

RADBOUD UNIVERSITY

MASTER THESIS

---

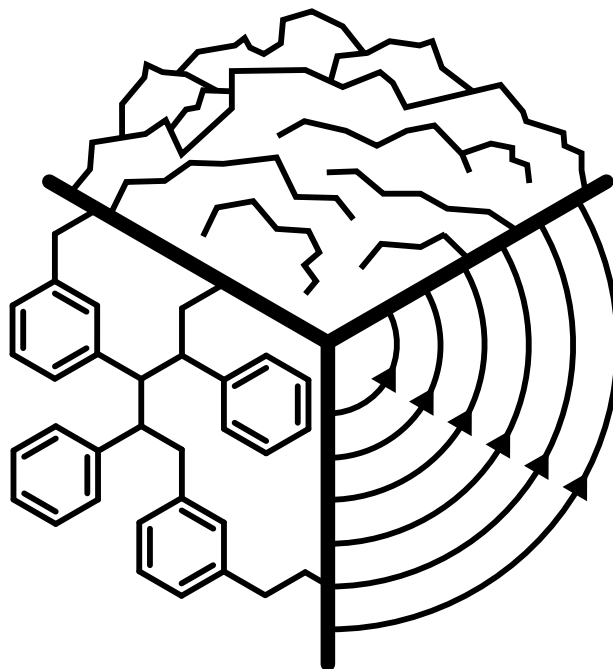
# Calcium Enrichment for the Study of Neutrinoless Double Beta Decay

---

*Author:*  
Milo VERMEULEN

*Supervisor:*  
Prof. Dr. Nicolo DE GROOT

*Second corrector:*  
Dr. Hugo MEEKES



October 27, 2016



## *Abstract*

This thesis is aimed at finding a method to enrich calcium in its heaviest naturally-occurring isotope:  $^{48}\text{Ca}$ . Motivation for this project came primarily from the CANDLES project, which seeks to study neutrinoless double beta decay in the aforementioned isotope, but currently uses unenriched calcium containing just 0.2%  $^{48}\text{Ca}$ . The Manhattan Project and recent attempts at calcium enrichment by CANDLES researchers provided inspiration for enrichment experiments attempted in this project. Mass-dependent effects were observed for two of the three classes of experiments: mineralisation yielded an enrichment factor of 1.009(8) and ion exchange produced a factor of 1.077(13). Electrophoresis was extensively studied, but ultimately no more than a simulation and a preliminary experiment were produced. Especially with regards to ion exchange, the thesis provides a realistic alternative to currently studied calcium enrichment methods.



## Acknowledgements

This project was an ambitious one, delving into a subject that is mostly unknown within the modern high-energy physics community and is smeared out over many different disciplines: materials science, chemistry, fluid dynamics and numerous others are all important fields with regard to element enrichment. For this reason, a large and diverse group of people was asked for support.

My gratitude goes out to the solid state chemistry department, especially Prof. Dr. Elias Vlieg, Dr. Willem van Enckevort and Dr. René de Gelder, for their advice on crystal growth and their attempts to find a gaseous compound containing calcium. Although crystal growth was ultimately not considered, it did spark the idea of mineralisation.

Special thanks go to Dr. André Eppink, Elke van Loenhout and Wiesiek Szweryn of the practical laboratory of physics. They provided almost all of the labware for the performed experiments and cleaned out their fume hood in case solvents such as methanol or acetone would be used. None of the experiments would have been possible without their help.

Similarly, the help of Dr. Tom Bloemberg and Luuk van Summeren of the practical laboratory of molecular sciences is much appreciated. They provided many of the chemicals needed for almost all experiments. Lye, EDTA, murexide and over twenty litres of demineralised water were selflessly offered. Additionally, they assisted in the acidification of some samples prior to mass spectrometry.

All of the isotope ratios were measured in Radboud University's general instrumentation department. Specifically the mass spectrometer and automated analyser were used extensively, and were operated by Paul van der Ven. Thanks go out to him for the analysis of countless samples and his explanation of the mass spectrometer's workings.

FTIR spectra were measured with the help of Prof. Dr. Jos Oomens, who selflessly provided some of his valuable time to discuss the possibilities of infrared spectroscopy and to demonstrate the workings of the FTIR spectrometer. My thanks go out to him and his seemingly endless patience for unusual student projects.

I am indebted to the staff of the university's technocentrum for their assistance in the creation of the preliminary electrophoresis experiment, which Jeroen Michiels ultimately performed. Special thanks go to René Habraken, technical staff member of the high-energy physics department, for always being available to advise and support. The many brain-storming sessions yielded countless ideas that impacted the project immensely.

My thanks go to Bob Stienen, Ruud Peeters and David Venhoek for reviewing and critiquing critical sections of this thesis. With their fresh insights, many incoherences and ambiguities were brought to light and could be corrected for the final version.

Additionally, my gratitude goes out to Dr. Hugo Meekes, who agreed to be the second corrector for this thesis.

Lastly, I would like to thank my supervisor, Prof. Dr. Nicolo de Groot, for his advice and support throughout the year. Although neither of us had very well in mind what to expect, our discussions sparked the first ideas and ultimately shaped the project into its current form.



# Contents

<b>Abstract</b>	iii
<b>Acknowledgements</b>	v
<b>Introduction</b>	1
<b>1 Neutrinoless double beta decay</b>	3
1.1 Majorana particles . . . . .	5
1.2 Experiments . . . . .	6
<b>2 Enrichment methods</b>	7
2.1 Centrifuge . . . . .	8
2.2 Calutron . . . . .	8
2.3 Gaseous diffusion . . . . .	10
2.4 Thermal diffusion . . . . .	11
2.5 Cascades . . . . .	12
2.6 Calcium . . . . .	13
2.7 Crown ether resin and chromatography . . . . .	14
2.8 Electrophoresis . . . . .	18
<b>3 Mineralisation</b>	23
3.1 Experiment . . . . .	23
3.2 Results . . . . .	26
3.3 Discussion . . . . .	28
<b>4 Ion exchange resins</b>	31
4.1 Experiment . . . . .	32
4.2 Results . . . . .	34
4.3 Discussion . . . . .	38
<b>5 Electrophoresis</b>	43
5.1 Experiment . . . . .	45
5.2 Results . . . . .	56
5.3 Discussion . . . . .	60
<b>6 Conclusions</b>	65
<b>A Mineralisation data</b>	67
<b>B Ion exchange resin data</b>	69
<b>C Simulation data</b>	71
<b>D Static electric field data</b>	73
<b>Bibliography</b>	75



# Introduction

At the dawn of the 20th century, multiple scientists independently discovered something peculiar. They had been studying newly discovered radioactive elements and their decay products, and found that more elements were produced than were thought to exist. From the established periodic table of the elements, it was predicted that there would be eleven elements spanning from lead to uranium. Experiments suggested 40. Additionally, several of these elements appeared to be chemically identical, leading to the idea that different atoms could occupy the same place in the periodic table. The name “isotope” was coined, meaning “same-place” in Greek, to denote these doppelgangers. Other evidence for the existence of isotopes emerged around the same time: it was found that naturally occurring thorium decays differently than thorium gained from decaying uranium. While the former undergoes alpha decay (now known to be the process  $^{232}_{90}\text{Th} \rightarrow {}^4_2\text{He} + {}^{228}_{88}\text{Ra}$ ), the latter decays by emitting a beta particle ( $^{234}_{90}\text{Th} \rightarrow {}^0_{-1}\text{e} + {}^{234}_{91}\text{Pa}$ ) and produces a radically different element. Additionally, elements were found to have a mass that was not a multiple of the nucleon mass, suggesting that multiple species containing different numbers of nucleons exist within a single element. For example, natural boron contains 20%  ${}^{10}\text{B}$  and 80%  ${}^{11}\text{B}$ , giving boron as a whole a mass of 10.8 atomic mass units and signifying it would have 10.8 nucleons in its core if it were to be composed of a single isotope.

**Notation of isotopes.** Atoms are composed of protons, neutrons and electrons. The notation  ${}^Z_A\text{X}^C$  is used to denote the abundance of these components in a compact fashion and distinguish between different elements and isotopes. X is the name of the element in question, for example H for hydrogen or Fe for iron. A signifies the number of protons in the atom’s core. Since this number uniquely determines the nature of the element, the name X is somewhat redundant. Z is the mass number of an atom and is the sum of the proton number A and the neutron number N. The number of neutrons may vary from atom to atom within the same element, and this is reflected by a different Z. For example,  ${}^{235}_{92}\text{U}$  and  ${}^{238}_{92}\text{U}$  are both isotopes of uranium, possessing 92 protons by definition. However, one isotope has 143 neutrons while the other has 146, resulting in the mass numbers 235 and 238. The number of electrons is assumed to be the same as the number of protons unless the atom is ionised. In this case, the number C denotes the charge of the ion. A helium atom that has lost two of its electrons, for example, is doubly charged and is denoted  ${}^4_2\text{He}^{2+}$ . Atoms taking up additional electrons obtain a negative charge.

 ${}^Z_A\text{X}^C$ 

Even though two isotopes of the same element are virtually indistinguishable from a chemical point of view, they can possess some different qualities. One of the better-known and more spectacular examples is uranium. The vast majority of uranium atoms consists of  ${}^{238}_{92}\text{U}$  and contains 146 neutrons per atomic nucleus. Although this isotope can be converted to the valuable plutonium ( ${}^{239}_{93}\text{Pu}$ ), it is rather unimportant relative to its lighter brother:  ${}^{235}_{92}\text{U}$ . This atom’s ability to release great amounts of energy when its core is split allows it to be used in nuclear power plants and nuclear weapons, and its discovery resulted in a scramble to isolate as much of it as possible during the second world war and subsequent cold war. Thanks to the immense power that comes with the possession of enriched uranium, large amounts of resources have been poured into separating isotopes. Advancements are still being made on the topic of enrichment today, even though the dawn of the atomic age is now more than sixty years in the past.

Modern enrichment plants are large and efficient, relying on all the technology that decades of intensive research has wrought. Uranium has partially made way for hydrogen, which is separated into protium and deuterium. The former contains only a proton whereas the latter consists of a proton and a neutron. Deuterium is used in research, certain nuclear fission power plants and thermonuclear weapons, and it is expected to play an integral part in upcoming nuclear fusion power plants. Tied to the production of thermonuclear weapons is the enrichment of lithium. The isotope  $^6\text{Li}$  is required to produce tritium, which is the next step up from deuterium with one proton and two neutrons at its core. Uranium enrichment methods are wholly unsuitable for both hydrogen and lithium and thus new methods have been specifically tailored to separate the isotopes of these elements. For many other stable isotopes, a general isolation method exists that is effective but very energy-inefficient. Minute quantities of rare isotopes may be separated from the bulk of an element by guiding ionised material through a magnetic field. A device called a calutron does exactly this and will be discussed in greater detail in section 2.2.

In order to avoid costly methods and to greatly speed up production, this project focuses on cheap and effective ways to enrich calcium and obtain  $^{48}\text{Ca}$  in as high a concentration as possible. Calcium exists in a wide variety of isotopes, featuring nuclear weights between 40 and 48 nucleons, with  $^{40}\text{Ca}$  taking up almost 97% of all natural calcium and only 0.2% consisting of  $^{48}\text{Ca}$ . The unusually large mass difference between these stable isotopes can be explained by nuclear ‘magic numbers.’ Magic numbers 2, 8, 20, 28, 50, 82 and 126 have been identified and  $^{40}_{20}\text{Ca}$  as well as  $^{48}_{20}\text{Ca}$  fit wonderfully into these figures, making them extraordinarily stable. They are considered doubly magic nuclei because both their protons and neutrons are present in the list of magic numbers: 20-20 (protons-neutrons) in the case of  $^{40}_{20}\text{Ca}$  and 20-28 in the case of  $^{48}_{20}\text{Ca}$ . The shell model that these magic numbers originate from will be explained in more detail in section 1.

As with almost all other isotopes that are actively isolated,  $^{48}\text{Ca}$  is necessary for a specific nuclear decay. In this case, the relevant decay is called neutrinoless double beta decay and will be further discussed in section 1. Additionally,  $^{48}\text{Ca}$  possesses an unusually large number of neutrons relative to its nuclear charge and is thus ideal for use in the creation of superheavy elements. For these productions, heavy atoms are bombarded with lighter, positively charged ions. If the ions can overcome the Coulomb barrier (both atomic nuclei are positively charged), the atomic cores may snap together by the strong force and form a new superheavy element. In order to make the Coulomb barrier as small as possible, it is advantageous to use nuclei that contain a relatively large number of neutrons. After all, neutrons contribute to the mass of a nucleus while they do not add to its electric charge.

# Chapter 1

## Neutrinoless double beta decay

Protons and neutrons are the building blocks of the atomic nucleus. The electrons exist outside of the core in a shell structure and determine nearly all the properties of the atom, despite only making up a small fraction of the total atomic mass. Since protons and electrons have opposite charges and the neutron is electrically neutral, the number of protons in the core determines the number of electrons that can be bound. This number is not fixed: the removal or addition of electrons can occur through collision with any other particle and commonly occurs under the influence of the sun's UV rays. This process is called ionisation. The number of protons in an atom, on the other hand, can only be changed by nuclear processes such as radioactive decay and nuclear fusion, and are rare in comparison to ionisation. Atoms are therefore classified by the more stable number of protons in their core. There are more forces at play within an atom than the electromagnetic force: the strong nuclear force is responsible for keeping the overwhelmingly positively charged nucleus from exploding and, unlike the electromagnetic force, it manifests itself within protons and neutrons alike. It may seem that an infinite number of neutrons may be added to a nucleus thanks to their stabilising power through the strong force while lacking a repulsive positive electric charge. However, there is a number of neutrons for which the atomic core is the most stable. The variance around this number results in the formation of isotopes: nuclei with the same number of protons but differing amounts of neutrons.

Two general theories exist to model the structure of the atomic core: the liquid drop model and the shell model [1]. The liquid drop model approaches nuclear stability from a pragmatic point of view. It considers all relevant forces and effects within the atomic core and constructs a binding energy from their combination. Table 1.1 gives an overview of the different terms.

TABLE 1.1: The various energy terms of the liquid drop model.

Energy term	Proportional to	Force type
Volume	A	Strong force
Surface	$A^{2/3}$	Strong force
Coulomb	$\frac{Z(Z-1)}{A^{1/3}}$	Electromagnetic force
Asymmetry	$\frac{(A-2Z)^2}{A}$	None (Pauli exclusion principle)
Pairing	$\pm A^{-1/2}$	None (Pauli exclusion principle)

Each of these terms requires a weighting factor that can be approximated by calculation but is more commonly taken from experiment. From the terms and their weighting factors, a total binding energy can be determined that can be used to ascertain the most stable isotope of a

certain element. The formula used to do this is called the semi-empirical mass formula and derives its name from the tuning of weighting factors to empirical observations.[2]

Once the structure of the atom became clear, it was found that nuclei containing certain numbers (2, 8, 20, 28, 50, 82 and 126) of protons or neutrons were more stable than others. These magic numbers were theorised to be the number of nucleons needed to fill a nuclear shell. Thus, with great resemblance to the atomic shell model for electrons, the nuclear shell model was born. Similar to the behaviour of electrons, protons and neutrons occupy the lowest unfilled shell in accordance with the Pauli exclusion principle, which forbids identical fermions from occupying the same state. Protons and neutrons have their own sets of shells and thus permit the formation of doubly magic nuclei in which both the proton number and neutron number are magic. Examples of doubly magic nuclei are  ${}^4_2\text{He}$ ,  ${}^{16}_8\text{O}$  and the main focus of this project,  ${}^{40}_{20}\text{Ca}$  and  ${}^{48}_{20}\text{Ca}$ . These doubly magic nuclei exhibit extraordinary stability and allow heavy isotopes to exist stably or with very long lifetimes where they would otherwise not have been able to exist. Although the shell model is reasonably successful at explaining the smaller magic numbers, it requires some modification at higher atomic masses.[2]

In the shell model, protons and neutrons have separate sets of energy levels. If there is a great inequality between the two kinds of nucleons, energy may thus be gained by converting an overabundant nucleon so that it may assume a lower energy state. This is called beta decay: a process involving the weak nuclear force that causes a neutron to be transformed into a proton or vice versa.  ${}^{14}_6\text{C} \rightarrow {}^{14}_7\text{N} + {}^0_{-1}\text{e}^- + \bar{\nu}_e$  and  ${}^{22}_{11}\text{Na} \rightarrow {}^{22}_{10}\text{Ne} + {}^0_{+1}\text{e}^+ + \nu_e$  are examples of  $\beta^-$ - and  $\beta^+$ -decay within atoms, respectively. Because an electron is also called a  $\beta$ -particle,  $\beta^-$ -decay is often abbreviated to  $\beta$ -decay. Only one quark actually participates in the process: it emits an intermediate W-boson that produces the final electron and antineutrino. Interestingly, there exists a process whereby two accounts of beta decay happen simultaneously in the same nucleus. The process can be visualised in a Feynman diagram (with time flowing from left to right) and is pictured in figure 1.1a. Only a handful of isotopes are able to perform double beta decay, however, and even among those elements the decay is extremely rare. In table 1.2, it can be seen that half-lives are on the order of  $10^{20}$  years and that the decay energy amounts to a few MeV in all cases. This indicates that double beta decays are few and far between, and that the few that do occur can easily be drowned out in background radiation.[3]

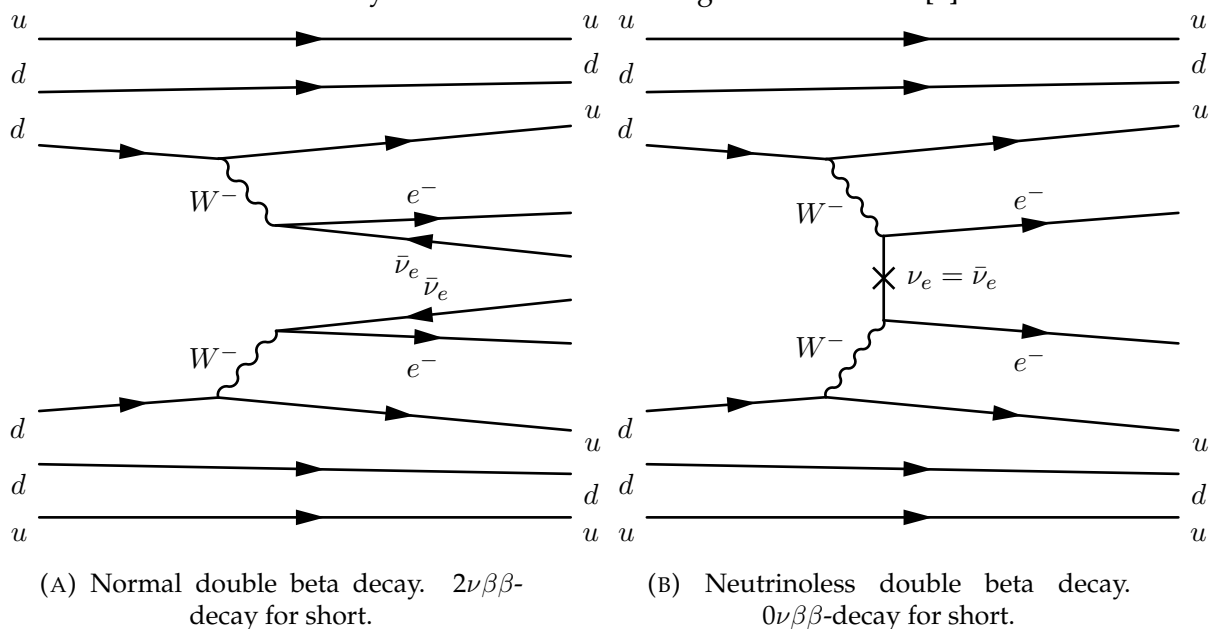


FIGURE 1.1: Two cases of double beta decay in which two neutrons simultaneously decay to protons by undergoing beta decay. The second diagram is only possible in the case that neutrinos are Majorana fermions.

TABLE 1.2: The known double beta decay candidates listed with their half-lives [4], decay energies and natural abundances[5].

Isotope	Half-life [years]	Decay energy [MeV]	Abundance [%]
$^{48}\text{Ca}$	$4.3 \cdot 10^{19}$	4.2737	0.187
$^{76}\text{Ge}$	$1.4 \cdot 10^{21}$	2.0391	7.8
$^{82}\text{Se}$	$1.1 \cdot 10^{20}$	2.9955	9.2
$^{96}\text{Zr}$	$3.9 \cdot 10^{19}$	3.3477	2.8
$^{100}\text{Mo}$	$0.95 \cdot 10^{19}$	3.0350	9.6
$^{116}\text{Cd}$	$3.75 \cdot 10^{19}$	2.0040	11.8
$^{124}\text{Sn}$	$> 1.8 \cdot 10^{17}$	2.8091	7.6
$^{128}\text{Te}$	$> 2 \cdot 10^{24}$	2.2877	5.6
$^{130}\text{Te}$	$> 0.8 \cdot 10^{21}$	2.5303	34.5
$^{136}\text{Xe}$	$> 2.3 \cdot 10^{20}$	2.4619	8.9
$^{150}\text{Nd}$	$1.7 \cdot 10^{19}$	3.3673	5.6

## 1.1 Majorana particles

Double beta decay is not only interesting because it is such a rare process. It also presents intriguing possibilities to probe the properties of the neutrino, an extremely elusive particle. It has been theorised that it could be its own antiparticle, which would make it an elementary Majorana fermion. If this were the case, neutrinoless double beta decay would occur: neutrinos would cancel each other since they are both particle and antiparticle at the same time. In this case, no energy would go missing in the form of the nigh-invisible neutrinos. The entirety of the decay energy would be put into the electrons, creating a markedly different energy spectrum that is shown qualitatively in figure 1.2. The process of neutrinoless double beta decay is shown fully in figure 1.1b.

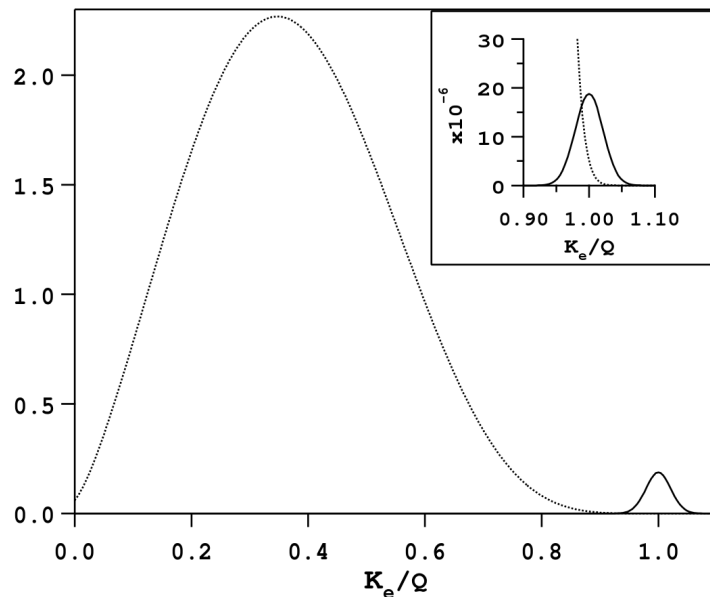


FIGURE 1.2: The frequency of double beta decay (in arbitrary units) as a function of the electron energy  $K_e$  normalised by the total energy released in the reaction  $Q$ . The main graph shows regular double beta decay (dotted line) and neutrinoless double beta decay (solid line). The latter is magnified by a factor  $10^4$ ; its true magnitude is displayed in the inset.[6]

## 1.2 Experiments

Experiments have been performed and are currently under way in an attempt to observe double beta decay in both its regular and neutrinoless variants. This effort is hampered by the rarity of such decays, indicated by the long half-lives shown in table 1.2. Background radiation from cosmic rays and terrestrial sources further obscure any potential signals. Cosmic radiation is relatively easily shielded from by building the experiment deep underground, but terrestrial sources of radiation are present in the earth and building materials. Sensitive experiments thus require the use of refined construction materials containing decreased amounts of radioactive isotopes. Potassium, thorium and uranium are the main sources of terrestrial radiation and contain multiple instances of beta decay in their decay chains. Moreover, the decay energies of these chains frequently overlap with those for double beta decay, ranging mostly from 1 to 3 MeV [3]. It is therefore important to limit the abundance of these elements in the direct vicinity of the detectors and to filter out any external radiation that does enter the experiment. This can be done by a veto system: a particle detection mechanism just outside of the double beta decay area that detects and registers any particles that enter from the outside. If such an event coincides with a detected signal within the experiment area, the event may be considered to have an external origin.

The many experiments that have been conducted in the search for neutrinoless double beta decay have used a wide variety of elements from the list in table 1.2. A select few are briefly summarised here.

- EXO-200 (Enriched Xenon Observatory) is a United States experiment that uses 200 kg of enriched liquid xenon both as the object of study and as a scintillator: when electrons are liberated during beta decay, they generate light within the liquid. This light is then captured and measured by avalanche photodiodes.[7]
- CUORE (Cryogenic Underground Observatory for Rare Events) uses 741 kg TeO<sub>2</sub> which contains 206 kg tellurium. One advantage of this particular element is that it consists for 34.5% of <sup>130</sup>Te, an isotope that undergoes double beta decay. It was therefore deemed unnecessary to invest in expensive enrichment procedures: natural tellurium was used instead. A measurable temperature rise occurs when the energy of a double beta decay is absorbed into the TeO<sub>2</sub> crystals and can be detected via cryogenically cooled bolometers.[8]
- GERDA (GERmanium Detector Array) employs a slightly different strategy: it is an experiment that features bare enriched germanium diodes that are submerged within cryogenic liquid argon and shielded from outside radiation by an additional water layer and copper shield. Again, the detectors serve both as the producer of double beta decay and as the detector, functioning as semiconductor detectors in this case.[9]
- The NEMO (Neutrino Ettore Majorana Observatory) experiments are extraordinary in that their sources are separate from their detectors. In NEMO3 and the more recent SuperNEMO, neodymium-containing foils are strung between gas tracking chambers, which are in turn bordered by calorimeters. The NEMO experiments have used molybdenum and selenium as their sources, with both materials enriched in the appropriate isotopes for double beta decay.[10]
- The CANDLES (CAlcium fluoride for the study of Neutrinos and Dark matters by Low Energy Spectrometer) experiments use CaF<sub>2</sub> crystals and make use of the double beta decay properties of <sup>48</sup>Ca. The crystals function once again both as the source and scintillator, with photomultiplier tubes surrounding them to detect any events within the experiment. Natural calcium is used due to difficulties in its enrichment. Unfortunately, a measly 0.187% of all calcium participates in the production of double beta decay events.[11]

## Chapter 2

# Enrichment methods

In this section, existing enrichment methods will be discussed. While the enrichment of calcium specifically is a very recent topic of research, the isolation of isotopes has been of great interest since their discovery and was rapidly accelerated by the Manhattan Project during the second world war.

In chemistry, sample purification has been extensively studied and has proved essential for modern industry. Contamination of fuels or alloys with unwanted elements could cause unexpected reactions that may decrease the quality of a product at best and cause serious harm at worst. It is an unfortunate fact that few useful elements and compounds exist in a readily usable form. For example, metallic ores are almost always a mixture of multiple elements: iron appears as its oxide forms in the minerals hematite and magnetite, aluminium is present in its hydroxide forms as gibbsite and boehmite, and lead exists in its sulfide form as galena. There is a myriad of ore processing methods and likewise countless exist for the purification of plastics, fuel, construction material, water and air, among many others.

Separation of different elements and compounds can be realised by making use of the fact that two different molecules have differing properties. In some cases it is as simple as heating the sample: ethanol has a much lower boiling point than water and can be isolated by heating the mixture to a point where the ethanol evaporates and the water does not. This process is called distillation and is also used in oil refinery for the production of petrol and other fuels. As another example, separating a solid from a fluid can be effected by passing the mixture through a filter. Large particles cannot pass the barrier that the filter represents, while the individual fluid molecules continue relatively unopposed. On a more molecular level, lead may be refined from galena by roasting the ore ( $2 \text{ PbS} + 3 \text{ O}_2 \rightarrow 2 \text{ PbO} + 2 \text{ SO}_2$ ) and making it react with carbon in coke ( $2 \text{ PbO} + \text{ C} \rightarrow 2 \text{ Pb} + \text{ CO}_2$ ). Many more of these processes exist and entire books have been written even on individual methods. Let it therefore suffice to say that the vast majority of element separation occurs on a basis of differing chemical properties.

It is exactly this principle that makes existing infrastructure worthless when considering isotope separation. Even though the core of an atom makes up nearly all of its mass, it is the outer electrons that determine the bulk of its properties. These electrons structure themselves around the nucleus strictly according to their number, which in turn is dictated by the charge of the atomic core. In short, most properties of an atom are determined by the number of protons in its core. Isotopes, by definition, possess the same number of protons but differ in their neutron content. The chemical behaviour of isotopes is thus nearly identical, even though they can differ substantially in mass. The processes discussed above will therefore likely not be sufficient for significant isotope separation.

The same was noted when, during the second world war, large amounts of a specific isotope were suddenly in high demand. The United Kingdom, the United States and Canada had banded together with the goal of constructing the first atomic bombs under the Manhattan Project. As with rocket science, great advances were made in little time thanks to a large military effort. The following sections are structured in such a way that they follow the chronological development of isotope separation technology during the course of the Manhattan Project. They serve to shed light on the difficulties that arise when attempting to isolate a specific isotope, as well as the methods that were devised to overcome these challenges.

## 2.1 Centrifuge

The method that was first attempted for the large-scale enrichment of uranium was the gas centrifuge. It consists of a cylinder that is filled with uranium-hexafluoride and brought to a high rotation speed. The earliest centrifuges were approximately 20 cm in diameter and their periphery attained speeds of 300 m/s [12]. In order to reduce friction at a rotation speed of 500 rev/s, the cylinders were held in place with magnetic bearings and were placed inside a vacuum. Modern centrifuges, in contrast, can reach peripheral speeds of 600 m/s and are magnetically balanced on a pin to further reduce friction. The uranium gas inside the centrifuge is rapidly spun around the central axis, making the atoms inside sort themselves according to mass. The heavier isotopes are flung outwards slightly more strongly than the lighter ones and can be scooped up at the extremities of the cylinder whereas the desired lighter isotopes mostly collect in the centre of the device and are extracted from there. A diagram of a uranium centrifuge is shown in figure 2.1. A single centrifuge can accomplish an enrichment factor between 1.2 and 1.5, which is huge compared to most other methods.[12]

**Notation of degrees of enrichment.** In order to display the results of an isotopic measurement in a comprehensible fashion, a differing abundance of a specific isotope  $x$  is often quantified in terms such as  $\alpha$ ,  $\varepsilon$  and  $\delta^x\text{Ca}$ . These measures are described as follows:

$$\alpha = \frac{(^x\text{Ca}/^{40}\text{Ca})_{\text{sample}}}{(^x\text{Ca}/^{40}\text{Ca})_{\text{standard}}} \quad (2.1)$$

$$\varepsilon = \alpha - 1 \quad (2.2)$$

$$\delta^x\text{Ca} = \varepsilon \cdot 1000 \quad (2.3)$$

In this equation,  $\alpha$  signifies the enrichment factor. If the sample has a 4% higher concentration of isotope  $x$  than the standard, this factor takes the value of 1.04. The separation coefficient  $\varepsilon$  would then be 0.04. Because of the often minuscule effects, the value is multiplied by one thousand for ease of reading and writing. The final value is then expressed in permille and the above example would result in  $\delta^x\text{Ca} = 40\text{\textperthousand}$ . Note that the deviation will attain negative values for samples that are depleted of the relevant isotope. For example, an enrichment factor of 0.998 returns a value of  $\delta^x\text{Ca} = -2\text{\textperthousand}$ .

Despite its advantages, the method was abandoned early on in the Manhattan Project for a number of reasons. Firstly, there are many problematic resonances the centrifuge has to pass to attain its final rotation speed. These can be altered to a certain degree by varying the physical properties of the centrifuge, but the problem persist. Secondly, the method cannot easily be scaled. It was hypothesised that a staggering 17,000 centrifuges would be required to produce any significant amount of highly enriched uranium. After a pilot plant proved even less efficient than was previously thought, the idea was abandoned altogether [12]. Today, the resonance problem is solved by swiftly accelerating through problematic frequency regions. Significant advances in materials science have opened up new possibilities for the gas centrifuge as well: they can be built much taller than they could be before, alleviating the scaling problem somewhat by allowing more material to be processed in parallel. Thanks to these improvements, the gas centrifuge became the main method of uranium enrichment during the cold war and is still the dominant method today.

## 2.2 Calutron

The idea of a mass spectrometer was not new by the time enriched uranium got in demand. In 1918, A. J. Dempster devised an apparatus that could separate what he called positive rays:

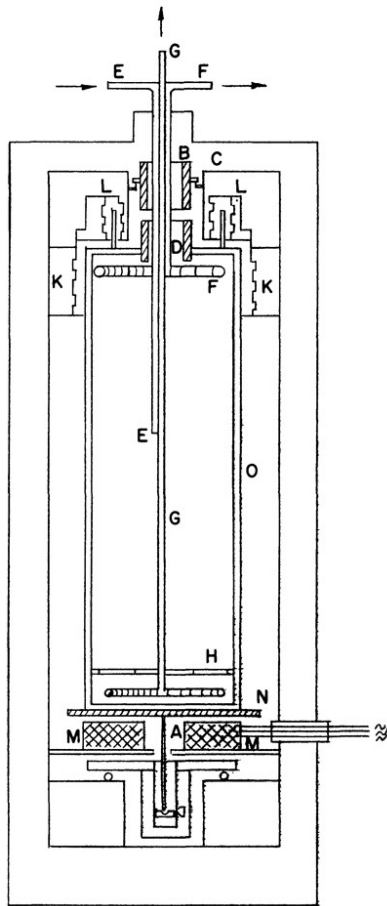


FIGURE 2.1: A Zippe type ultracentrifuge for the enrichment of uranium. The input feed (E) pumps gas into the centrifuge barrel (O), which is then extracted by scoops (F and G).[13]

positively charged ions. In his device, he accelerated these charged particles and made them pass through a perpendicular magnetic field so that they described semicircles in accordance with their  $q/m$  ratio, where  $q$  is the charge of an ion and  $m$  is its mass. Ions with a large charge are more strongly affected by the magnetic field and move in a smaller semicircle. Likewise, lighter ions possess less momentum than their heavier companions and split off to form a smaller semicircle as well. This is used to distinguish between isotopes, which by definition differ in little else than their mass.[14]

A calutron is essentially a mass spectrometer that is focused on quantitative production instead of qualitative measurement. The principle is identical: ionised material is accelerated and made to describe a semicircle under the influence of a magnetic field. Special pockets collect the isotopes at the end of their paths to keep the separated material apart. Figure 2.2 shows an overview of the main calutron function. Calutrons were essential in the making of the first atom bombs: over 1,000 of the enrichment devices were built under the Manhattan Project and 76 were kept in operation long afterwards. Even though every atom has its own characteristics when it comes to ionisation, focusing and deflection, the main principle behind the calutron is sufficiently universal for application in the enrichment of most isotopes. Coupled with the extremely high enrichment factor and the ability to collect all isotopes of an element at once, this makes the method highly attractive for the isolation of any isotope.[15]

Unfortunately, all of these advantages come at a price. Isotopes in the calutron can only be separated according to their weight as long as they do not experience significant forces other than the Lorentz force brought about by the magnetic field. It is thus essential that the ion beam travels in a vacuum and that the ions affect each other minimally. Since they have like charges,

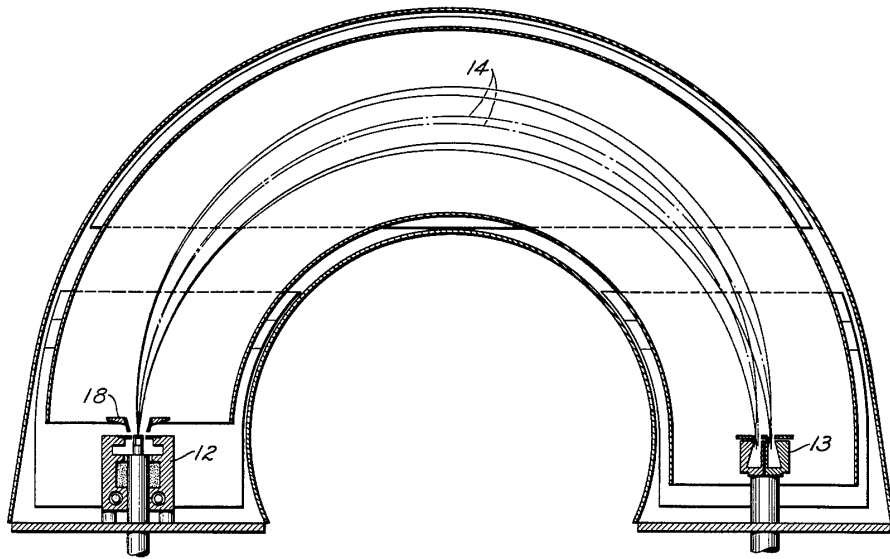


FIGURE 2.2: A schematic overview of a calutron. Uranium is ionised by an oven (12) and accelerated by electrodes (18). The beam then splits into its isotopes (14), which are captured in separate pockets (13).[16]

the atoms repel each other and expand the beam, causing increased cross-contamination at the collection pockets. Ideally, ions would pass the machine individually, with sufficient distance between subsequent charges that they would not affect each other at all. The nature of mass-production dictates a different setup, however. For production to be of any significance, the ion current in the calutron must be as large as possible without significantly affecting the enrichment factor of the machine. This limitation defines the main drawback of the method: only minute quantities of highly enriched elements can be produced at a time. Not only does this cause an extremely long preparation time for samples above a kilogram, but it also costs an immense amount of electricity to produce such a quantity. Although the exact price for enriched isotopes is not easily found, estimates place  $^{48}\text{Ca}$  on the order of \$10,000 per gram, making an experiment utilising a tonne of the material prohibitively expensive. Nevertheless, for many elements it is the only method that will allow any enrichment at all and thus it remains widely popular to this day.

### 2.3 Gaseous diffusion

Another successful enrichment method that sprung up under the Manhattan Project is the application of gaseous diffusion. In a gas, the lighter molecules will move slightly faster than the heavier ones. This effect is described by Graham's law, which states that the diffusion speed of a gas is proportional to the square root of its molecular mass. The effect can be made intuitive by considering a mixture of two gases at a constant temperature. Since the average kinetic energy of a gas molecule is only dependent on the macroscopic temperature, it is the same for all molecules in a mixture. Thus:

$$\frac{1}{2}m_1v_{1,\text{avg}}^2 = \frac{1}{2}m_2v_{2,\text{avg}}^2 \quad \Rightarrow \quad \frac{v_{1,\text{avg}}}{v_{2,\text{avg}}} = \sqrt{\frac{m_2}{m_1}} \quad (2.4)$$

Where  $v_{1,\text{avg}}$  and  $v_{2,\text{avg}}$  are the velocities of the gases and  $m_1$  and  $m_2$  are their masses. This principle finds practical application with semipermeable membranes. The small holes that are

set into these plates act somewhat like a filter: the lighter molecules pass through more easily than the heavier ones, and cause separation dependent on molecular mass.

Gaseous diffusion was employed as a method to enrich uranium during the second world war. To this end, the unenriched gas was placed under high pressure and forced along semipermeable membranes, behind which was a region of much lower pressure [17]. As described by Graham's law, the  $^{235}\text{U}$  diffuses into the low-pressure space slightly better than the  $^{238}\text{U}$ , creating a small enrichment just beyond the barrier. The arrangement is shown in figure 2.3. The diffusion rate of a gas through a semipermeable membrane is proportional to its average molecular velocity. Therefore, the ratio between the two uranium species on the low pressure side is enhanced by the mass ratio in equation 2.4.

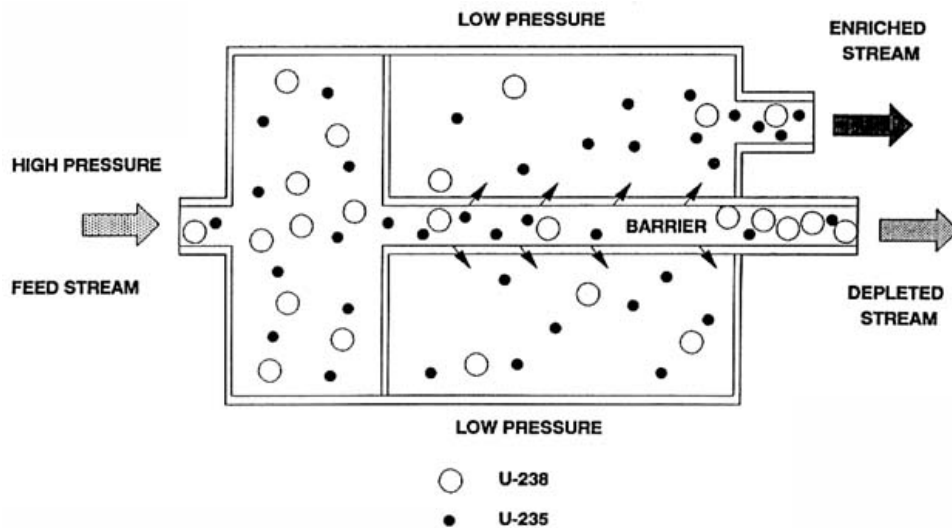


FIGURE 2.3: An overview of a gaseous diffusion enrichment scheme.[18]

Uranium was converted to uranium-hexafluoride to form a gas near room temperature and atmospheric pressures. Although the formation of this compound is a necessity as there are no other viable candidates, it poses many challenges in its creation and handling. Uranium-hexafluoride is highly toxic and corrosive, requiring specific compounds in the enrichment facility's transport pipes, valves and lubricants to prevent detrimental chemical reactions. The gas forms a solid compound when brought into contact with water and solidifies spontaneously at a temperature below  $64^\circ\text{C}$  [19]. Even after going through the effort to accommodate the gas, the full mass difference between uranium isotopes cannot properly be taken advantage of. Both isotopes are perpetually bound to six fluorine atoms, making the mass ratio much smaller than would be the case if uranium were a monoatomic gas in itself. Uranium-hexafluoride containing  $^{235}\text{U}$  weighs approximately 349 atomic mass units and  $^{238}\text{U}$  352. Equation 2.4 shows that the ratio between drift velocities would then be  $v_{^{235}\text{U},\text{avg}}/v_{^{238}\text{U},\text{avg}} = 1.004$ . In other words, the single stage efficiency can only be expected to yield an enrichment of 0.4%. A stark contrast to the gas centrifuge detailed above. Gaseous diffusion is much simpler to realise, however, and single stages can be scaled much more easily than the centrifuge. For these reasons, the method is still in extensive use these days.[20]

## 2.4 Thermal diffusion

Another known principle was put to the test under the Manhattan Project: thermal diffusion. At its core, it relies on the fact that a mixture of gases under a thermal gradient will exhibit a gradient in its gas species, given that there is some difference between the gas molecules. Although the theory behind this principle is not very transparent and was poorly understood

at the time of the second world war, a concentration gradient can be readily observed in a practical setting. The separated species have a tendency mix again, however: regular diffusion works against any concentration gradient and grows stronger as said gradient becomes larger. Thus, after a while, an equilibrium between thermal and regular diffusion will be obtained at which the largest possible separation between gases is reached.[21]

Thermal diffusion is not performed in large volumes. Modern plants employ concentric cylinders with a small gap between them filled with gas. These vertical cylinders are often made quite tall to increase the single stage enrichment factor and are heated on the internal cylinder while being cooled on the external one. This causes a convection current and a slight separation between uranium isotopes. The lighter uranium-hexafluoride is drawn to the warm cylinder wall and is carried upwards while its heavier brother is attracted to the cold wall and rides the convection current down to the bottom of the apparatus. The enriched and depleted gases are then extracted from the top and bottom of the device, respectively. An alternate scheme exists in which the inner cylinder is replaced by a hot wire which is heated electrically. The hot wire setup decreases the amount of parasitic convection currents within the apparatus. However, electric heating is not always the cheapest option. Concentric cylinders can be heated by sending hot steam down the middle of the apparatus instead. This is especially useful when the enrichment plant is built close to a power plant, where steam is abundant.[21]

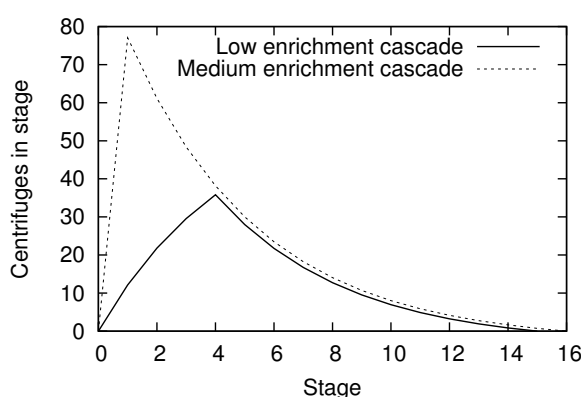
## 2.5 Cascades

With the possible exception of the calutron, all the above methods are woefully insufficient when it comes to realising a significant enrichment factor. This was known at the time of the Manhattan Project as well:  $^{235}\text{U}$ , at an initial concentration of 0.72%, needed to be boosted to over 80% for the production of nuclear weapons. An enrichment factor of over 100 was thus required, something that was not even realised by calutrons at the time and was very much above the factor 1.5 that gas centrifuges could offer in theory. The solution was simple: use enrichment stages in series, with the enriched output from one stage being used as input feed by the next. In the example of gas centrifuges, it was initially estimated that 29 subsequent enriching stages would be needed to produce sufficiently enriched uranium for the production of nuclear weapons. In the end, and without using the now-popular gas centrifuge, the Manhattan Project fed the enriched output from one enrichment plant into the next. Thermal and gaseous diffusion produced the initial enrichment, and the calutron processed the material into its final highly-enriched form.

Estimating the amount of required enriching stages is relatively simple once the initial and final enrichments are known and the enrichment per stage is well-defined. In a laboratory, a single enrichment apparatus could be used in which the enriched output is fed back into the input feed of the machine and the depleted output is discarded. Highly enriched samples may be prepared in this manner, but in minute quantities. Although the setup for mass production is much more complex, it can be made intuitive by posing a number of requirements. Firstly, using a single machine for all stages does not allow for a continuous enrichment process: there should be at least one device per stage and preferably many per stage working in parallel. Many stages working in series is called a cascade. Secondly, it would not do to discard the depleted output of all enrichment stages. Although it does not fit the requirements the final product should meet, the depleted output of the final stage is at least as enriched as the initial input feed and could be used again. The enriched output of one stage is fed into the next and the depleted output is fed into the previous stage. This way all stages have a well-defined enrichment factor assigned to them and enriched material is always mixed with other material enriched to the same degree. Thirdly, to minimise waste, there should be a number of stripping stages. These stages function the same as the enrichment stages, but they process material which has a lower abundance of the desired isotope than natural material. Elements which

are abundant in nature require fewer stripping stages: the energy put into stripping depleted material may not be worth it if raw material is readily available. Lastly, all stages should not be the same size. The material flow at the product and waste ends are much smaller than that at the first stage. This is because the input feed and recycled material both pass through the middle stages.

Calculating the optimal number of devices per stage is not straightforward to do analytically, but an example of an ideal cascade profile is shown in figure 2.4. Raw material is fed into the widest part of the profile and processed material exits at either end. The enriched product flows out of the narrow higher stages of the cascade while the waste exits out the lower stages. It is worth noting that only one of the pictured profiles features a stripping section. Additionally, stages contain non-integer numbers of centrifuges. This highlights the purely mathematical nature of the model. Real world centrifuge cascades have to compensate for their integer nature with extra centrifuges. In this section, it was assumed that all devices in all stages are identical and that their enriched and depleted outputs are approximately equal in volume.[22]



Enrichment	Low	Medium
Total stages	14	15
Enrichment stages	11	15
Stripping stages	3	0
Total centrifuges	206	344
Input enrichment	0.2%	0.2%
Product enrichment	2%	5%
Waste enrichment	0.08%	0.16%
Input stage	4	1
Product feed fraction	1/16	1/97
Waste feed fraction	15/16	96/97

FIGURE 2.4: Two centrifuge cascade profiles with an individual stage enrichment factor of 1.25, enriching the same material. Their statistics are presented in a table. Raw material enters a cascade at its input stage, after which it either exits from the cascade's head (stages 15 and 16) as enriched product or at its tail as depleted waste (stage 0). Note the difference in the number of required stages and the fraction of the material that exits the cascade as product.[23]

## 2.6 Calcium

The methods named thus far are all effective in their own ways. Some feature a higher enrichment factor while others allow for easy upscaling and mass-production. Yet others are more energy-efficient and permit enrichment schemes to operate for extensive lengths of time at minimal cost. One characteristic that ties the different methods together is that they process materials in a sparse form. That is to say, most methods of the Manhattan Project made use of uranium-hexafluoride in its gaseous state. The calutron is the exception to this and uses an ion beam that is even sparser than the gases used in other devices. The reason for this can be made intuitive by considering the degree of mutual interaction different molecules may have within an enrichment process. Because they are small by nature, individual isotopic characteristics would be overshadowed if interactions between molecules were significant. In the example of thermal diffusion, different isotopes are required to move in different directions altogether. One is attracted to increased temperatures while the other moves towards cooler regions. If these effects are intertwined in some way, it is very likely that the end result would be zero.

The unfortunate nature of calcium prevents it from forming gaseous compounds near room temperature and atmospheric pressure. Fluorine, the atom that makes a gas out of uranium,

forms a solid crystal with calcium.  $\text{CaF}_2$  has a melting point of 1423 °C and evaporates around 2500 °C, a far cry from room temperature [24]. Operating existing enrichment schemes at these temperatures is likely not strictly impossible, but it does bring about additional challenges. The materials that come into contact with the scorching calcium gas would have to keep their strength and resist any chemical reaction with the gas under the heat. Safety of researchers and workers would also be compromised if the superheated gas were to be brought into motion: simple leaks would be dangerous and exploding ultracentrifuges downright disastrous. Considering the scope and resources of this project, it was decided not to investigate superheated fluids.

Other possibilities for enriching calcium include dissolving a calcium salt in a solvent, using solid calcium dust, and ionising individual calcium atoms as is done in the operation of the calutron. Although dust and ions have their advantages, their scalability is poor and they generally require considerable amounts of power per unit product to function. Therefore, calcium is mostly considered in its dissolved state throughout this project. The simple act of dissolving a calcium salt causes the individual atoms to obtain a charge as though they were ionised, but the effect comes at a price. The solvent molecules responsible for forcing the salt apart crowd around the ions and form a solvation shell that negates much of the mass difference between isotopes. The exact number of water molecules that cling to an ion is difficult to determine and varies depending on the method used, but experiment places the hydration number between 5 and 10 [25]. Taking the hydration number to be 8, for example, the large mass ratio between calcium isotopes  $m(^{48}\text{Ca})/m(^{40}\text{Ca}) \approx 1.2$  is reduced to  $m(^{48}\text{Ca} + 8 \text{H}_2\text{O})/m(^{40}\text{Ca} + 8 \text{H}_2\text{O}) \approx 1.04$ . Heavier solvents such as methanol can have a slightly lower solvation number but are much heavier than water: in the case of six methanol molecules per calcium ion, the mass ratio reduces to  $m(^{48}\text{Ca} + 6 \text{CH}_3\text{OH})/m(^{40}\text{Ca} + 6 \text{CH}_3\text{OH}) \approx 1.03$  [26]. Additional variation in these ratios exists thanks to isotopic variance within solvent molecules and variance of solvation number per calcium ion:  $^{48}\text{Ca} + 7 \text{H}_2\text{O}$  is already much lighter than  $^{40}\text{Ca} + 8 \text{H}_2\text{O}$ , despite the heavier calcium isotope.

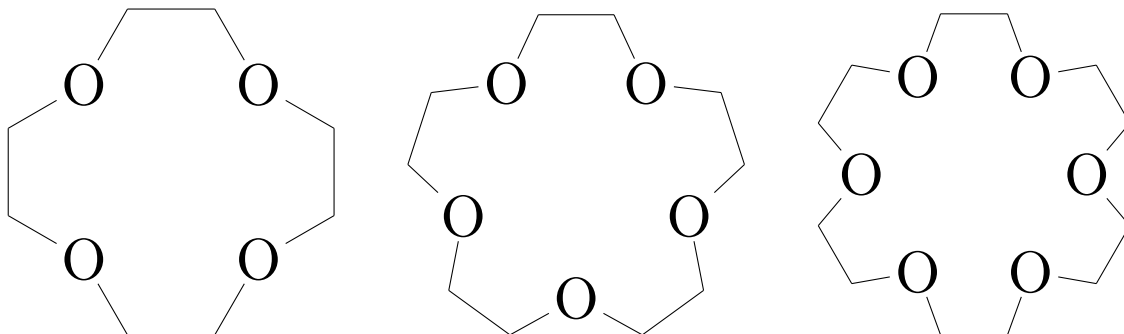
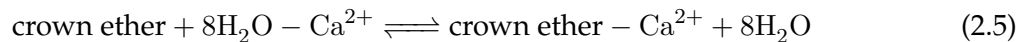


FIGURE 2.5: Various crown ethers.

## 2.7 Crown ether resin and chromatography

Ions in solution are surrounded by solvent molecules that arrange themselves in a solvation shell structure. This extra mass is in most cases inevitable, but sometimes it can be shed. Crown ethers are cyclic molecules consisting of ethers, which are carbon chains that incorporate an oxygen atom as part of the main chain. Their name is derived from their characteristic shape, shown in figure 2.5, which resembles the shape of a crown and allows the molecules to adsorb, or crown, a cation in their centre [27]. An equilibrium arises when crown-ethers are brought into contact with an electrolytic solution: the population of cations is split between occupying solvation shells and crown ethers. In the example of calcium, the following equation represents

the appropriate equilibrium:



In practice, however, it is assumed that available crown ethers always adsorb calcium ions unless ions of another type are present in sufficiently high quantities. The preference for a crown ether to adsorb one cation over another is described by a selectivity coefficient and is to a large extent correlated with the cation's diameter. This theory is supported by a comparison of ionic diameters to selectivity coefficients of an ion exchange resin. Although this specific ion exchange resin works by an entirely different mechanism compared to crown ethers, the solvation shell still has to be shed before cations can be bound and thus the same theory is viable. In figure 2.6, it can be seen that a larger ionic diameter in general does imply a higher selectivity coefficient, i.e. a higher affinity for adsorption into an ion exchange resin.[28][29]

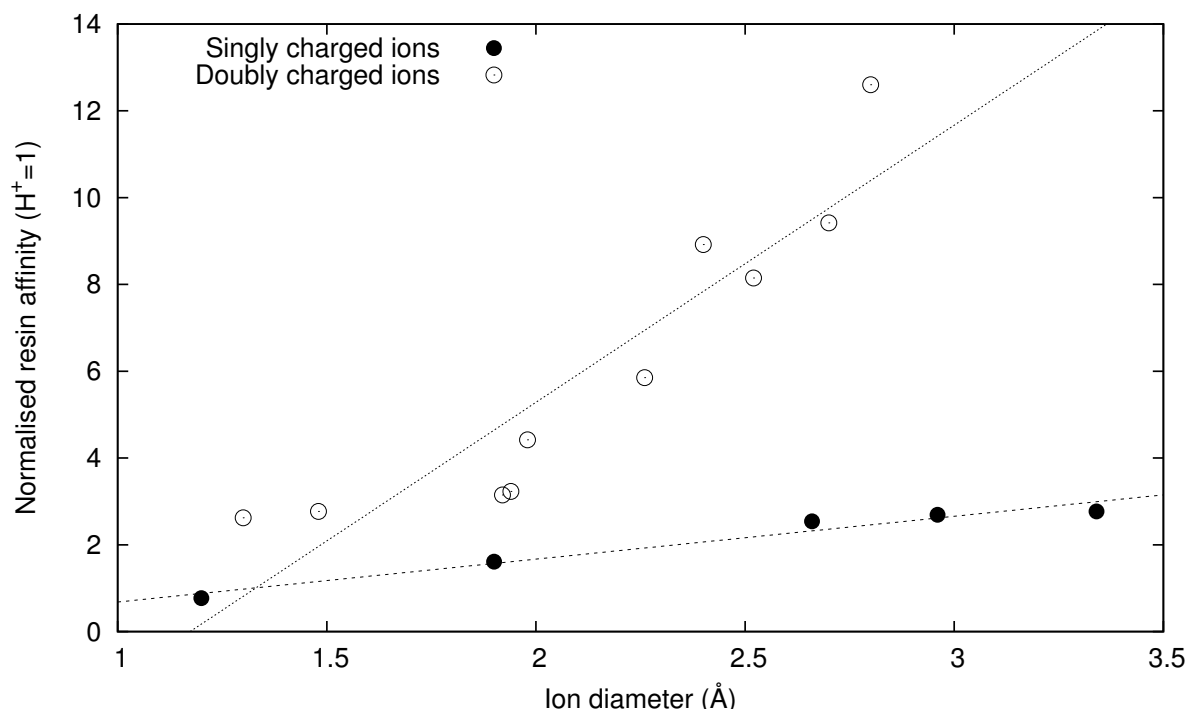


FIGURE 2.6: Cation diameters correlated with their affinity for binding to a polystyrene sulfonate cationic ion exchange resin. Data from [28] and [29] was used to create this figure.

Ion exchange resins are in extensive use wherever certain ions need to be removed from a solution. Water softening and purification is the simplest example of their uses, but they are also used in the separation of ions that are otherwise chemically similar. In private use, they are most often used in the preparation of drinks (especially coffee) and the maintenance of aquarium water. In both cases, they serve to extract calcium and magnesium from water in order to reduce its hardness. Since the resin merely exchanges ions, different ions are released into the solution upon adsorption of  $\text{Ca}^{2+}$  and  $\text{Mg}^{2+}$ . In many cases this will be  $\text{Na}^+$ , making the solution slightly salty. Other resins release  $\text{H}^+$  instead, making the solution more acidic. This can be counteracted by capturing the  $\text{Cl}^-$  using another resin and replacing it with  $\text{OH}^-$  groups which then combine with  $\text{H}^+$  to make water. In this way, water can be purified to a high degree. One of the most used ion exchange resins consists of polystyrene sulfonate and can be loaded with cations such as  $\text{Na}^+$  and  $\text{H}^+$ . It is therefore called a cationic ion exchange resin. When the resin comes into contact with an electrolytic solution, ions are exchanged between the resin and solution according to their ion selectivity coefficients. Polystyrene sulfonate is normally loaded

with sodium or hydrogen, both of which have relatively low selectivity coefficients and are thus easily replaced by ions in solution such as calcium and magnesium. The sulfonate groups in the resin each bind one elementary charge, such as one  $H^+$  or one  $Na^+$  ion. Two sulfonate groups bind to a doubly charged ion such as  $Ca^{2+}$  or  $Mg^{2+}$  to remove it from solution. Figure 2.7 gives a representation of an exchange process in which sodium is released and calcium is bound. The method of binding is considerably different from the crown ether process, but there are indications that the same enrichment mechanisms may still apply. As shown in figure 2.6, the ionic diameter and sulfonate selectivity coefficient of a cation are positively related. Something that has also been suggested for crown ether resins. Additionally, the solvation shell has to be shed no matter what type of cation adsorber is used. Thus, cations that shed their shells more easily are more readily adsorbed regardless of the resin.

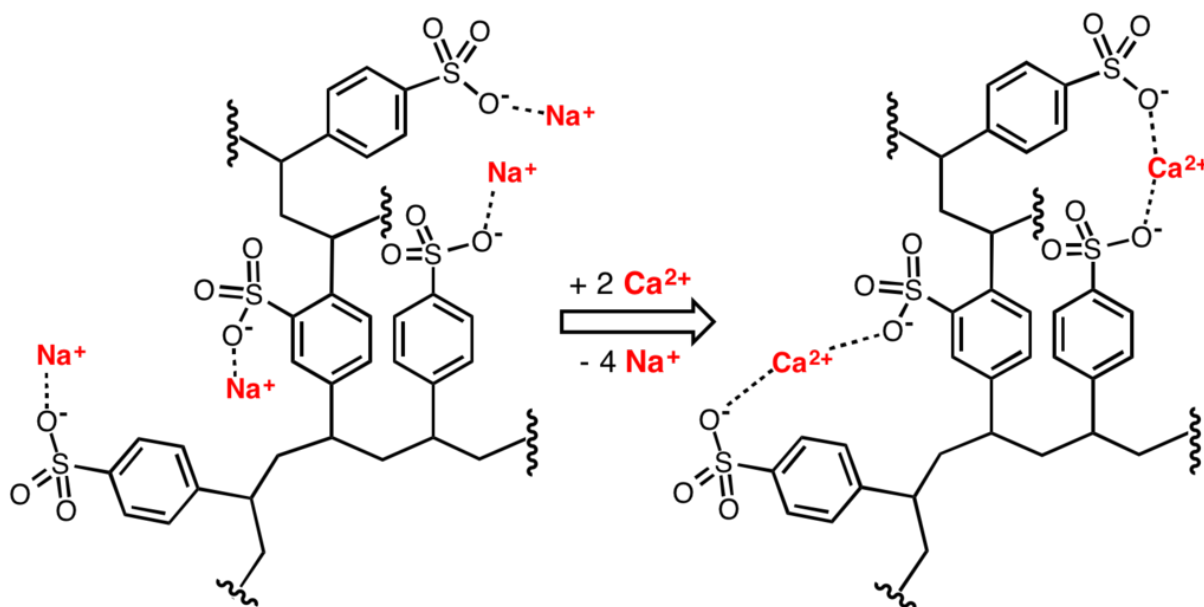


FIGURE 2.7: An ion exchange process involving polystyrene sulfonate. Two sodium ions are exchanged for a single calcium ion.[30]

## Chromatography

The dominant method to process a calcium chloride solution with ion exchange resin is chromatography. A resin is packed into long narrow columns and the solution is allowed to migrate along its length, gradually losing calcium to the resin it encounters. If there is some preference for the resin to adsorb lighter isotopes over heavier ones, the resulting flow should be enriched in  $^{48}Ca$ . There are a number of advantages to chromatography. Firstly, an actual production process would likely feature a fixed resin and a flowing solution, as is the case in chromatography. This does not require any tiny beads to be filtered from the solution later and does not cause any clogging or jamming due to the beads flowing wherever the solution carries them. Secondly, a chromatography column provides a compact cascade all by itself. Conventional cascades are based on multiple identical stages which receive and produce material in the same form. A chromatography experiment, on the other hand, receives a solution and produces both a solution and keeps material stuck in a resin. Thirdly, the method allows to determine which enrichment process dominates in an ion exchange enrichment experiment. One process is based on a kinetic effect and the other follows from equilibrium considerations. These two processes produce different results in a chromatography experiment. Cascade and enrichment effects are discussed more in-depth in the following paragraphs.

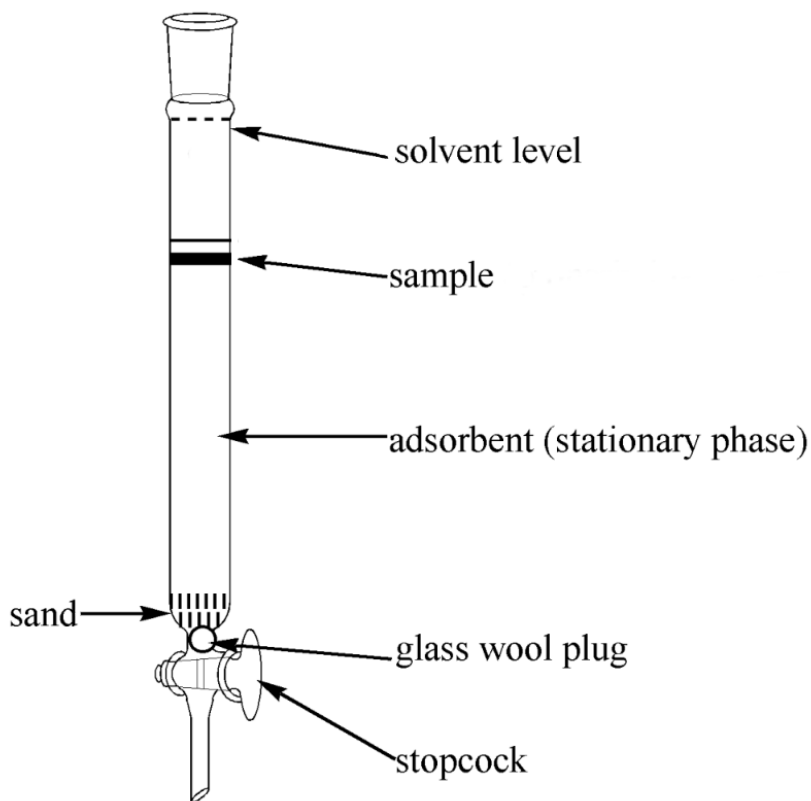
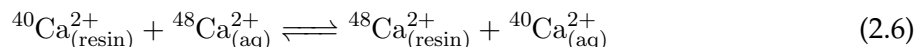


FIGURE 2.8: An example of a chromatography setup. A sample in the liquid phase seeps through the stationary phase, splitting into bands.[31]

A chromatography experiment theoretically provides an infinite number of infinitely small enrichment stages and links these up linearly. At every point in the column, ion adsorption groups select ions from the solution as they pass by, continuously enriching the fluid in heavy calcium. While such a continuous staging process may seem convenient, in practice it limits the enrichment process greatly. For example, there are no stripping stages and there is no looping mechanism. Anything that is adsorbed is as good as lost and cannot be reintroduced easily into the fluid to shed more of its  $^{48}\text{Ca}$ . This becomes especially wasteful at the very end of a chromatography stage where maximally enriched calcium is for a large part adsorbed. There is a way to regain the calcium from the column, but this involves flushing the column with a brine solution or strong acid and invariably mixes all the calcium that is contained within. Thus a chromatography stage would have to be started with an obscene amount of solution if anything of substance were to be produced.

Chromatography can help determine which of two enrichment processes provides the greatest contribution. In the kinetic effect, enrichment is owed to  $^{40}\text{Ca}$  having a higher reaction speed than  $^{48}\text{Ca}$  and therefore occupying the resin before the heavier isotope can. Chromatography would not be a suitable enrichment method if this were the case: the front boundary of the migrating solution would gradually be enriched in  $^{48}\text{Ca}$ , but a growing overabundance of the heavier isotope would allow  $^{48}\text{Ca}$  to be adsorbed in greater quantities as well, stalling enrichment. The solution directly behind the front boundary would only ever encounter occupied resin and would remain unchanged. The equilibrium effect, on the other hand, works by allowing  $^{40}\text{Ca}$  and  $^{48}\text{Ca}$  ions to swap places between resin and solution as shown in the following equation:



where the (resin) subscript indicates an ion that has been fixed to the crown ether resin. The

entire solution is thus able to participate in the reaction and the front boundary isn't simultaneously enriched and depleted of  $^{48}\text{Ca}$ .

Several ion exchange enrichment experiments have been performed in the past, all of them employing chromatography, but of two different kinds. Elution is the most common form of chromatography, being used for the analysis of fluids and providing a suitable method for a proof of concept. In it, a mixture of compounds is split into its components by forcing it through a stationary phase. This can be a porous solid or a liquid, depending on the sample and specific experiment goals. The sample is driven through this stationary phase by a mobile phase, or eluent, which is most often liquid or gaseous. The various components in the sample have slightly different attractions to the stationary phase and thus move through it at differing velocities. This causes the sample to split into bands of different species that can be detected by eye or by collecting fractions of the fluid at the end of the experiment and analysing them separately. Bands that move through the stationary phase naturally expand into Gaussian distributions and counteract the chromatographic separation. The separation between bands should thus be significantly larger than their widths, which is often the case for different chemical species present within a sample but not necessarily for different isotopes. Enrichment by chromatography is therefore always a struggle against band broadening effects.[32]

Displacement chromatography works by a slightly different principle. There still exists a stationary and mobile phase, but in this case the mobile phase does not flow through the stationary phase as straightforwardly as with elution chromatography. Instead, displacement chromatography depends on the fact that there is a limited number of binding sites on the stationary phase and that some components of the sample bind more strongly to it than others. After the sample is loaded into the column, a displacement fluid is injected that has an even higher affinity for the stationary phase than the sample. As it reaches the bound sample, it causes the sample components to be rejected from the binding sites and drives them forward. Something similar happens between sample components, where higher affinity constituents take the place of less strongly binding particles and push them forward. The result is a series of broad but pure bands that are in direct contact with each other. Unlike elution chromatography, this method is not hindered by broadening effects of bands: components moving ahead of their band encounter an environment in which they bind relatively easily and thus slow down significantly until their band arrives.[32]

## 2.8 Electrophoresis

Enrichment requires movement. In all of the enrichment schemes outlined so far, an element has been moved from one place to another, with certain isotopes taking a different route and splitting off from the bulk. Gaseous compounds are well-suited for this principle: they allow free movement of individual molecules with minimal mutual interaction. Diffusion is therefore relatively fast and allows for enrichment schemes such as gaseous and thermal diffusion, as well as centrifugal enrichment. In liquids and solutions, the higher density and greater viscosity stifle free movement greatly, diminishing the diffusion coefficient with a factor of  $10^4$  to  $10^5$  compared to the gaseous case [33][34]. Ions in solution thus need some encouragement before they start moving. Fortunately, they possess an electric charge and may be coerced into motion by an electric field. This process, called electrophoresis, is mostly used in a manner reminiscent of chromatography to identify larger molecules such as DNA. A sample is placed into a medium and a high voltage is applied that pulls it through the liquid. As can be seen in figure 2.9, mixed samples split up into their constituent parts according to properties such as size and charge, allowing for the identification of sample contents. A similar principle applies to the splitting of elements into their isotopes. Slight differences in mass and size could, over long distances, produce macroscopic separation and allow for significant enrichment.

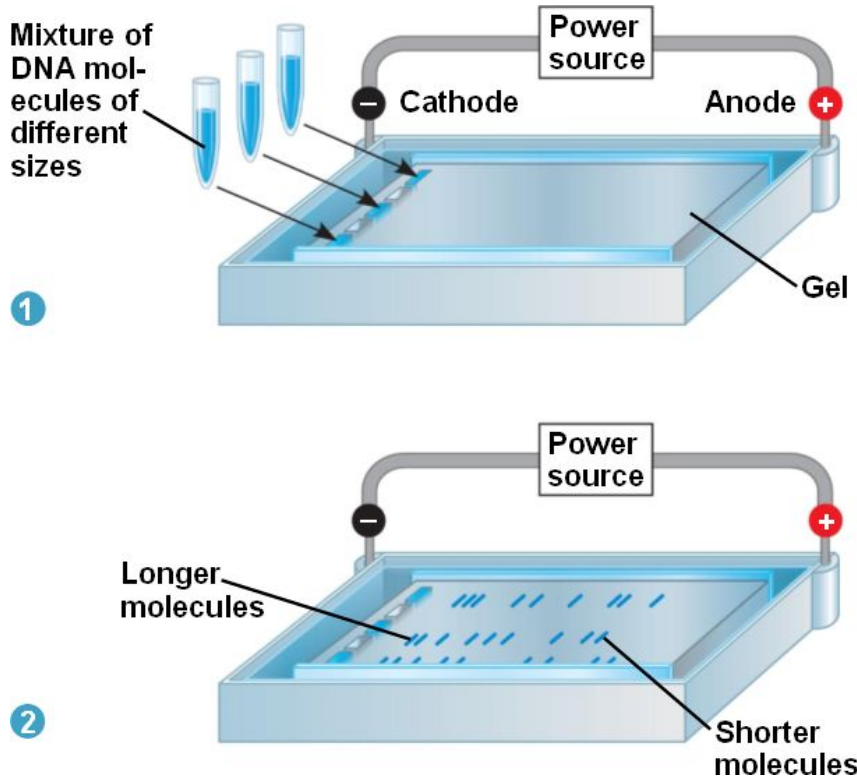


FIGURE 2.9: An example of electrophoresis. In the pictured experiment, DNA molecules of various lengths move through a gel, attracted by a positive electrode. Longer molecules experience more resistance and attain lower velocities than shorter molecules, thus splitting samples into their constituents.[35]

It has been theorised that elemental ions in solution rapidly jump from equilibrium position to equilibrium position with a frequency of  $10^{10}$  to  $10^{11}$  Hz and velocities of over 100 m/s [36]. This violent thermal motion is only very slightly influenced by an external electric field, effectively creating a drifting motion that is almost instantaneously proportional to the external field. Calcium isotopes have been shown to exhibit differing drift velocities in a solution under the influence of an electric field. This effect is, however, minute: it was determined that the mass dependence of the ions' diffusion coefficient in water can be described as  $D \propto m^{-\beta}$  where  $\beta = 0.0045 \pm 0.0005$  [37]. The Einstein relation links the diffusion coefficient to the electric mobility  $\mu_E = v/E$  so that the velocity ratio between isotopes in solution can be determined [38]:

$$\frac{v}{E} = \mu_E \xrightarrow{\text{Einstein rel.}} \frac{q}{k_B T} D \quad \Rightarrow \quad \frac{v_{40}}{v_{48}} = \frac{D_{40}}{D_{48}} = \left( \frac{m_{48}}{m_{40}} \right)^{0.0045} \approx 1.00082 \quad (2.7)$$

where  $E$  is the external electric field,  $q$  is the ionic charge,  $k_B$  is the Boltzmann constant and  $T$  is the temperature of the system.  $v_x$ ,  $D_x$  and  $m_x$  signify the velocity, diffusion coefficient and mass of a  ${}^x\text{Ca}^{2+}$  ion, respectively. It can be seen that the velocity difference between calcium isotopes is tiny in comparison to the one shown in equation 2.4 under gaseous diffusion. Additionally, the approximate induced velocity of a calcium ion is known to be 61.7 nm/s in a unit electric field (1 V/m) [36]. Even though the velocity increases linearly with the applied field, considerable fields are thus required to move ions along a macroscopic distance within an acceptable timeframe.

Because the difference between isotope drift velocities is so small, large distances have to be crossed before any separation becomes apparent. Equation 2.7 shows that, after a travel distance of ten metres, the isotope species would have moved less than a centimetre apart. Thermal diffusion and convection currents within the experiment, however small, would quickly

nullify any separative work that had been done. Moreover, the practical challenges of having to apply a strong constant electric field over such a long distance are daunting: even if the extremely high voltage could be safely contained to the solution, resistive heating within the liquid would quickly cause it to create convection currents and even boil. Therefore, other methods are in use to maximise the effective path length of the ions while keeping the experiment length to a minimum.

One such method is called **capillary electrophoresis**. It depends on one or more 20-200  $\mu\text{m}$  thin capillaries filled with solution. Multiple modes of capillary electrophoresis exist, many of which depend on electro-osmotic flow. In this method, the capillary walls are ionised by the solution within so that an electrical bilayer forms that can transport a liquid by the application of an electric field. An example of a capillary electrophoresis setup is shown in figure 2.10. One advantage of capillary electrophoresis methods is that heat dissipation is made easy, allowing for much higher electric fields to be built up before resistive heating causes the solution to pass its boiling point. The obvious disadvantage of using a capillary with a 20-200  $\mu\text{m}$  diameter is that the production throughput is abysmal. A large number of the tubes would be required for mass-production, compounding any clogging and contamination problems greatly.[39]

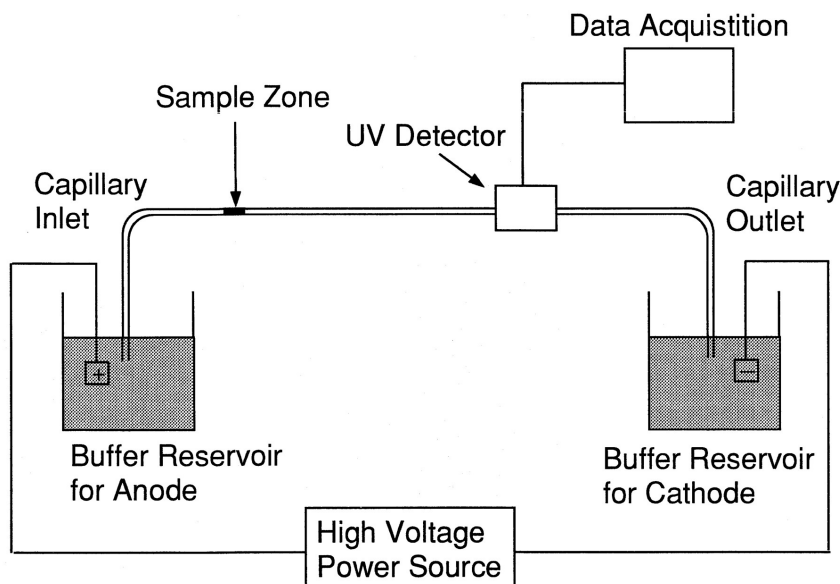


FIGURE 2.10: An overview of a capillary electrophoresis experiment. The sample is driven from a positive to a negative electrode through a thin capillary.[40]

A different method of electrophoresis that does not suffer these problems is called **counter-current electrophoresis** and is able to process relatively large volumes at once. Its design depends on a combination of an electrophoretic flow and a regular flow induced by a pump. These flows are set to be opposed and equal so that the ions that are to be separated stay within the electric field at all times. This allows a compact experiment to simulate an arbitrarily large path length as long as it is given enough time. Heating still limits the electric field that can be applied, but the constant introduction of new solvent alleviates the problem somewhat. In contrast to the other electrophoresis schemes discussed so far, this method has the added advantage of being able to produce an enriched output flow that is continuous. By adjusting the two flows such that the electric field is just strong enough to pull the fast isotopes upstream but not strong enough to keep the slower ones from flowing downstream, two distinct flows can be isolated to be used in a cascade formation. Figure 2.11 shows an example of a counter-current electrophoresis example. Thanks to the configuration of the electrodes, positively charged ions are predominantly pulled downward toward output D. The liquid current flowing from A to B can be tuned such that the flow velocity is smaller than the  $^{40}\text{Ca}$  electromigration but larger

than that of  $^{48}\text{Ca}$ , causing enrichment in output B and depletion in D.

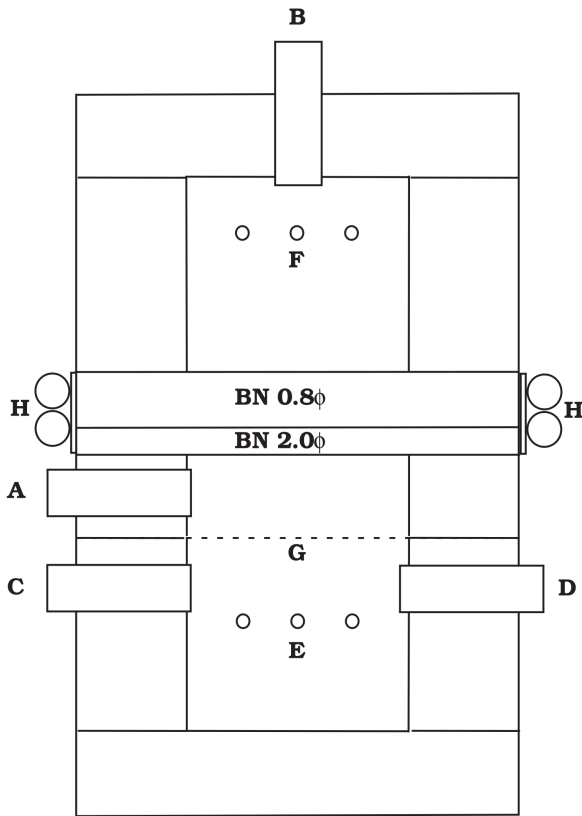


FIGURE 2.11: A counter-current electrophoresis experiment. Calcium solution is fed into A and a solution of HCl is pumped into C. B and D are outputs. G is an ion exchange membrane and only allows the passage of ions. F and E are electrodes that possess a positive and negative charge, respectively. Lastly, H has to do with the experiment thermostat and does not participate in the experiment's basic function.[41]

Three classes of experiment have been performed during the course of this project to explore the possibilities of calcium enrichment. The first is based on crystallisation and depends on calcium isotopes having a different tendency to stay in solution. The second works with a difference between isotopes to be adsorbed and held within an ion exchange resin. Finally, the third method relies on isotopes having differing drift velocities through solution under the influence of an electric field. The following sections give a brief overview of these methods' working principles and their general operations within the project.



# Chapter 3

## Mineralisation

Although history has seen large efforts to effect isotope separation, nature causes small enrichments by itself: through mostly unknown mechanisms, the concentration of certain isotopes varies depending on the source. Studies have been performed on small shelled seacreatures such as *foraminifera* to examine isotope fractionation effects in biomineralisation. The inorganic mineralisation of aragonite, a common  $\text{CaCO}_3$  crystal, was also studied. It was found that the isotope fractionation in these is highly temperature-dependent and attained values up to  $\delta^{44}\text{Ca} = -3.53\text{\textperthousand}$  and  $-2.18\text{\textperthousand}$  in the sea creatures and calcium carbonate deposits, respectively [42][43]. Experiments on mammalian samples found differences even between different tissues of individual animals: the bones and soft tissue of an animal can vary up to  $1.5\text{\textperthousand}$  in  $^{44}\text{Ca}$  concentration. In one specific study, the total range of isotopic deviation was found to be  $5\text{\textperthousand}$ , with the largest deviation from the standard being  $\delta^{44}\text{Ca} = -3.14 \pm 0.16\text{\textperthousand}$  in cougar bone.[44]

The numbers associated with enrichment through mineralisation are promising, especially considering that they concern  $^{44}\text{Ca}$ . It is expected that  $^{48}\text{Ca}$  is separated equally if not more, but mass effects are difficult to predict in this case because complex biological processes are involved. Growing a cougar bone is more time costly than most enrichment methods that have been considered so far, however, and applying multiple stages to this process would be somewhat unethical, not to mention highly inefficient. Needless to say, the precipitation of aragonite is much better suited for mass production, despite its slightly lower enrichment factor. One advantage of enrichment by precipitation is that calcium carbonate is already largely processed by this method. Existing infrastructure designed for high product output may thus be used, decreasing the cost of the enrichment process. One caveat to this is that enrichment was found in a slightly different reaction than is mostly employed in  $\text{CaCO}_3$  production. The performed experiment mixes solutions of  $\text{CaCl}_2$  and  $\text{NaHCO}_3$  to precipitate calcium, while industrial processes force carbon dioxide through slaked lime in the following process:

$$\text{Ca(OH)}_2 + \text{CO}_2 \longrightarrow \text{CaCO}_3 + \text{H}_2\text{O}.\text{[45]}$$

Instead of precipitating the calcium from solution by adding another chemical, the calcium may be made to mineralise by itself. The solubility of calcium chloride in water is quite high, but there are two methods to extract it from solution. The first is to cool a saturated liquid down: a decrease in temperature generally decreases the solubilities of salts and thus the previously dissolved material is not able to stay in solution entirely. The second is to heat a saturated solution and evaporate a portion of the solvent. Without enough liquid to dissolve in, the solute mineralises into a solid form. The latter method is already used industrially: calcium chloride is prepared by evaporating the water from the solution and scraping the result into flakes. Rejected flakes and powder are redissolved to increase efficiency, demonstrating the ability of a common production method to send material back to an earlier stage. As explained in section 2.5, this is a convenient feature to have in an enrichment cascade as well.

### 3.1 Experiment

The source of calcium for this experiment was a commercial air dehumidifier refill pack. This consisted almost entirely of calcium chloride flakes hydrated to an unknown degree ( $\text{CaCl}_2 \cdot x\text{H}_2\text{O}$ )

and contained further unknown insoluble material. It is expected that a small fraction of the calcium chloride had undergone a reaction with carbon dioxide in the air to form calcium carbonate ( $\text{CaCl}_2 + \text{CO}_2 + \text{H}_2\text{O} \rightarrow \text{CaCO}_3 + 2\text{HCl}$ ) which is nigh insoluble compared to calcium chloride and causes a white tinge in suspension. Demineralised water was used with measured impurity concentrations of  $1 \pm 1$  ppm (parts per million, here defined as mg/L). A small heating plate and stirring magnet combination was used, as well as a scale with a precision of 0.05 g and a graduated cylinder with a precision of 0.1 mL. The low purity materials and low precision instruments were not expected to hinder a potential enrichment process significantly, since irregularites were expected to affect all calcium isotopes equally. Ultimately, only a ratio between isotopes is relevant, rendering any inaccurate measurements unimportant. Samples of processed calcium chloride solution were analysed by an inductively coupled plasma mass spectrometer (ICP-MS). Unfortunately, this spectrometer was unable to measure  $^{40}\text{Ca}$  because it uses  $^{40}\text{Ar}$  to induce a plasma. All other isotopes of calcium were measured, however, and any mass effect that would be visible in the  $^{48}\text{Ca}/^{40}\text{Ca}$  ratio was expected to also change  $^{48}\text{Ca}/^{44}\text{Ca}$  and  $^{48}\text{Ca}/^{43}\text{Ca}$ .



FIGURE 3.1: A photograph of a saturated calcium chloride solution that was cooled. The stirring magnet is visible inside the solidified ‘ice’.

The general idea of these experiments was to induce calcium chloride mineralisation by oversaturating a solution. The first way in which this was attempted was by creating a saturated solution at a temperature of 170° C and letting the solution cool to room temperature in order to cause the growth of minerals. The expected path of the solution in the concentration-temperature phase diagram is shown in figure 3.2. The plan was to split the mineralised material from the leftover solution by decantation and filtration. However, two factors made this impossible. Firstly, the solution did not follow the expected path by slowly expelling calcium chloride: it solidified almost instantaneously in its entirety once its temperature dipped below the point where oversaturation occurs. Crystal planes quickly grew in all directions and turned the liquid into an opaque white solid that resembled water ice in structure. This is shown in figure 3.1. When left standing for a few hours, a layer of water collected on top that would have eventually dissolved the ‘ice’ if given enough time. It is here that the second problem lies: calcium chloride is hygroscopic, meaning that it attracts water from the air, and deliquescent, meaning that it attracts enough water from the air to completely dissolve itself. Slow filtration in which a wet powder is left in a filter overnight does thus not work under normal circumstances. The filtered solid calcium chloride would attract moisture from the air, dissolve and pass through the filter. This can be demonstrated by leaving a flake of calcium chloride out of its container overnight: by morning it will have turned into a drop of saturated water.

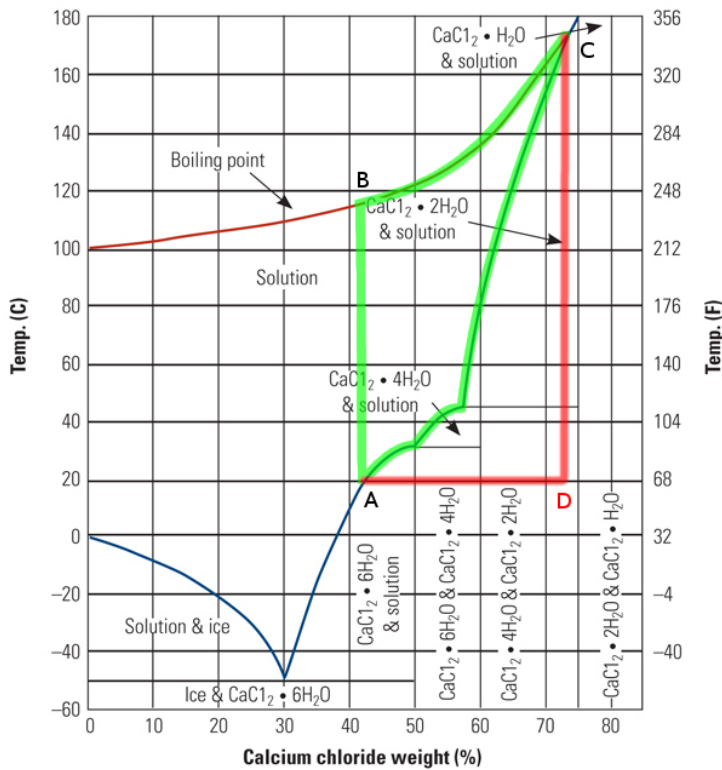


FIGURE 3.2: The concentration-temperature phase diagram of calcium chloride solution. Two paths are pictured, both going clockwise: the expected path in green (ABCA) and the actual path in green/red (ABCDA). Furthermore, the solid black curves in the graph signify the boiling and freezing points of the solution. The partial path AB signifies simple heating of the solution. During BC, the solution is heated while water is boiled off. From C to A, the solution cools, staying liquid and depositing solid calcium chloride crystals. CD signifies the solidification of the entire solution as it cools down to room temperature. In DA, the solid calcium chloride attracts water from the air and eventually dissolves again completely.[46]

Evaporation of water from a CaCl<sub>2</sub> solution is another process in which calcium chloride mineralises. A solution was stirred and heated so that it boiled lightly, removing water at a constant rate. Once saturation was reached, a calcium chloride skin formed on the surface of the solution and thickened into a crumbly white layer, shown in figure 3.3. This layer was skimmed off repeatedly and was weighed on the scale until a certain fraction of the initial calcium chloride had been extracted from the solution. Afterwards, the skimmed material was dissolved and the process was repeated, again removing a certain fraction before moving on to the next stage. When eventually the amount of calcium chloride was in danger of becoming too small to work with, the material was dissolved and analysed using an ICP-MS. Samples were also periodically taken during different stages of the experiment so that the results could be placed into context. Although the end goal of the project is to find a way to enrich calcium in the <sup>48</sup>Ca isotope, this experiment was more likely to deplete the final sample of heavier isotopes. It was shown in earlier experiments that precipitated aragonite contains less <sup>44</sup>Ca and more <sup>40</sup>Ca than the original solution. This isotope fractionation effect was also shown to be highly dependent on temperature, with lower temperatures (< 30° C) being required for enrichment [42]. Unfortunately, boiling occurs at much higher temperatures: as can be seen in figure 3.2, a saturated calcium chloride solution can attain temperatures of up to 170° C before starting to boil.



FIGURE 3.3: A photograph of solid calcium chloride produced by evaporating water from a solution.

## 3.2 Results

The results of the first mass spectrometry experiment are shown in table 3.1. As can be seen from this table, the sample set included only an intermediate and a final sample. Because this experiment was one of the first to be analysed and because the ratio between calcium isotopes tends to vary in nature, the demineralised water and some unprocessed calcium chloride were analysed as well. For this purpose, a stock solution was made by dissolving calcium chloride flakes in demineralised water. The intermediate sample was obtained by first skimming off some  $\text{CaCl}_2$  from the boiling stock solution, dissolving that in water and again skimming off some calcium chloride. The leftover solution was then analysed as the intermediate sample. Once more the skimming procedure was repeated, for a total of three times, and the product was analysed as well. No quick method of testing TDS values was available at the time of creation of these samples, and they were diluted by a factor of ten to avoid clogging the spectrometer. This was done with distilled water: water that has not only been demineralised, but has also had all biological contaminants removed. It is unlikely that this has influenced the results significantly.

TABLE 3.1: The mass spectrometry values obtained from the first mineralisation experiment. ppb values were scaled to naturally occurring isotopic ratios so that simple division directly yields an enrichment factor.

Sample	$^{43}\text{Ca (ppb)}_{\text{std}}$	$^{44}\text{Ca (ppb)}_{\text{std}}$	$^{46}\text{Ca (ppb)}_{\text{std}}$	$^{48}\text{Ca (ppb)}_{\text{std}}$
Water	28(10)	30(10)	-31(6) $\cdot 10^2$	17(12)
Stock $\text{CaCl}_2$	1616(12) $\cdot 10$	1623(14) $\cdot 10$	136(6) $\cdot 10^2$	1581(12) $\cdot 10$
Intermediate	633(3) $\cdot 10$	643(5) $\cdot 10$	38(4) $\cdot 10^2$	615(4) $\cdot 10$
Product	716(4) $\cdot 10$	726(4) $\cdot 10$	49(4) $\cdot 10^2$	697(4) $\cdot 10$

**Notation of errors.** Values that were obtained experimentally have their errors denoted by parentheses where space is short. This is especially useful where errors are several orders of magnitude from unity. For example,  $0.3456 \pm 0.0005$  becomes 0.3456(5) and  $5630 \cdot 10^5 \pm 12 \cdot 10^5$  becomes 5630(12) ·  $10^5$ .

From table 3.2, it can be seen that the stock solution does not have an enrichment factor of 1, as would ideally be the case. The enrichment factors were normalised to the stock solution in order to determine the effect of the experiment.

TABLE 3.2: Enrichment factors as calculated from the data in table 3.1.

Sample	$^{48}\text{Ca}/^{43}\text{Ca}$	$^{48}\text{Ca}/^{44}\text{Ca}$	$(^{48}\text{Ca}/^{43}\text{Ca})_{\text{norm.}}$	$(^{48}\text{Ca}/^{44}\text{Ca})_{\text{norm.}}$
Water	0.4(4)	0.3(3)	0.4(4)	0.3(3)
Stock $\text{CaCl}_2$	0.978(10)	0.974(11)	1.000(12)	1.000(16)
Intermediate	0.972(8)	0.956(9)	0.994(13)	0.982(14)
Product	0.973(7)	0.960(7)	0.995(13)	0.986(13)

A second experiment was performed with more stages and more recorded steps. If the stock solution is considered the 0th stage, its waste during an enrichment process can be considered the -1st stage. This waste was analysed, as well as two intermediate steps at stages two and three and the final product after stage five. The data is plotted in figure 3.4 and direct mass spectrometry measurements can be found in appendix A.

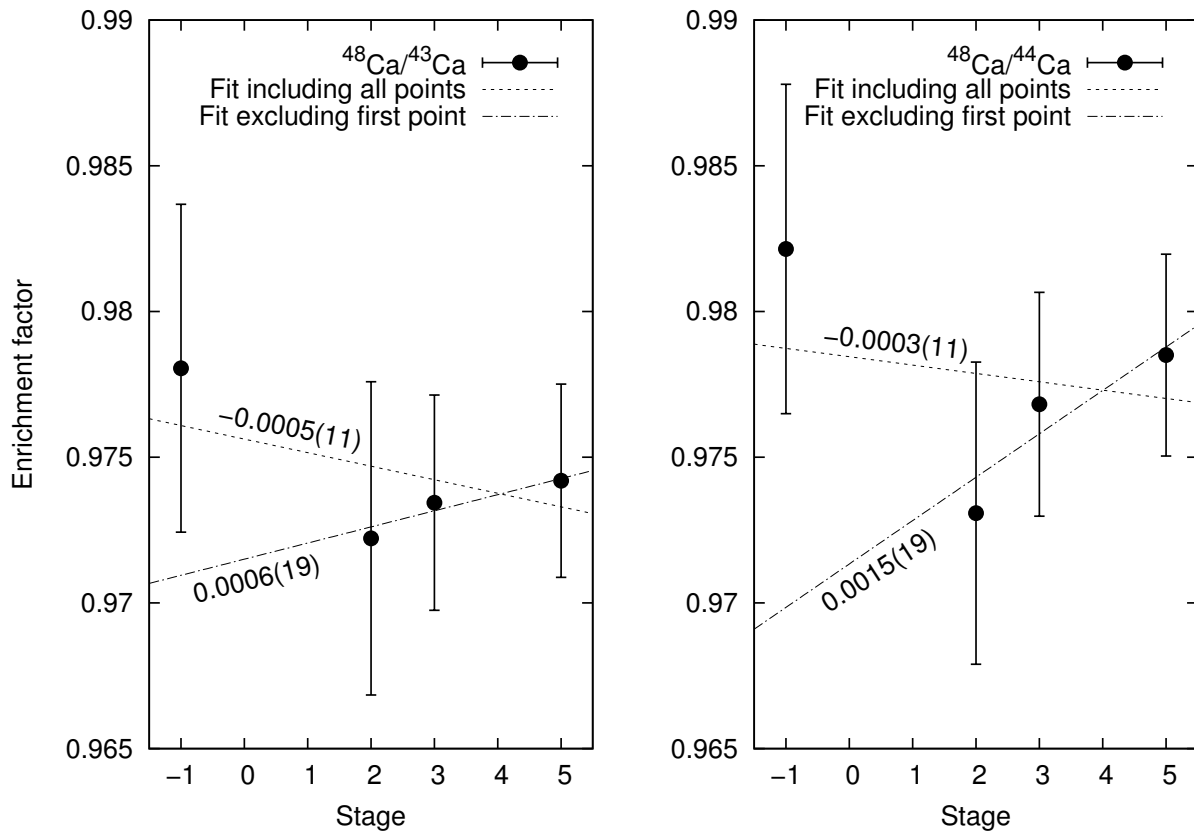


FIGURE 3.4: Enrichment factors of the second mineralisation experiment. The slope coefficients of all fits are given within the graph.

### 3.3 Discussion

The results of the first mineralisation experiment documented in table 3.1 show a few interesting features. Firstly, the stock  $\text{CaCl}_2$  appears to possess significantly different isotope ratios from the standard solution employed to calibrate the mass spectrometer. Whereas the calcium chloride used in the current experiments came from a humidifier refill pack in the form of industrially produced flakes, the ICP-MS uses a solution with precisely defined isotope ratios

that was specifically produced for the calibration of mass spectrometers. It is not surprising that calcium chloride originating from such different sources shows a difference in isotopic ratios. After all, calcium chloride shows large variation in nature, as discussed in section 3.

Secondly, it can be seen that the isotope ratios of the intermediate and final solutions match the initial solution quite closely. Even though there seems to be an overall depletion of  $^{48}\text{Ca}$ , it is important to keep the source of the intermediate sample in mind. As described in section 3.2, the stock solution was boiled and mineralised calcium chloride was skimmed off. This material was then dissolved and heated once again. The leftover solution after skimming off material was the source of the intermediate sample. It should thus possess an enrichment factor close to that of the stock solution, but with error margins this large it is impossible to make hard conclusions concerning the validity of that statement.

Lastly, the ratio  $^{48}\text{Ca}/^{44}\text{Ca}$  seems to have undergone a larger change than  $^{48}\text{Ca}/^{43}\text{Ca}$ . In the context of mass-dependent processes, this is a strange phenomenon. It would be expected that mass-dependent effects have the same sign independent of mass. For example, if  $^{44}\text{Ca}$  were to mineralise in greater concentrations than  $^{40}\text{Ca}$ , it is expected that  $^{48}\text{Ca}$  would mineralise in even larger concentrations. This does not seem to be the case for  $^{43}\text{Ca}$  and  $^{44}\text{Ca}$ , and there are two obvious factors that could be the cause. For one, calcium consists for 2.1% of  $^{44}\text{Ca}$  and just for 0.14% of  $^{43}\text{Ca}$ . This large difference in isotopic abundance may have influenced the experiment sufficiently to cause a slight deviation in the  $^{48}\text{Ca}/^{43}\text{Ca}$  ratio, although it is not known exactly how. Another possible explanation stems from the spin of the atomic nuclei.  $^{43}\text{Ca}$  has a nuclear spin of -7/2 whereas  $^{40}\text{Ca}$ ,  $^{44}\text{Ca}$  and  $^{48}\text{Ca}$  all possess a spin of 0. As was explained in section 2, the electrons of an atom determine its chemical properties almost exclusively. However, the nucleus exerts a small amount of influence in the form of its spin. Once again, the exact mechanism by which  $^{43}\text{Ca}$  acts differently from other calcium species is unknown.

The data from the second mineralisation experiment is plotted in figure 3.4, along with two kinds of linear fits: one fit including all points and one fit excluding the first point. One reason for excluding the first point is that it seems to be an outlier in regard to the slope coefficient of the fits. Fits including the outlier are completely unconvincing in their general appearance and have a sign that is opposite to the more intuitive fits that exclude the first point. These strange qualities are reflected in the physics of the experiment. When one stage of the enrichment process is performed, approximately half of the calcium chloride is extracted from a boiling solution. If one half, for example the skimmed off half, turns out to be enriched in  $^{48}\text{Ca}$ , it is only logical that the portion of calcium chloride left in solution is depleted in that same isotope. Especially considering the low enrichment attained at each stage, this forms another reason to exclude the first point: it does not make sense from a physical point of view.

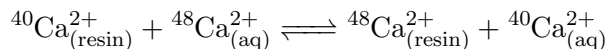
Aside from this, there are a few more points to make about the data, most of which correspond to the results of the first experiment. Firstly, none of the samples reached an enrichment close to 1 because the ICP-MS calibration solution has a significantly differing isotope ratio from the calcium chloride flakes used in the experiment. Unfortunately, no stock solution was analysed and thus normalisation is impossible. It can be seen that the stock isotope ratios of the first experiment fit the data of the second experiment reasonably well, but this data was collected in a different run of analyses and with a completely different calibration. Inserting such a datapoint into the set of the second experiment would thus not be truthful, especially considering the large errors already present within the data.

Secondly, and similarly to the first experiment, whatever effect causes some isotopes to mineralise more than others is not purely dependent on mass, as can be seen from the slope coefficients of the fits excluding the first points.  $^{48}\text{Ca}/^{44}\text{Ca}$  attains higher values at a steeper rate than its  $^{48}\text{Ca}/^{43}\text{Ca}$  counterpart. Even the possibly erroneous first point lies much higher. Once again, it is unknown whether this is because of differing abundances of isotopes or because spin effects have come into play.

## Chapter 4

# Ion exchange resins

In a recent experiment using chromatography, an isotopic effect was demonstrated. Long columns were packed with crown ether resin consisting of silica beads with embedded crown ether. A calcium chloride solution was then passed through the columns and the resulting fluid was collected by parts at the end of the experiment. It was found that the lighter  $^{40}\text{Ca}$  has a slight preference over  $^{48}\text{Ca}$  to be adsorbed into a crown ether resin. Two hypotheses were given to explain this. The first is a kinetic effect wherein the lighter isotope has a slightly higher reaction speed and occupies the crown ether binding sites before other isotopes can. The second hypothesis is based on an equilibrium effect which causes a leftward skew in equation 2.6, repeated here for convenience. The latter hypothesis was found to be the correct one: the equilibrium effect caused the  $^{48}\text{Ca}/^{40}\text{Ca}$  ratio to increase from its natural value of 0.00194 to 0.002595. An enrichment factor of 1.338.[47]



The experiment has demonstrated a promising enrichment method. It can be performed at room temperature and requires no high pressure pumps, ultracentrifuges or extreme temperature gradients. A solution of cheap calcium chloride may be pumped through crown ether resin or into the top of a column so that it flows down by gravity. The enrichment factor of a single metre column is quite small: a  $^{48}\text{Ca}/^{40}\text{Ca}$  fraction of 0.002039 was observed, signifying an enrichment factor of only 1.051. Still, through the proper enrichment cascade, many columns could work towards the mass production of a solution highly enriched in  $^{48}\text{Ca}$ . Indeed, the experiment above used a 200 metre column setup, which was essentially 200 one metre columns in series. One peculiarity about the enrichment method sets it apart from most others: depleted calcium is adsorbed into solid resin and needs to be flushed out before the resin can be used again. The waste is thus extracted separately from the product, making it impossible to run a continuous operation. Additionally, crown ether is quite expensive to synthesise and embed into a useful resin. Fortunately, the calcium can be washed out of the crown ether using HCl so that the resin may be reused. Research into cheaper synthesis of crown ether is underway. The method is also quite slow: the reported speed of the calcium boundary is approximately 20 m/day, costing a total of ten days to reach the aforementioned enrichment factor of 1.338 after 200 metres. The slow production that results from this may be alleviated by simply using broader or more columns at the cost of extra crown ether.[47]

Roughly the same group of researchers more recently performed a follow-up experiment. Using the same benzo-18-crown-6-ether resin, this time they opted for a concentrated acetic acid solution as the eluent. It was found that the adsorption of calcium ions into the crown ether resin is highly enhanced as the concentration of acetic acid is elevated. Although no definite explanation seems to be known at this time, it has been theorised that the acid forms an environment that is similar to the crown ether, both compounds being organic in nature. The theory given in section 2.7 supports this: without a strongly bound hydration shell, the ions are much more easily adsorbed into resins. After letting the calcium acetate solution pass through a metre-long column packed with resin, the exiting fluid was captured and analysed in parts. Again, it was found that  $^{48}\text{Ca}$  was enriched in the front boundary of the calcium ion

band. With  $\delta^{48}\text{Ca} = 4.6 \pm 0.9\text{\textperthousand}$ , calcium acetate was advertised as a much better choice for the enrichment of calcium than the previous experiment, which used HCl. However, the errors on both values are significant and the acetic acid poses some additional problems. The distinction between the two methods is thus not so clear-cut.[27]

## 4.1 Experiment

The materials used in ion exchange resin experiments were more or less the same as in the previously discussed methods. Commercial dehumidifier refill packs were used as the source of calcium chloride and demineralised water served as the solvent. In one of the experiments, a Fourier transform infrared (FTIR) spectrometer was used, whereas the others utilised the ICP-MS as before. Ion exchange resin was obtained as a refill pack for coffee-machines where it is thought to serve as a water softening agent. The resin consists of porous polystyrene beads with sulfonate groups occupied by placeholder sodium atoms. As explained in section 2.7, calcium ions have a greater tendency to fix to the ion exchange resin than sodium and are thus taken from solution. Meanwhile, sodium ions are released into the solvent, making the water slightly salty and leaving the total dissolved solids (TDS) value unchanged.

A batch process is somewhat simpler in setup than a chromatography experiment. In order to attain maximum enrichment in such an experiment, as much calcium needs to be removed from solution as possible. The experiment is therefore a sensitive balancing act. The capacity of the resin needed to be known and was roughly determined by titration using EDTA (ethylene-diaminetetraacetic acid). A pH between 11 and 12 is necessary for the EDTA to lose some of its hydrogen so that it may receive calcium ions. This was realised by adding a small amount of a sodium hydroxide solution. The indicator used was murexide, which forms a pinkish solution when it forms complexes with calcium ions and turns to bright blue when these ions are removed. Minute quantities of the indicator are needed, and thus it was used in a highly diluted form of a mixture with potassium sulfate. The exact quantities are not relevant since the amount of added indicator is not expected to influence the final result of the measurement. Nevertheless, care should be taken to make sure that the colour is visible enough for the colour change to be noticeable when it occurs. Additionally, adding an excessive amount of indicator would cause the solution to turn partially blue just because there are not enough ions for all the murexide to form complexes. Lastly, the indicator seems to slowly lose its colour and is noticeably more faded after as little time as half an hour. There is no indication, however, that the colour change from pink to blue is time-dependent.

After the capacity of the ion exchange resin was determined, an appropriate amount of calcium chloride was weighed and dissolved, and such a quantity of ion exchange resin was added that it left a small fraction of calcium chloride in solution. The resin beads were added slowly, at approximately 20 beads/s, while the solution was stirred vigorously. This way, the beads were each introduced to a freshly mixed part of the solution, increasing their adsorbing efficiency of  $^{40}\text{Ca}$ . Because of the nature of ion exchange reactions, the TDS was unchanged after ion exchange and the solution consisted primarily of dissolved NaCl at this point. The ICP-MS used for the final analysis is particularly sensitive to high TDS and the solutions needed to be diluted until their concentration was below 0.2% by mass, or approximately 2 g/L. A large amount of NaCl relative to  $\text{CaCl}_2$  thus decreases the total possible  $\text{CaCl}_2$  that can be analysed, greatly decreasing the accuracy of the measurement. Samples were made by extracting one to two drops of solution and diluting those until a TDS value of 50-150 was reached. The diluting process produced more than enough volume for multiple duplicates of the same sample. All duplicates of all samples were then delivered to the ICP-MS out of order, so that any bias developed during the course of measurement would be detected.

## FTIR spectroscopy

In another class of experiments, the ion exchange resin beads were themselves examined in a FTIR spectrometer. The idea of this experiment was to examine the difference between  $^{40}\text{Ca}$  and  $^{48}\text{Ca}$  in terms of bond strength to the sulfonate groups on the ion exchange resin. In the simplest mechanical model, an atom bound to a molecule vibrates according to a harmonic potential. The frequency of this vibration can then be described as follows:

$$\nu \sim \sqrt{\frac{k}{\mu}} \quad \text{where} \quad \mu = \left( \frac{1}{m_1} + \frac{1}{m_2} \right)^{-1} = \frac{m_1 m_2}{m_1 + m_2} \quad (4.1)$$

Here,  $\nu$  is the frequency of the vibration,  $k$  the force constant of the binding and  $\mu$  the reduced mass of the system. The latter is dictated by  $m_1$  and  $m_2$ , which are the mass of the atom in question and the mass of the rest of the molecule, respectively. A number of unreasonable assumptions have been made by applying this model to a calcium-loaded ion exchange resin. Firstly, the vibration only approximates harmonic oscillation for small amplitudes, as shown in figure 4.1. More accurate atomic potentials exist, but complicate the mathematics to an unreasonable degree for a qualitative investigation such as this. Secondly, whereas  $m_1$  is very well-described as a point-mass,  $m_2$  pertains to the rest of the participating molecule and could range from just two oxygen atoms to two sulfonate groups to a section of polystyrene. This mass is not rigid, nor is it a point mass, nor is it necessarily the same for all calcium atoms. In the assumption that  $m_2 \gg m_1$ , however, the reduced mass becomes  $m_1$ . Thirdly, and similarly to the previous point,  $k$  is not just the force constant between a calcium atom and the oxygen atoms it is bound to. It is a complex combination of force constants throughout the sulfonate groups and the rest of the polystyrene. Again, it is not necessarily identical for all calcium ions, but it is expected that an average effective force constant exists and that most calcium ions will experience a force constant very close to it.

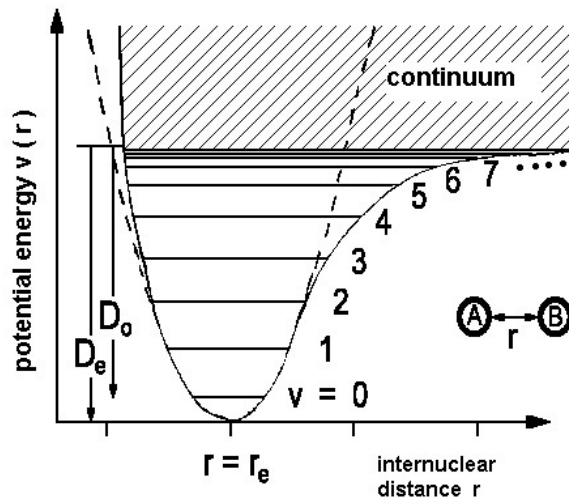


FIGURE 4.1: Potential energy of a diatomic molecule as a function of internuclear distance. The potential well is shown as a solid curve and features the lowest few vibrational modes, as well as the continuum. The harmonic approximation to the potential well is shown as a dashed line without vibrational modes.[48]

A small sample of resin was placed into a strong  $\text{CaCl}_2$  solution which was then stirred for over an hour to make sure that all sulfonate groups in the resin had been occupied by calcium ions. After decantation and washing of the resin with demineralised water, the beads were dried at a temperature around  $100^\circ\text{C}$  until all water had been evaporated. The beads were then crushed thoroughly using a mortar and pestle and mixed with a KBr powder. The

spectrometer produces a spectrum of light within a certain range and records the transmission of this light through a sample. KBr has the convenient property of being transparent to infrared light and thus makes for an excellent sample matrix. The ratio between resin powder and KBr is mostly a matter of experience: too much resin and the mixture becomes opaque to the infrared radiation, while too little will not produce a clear absorption spectrum. After the two powders were thoroughly mixed, the mixture was placed within a hand-press and clamped until a glass-like window had formed. This window was half a centimetre in diameter, very fragile and sensitive to moisture. Its holder is pictured in figure 4.2. After the window was placed in the spectrometer, the machine was placed under a soft vacuum and spectra were produced.

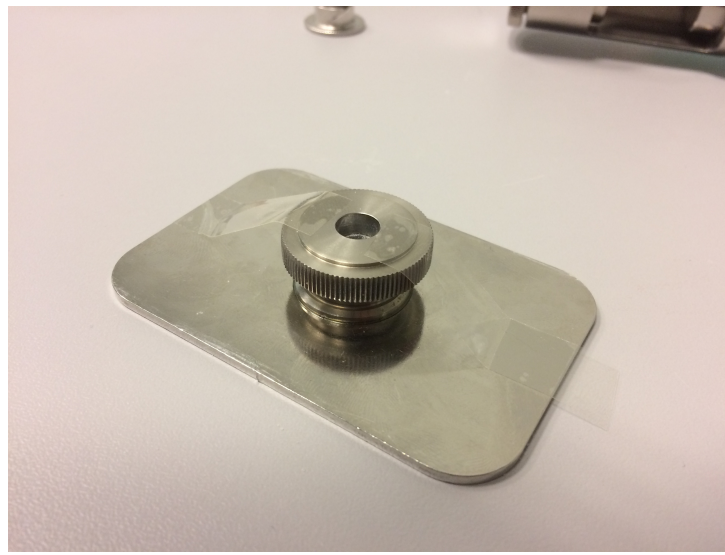


FIGURE 4.2: The arrangement by which the produced KBr window was held in place. The round disk on top holds the small window in its centre, and is in turn held in place with scotch tape on a plate that is slid into the spectrometer.

## 4.2 Results

The first ion exchange experiment consisted of a simple and purely qualitative test where it was investigated whether ion exchange showed any isotopic preference at all. 1.90(5) g of ion exchange resin was added to a solution containing 1.00(5) g of calcium chloride to remove what was thought to be approximately 95% of the calcium ions. Two of these experiments were performed to yield the final ratios shown in table 4.1. The full dataset is given in appendix B.

TABLE 4.1: Ion exchange enrichment factors as calculated from mass spectrometry data.

Experiment	$^{48}\text{Ca}/^{43}\text{Ca}$	$^{48}\text{Ca}/^{44}\text{Ca}$
1	1.025(15)	1.038(16)
2	1.01(5)	1.01(5)

In the second experiment using ion exchange resin, the ion exchange beads were added slowly and samples were taken regularly. Also, an unprocessed calcium chloride sample was submitted for normalisation. Figure 4.3 shows the progress of the enrichment factor throughout the experiment.

The third experiment attempted the same as the second, this time with more added resin. The results are plotted in figure 4.4. All direct mass spectrometry data can be found in appendix B, in the format specified in section 3.3.

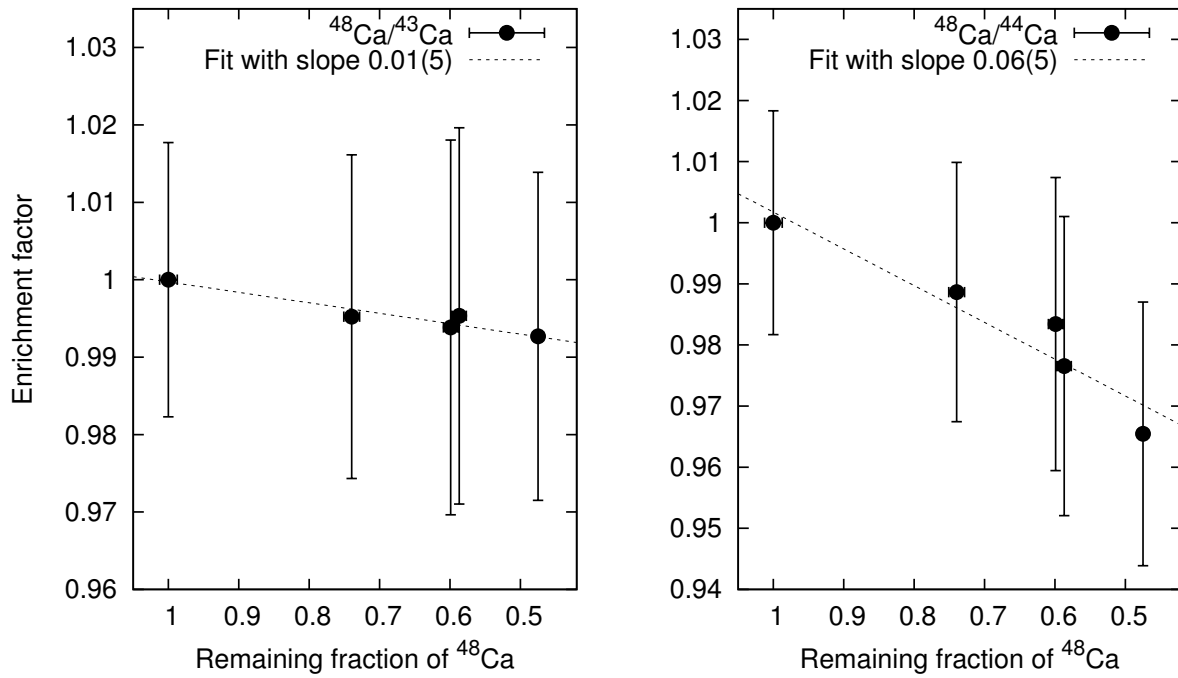


FIGURE 4.3: Enrichment factors of the second ion exchange experiment. Fits are presented with their slope coefficients.

From the mass spectrometry experiments, an approximate adsorption capacity of the ion exchange resin can be reduced. This is shown graphically by plotting the remaining  $^{48}\text{Ca}$  fraction against the relative amount of resin, depicted in figure 4.5.

A few ion exchange resin bead samples were dried and crushed according to the method described above, and then analysed via FTIR spectroscopy. The relevant data range is shown in figure 4.6.

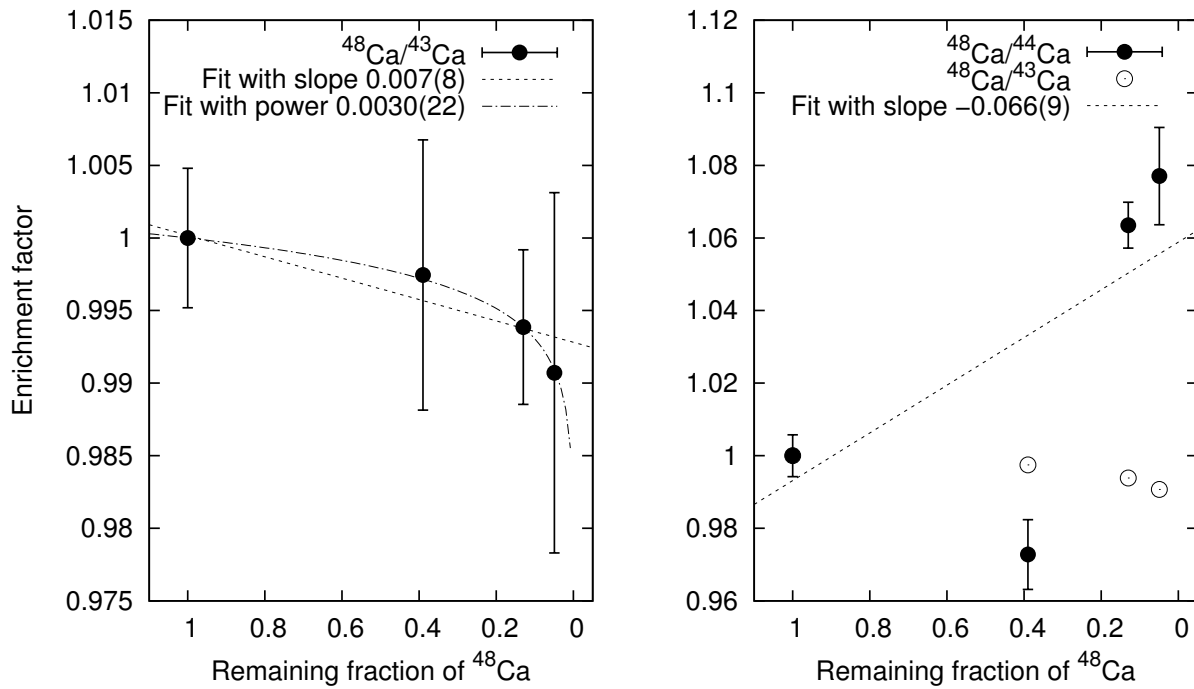


FIGURE 4.4: Enrichment factors of the third ion exchange experiment along with their fits and slope coefficients. The  $^{48}\text{Ca}/^{43}\text{Ca}$  data is repeated for comparison.

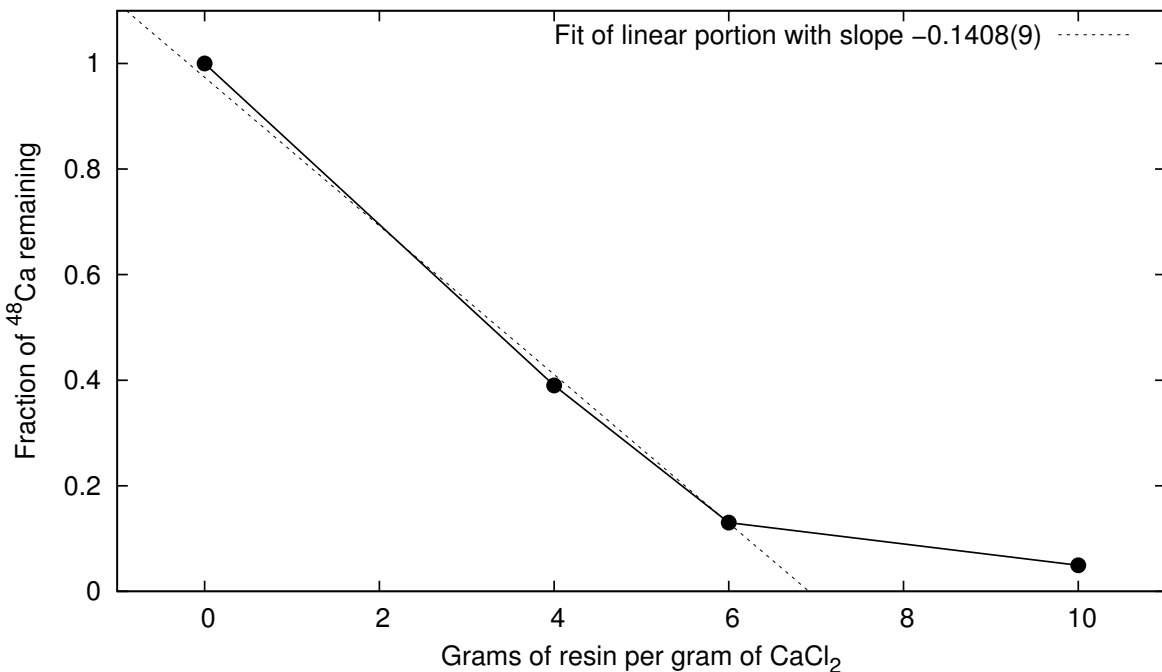


FIGURE 4.5: The fraction of  $^{48}\text{Ca}$  remaining in solution as a function of the relative amount of resin present, produced with data from the third ion exchange experiment. The fit was produced from the first three data points.

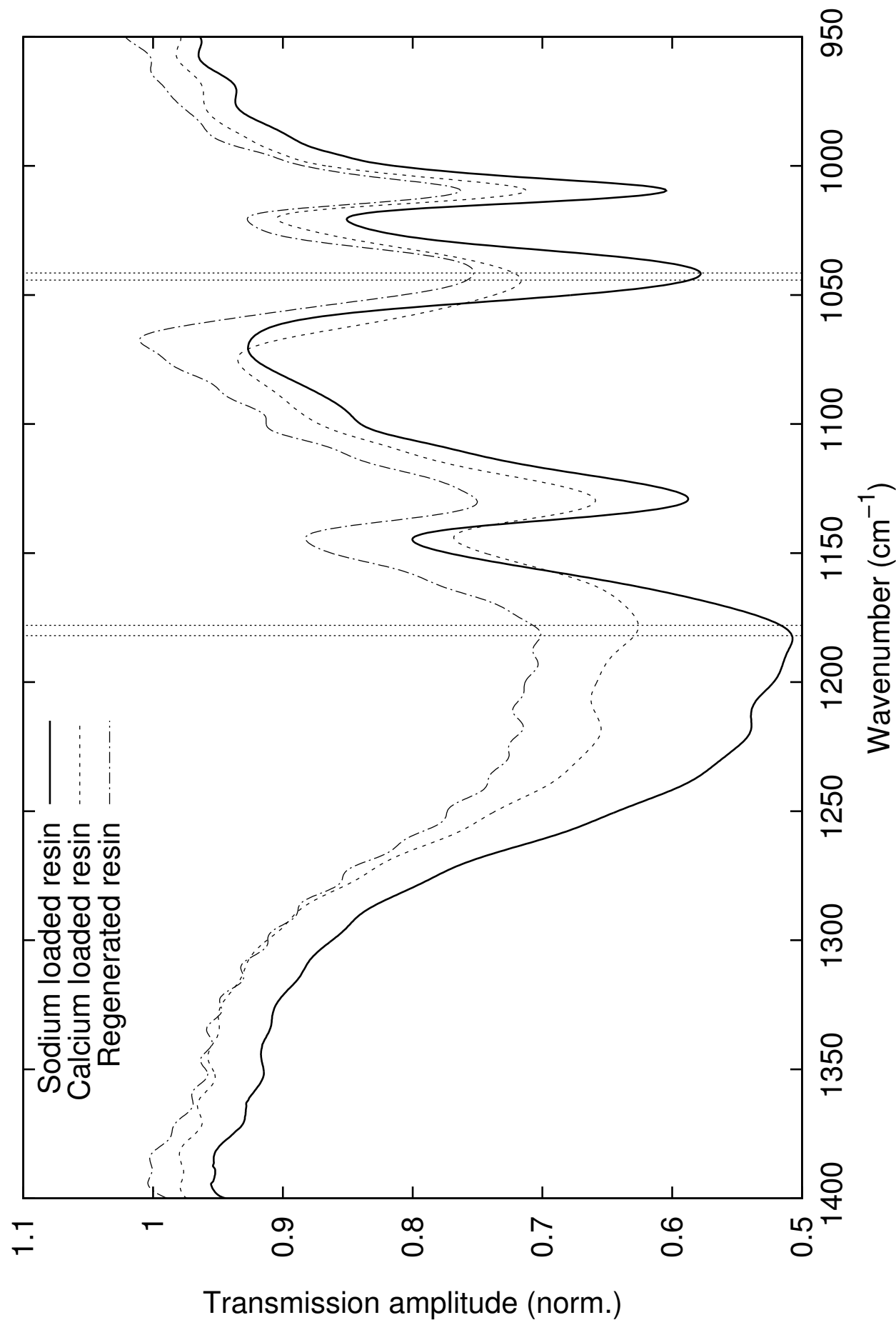


FIGURE 4.6: FTIR spectra of untreated resin, calcium-loaded resin and regenerated resin. The former and latter are both primarily loaded with sodium ions. Vertical lines signify shifted absorption peaks between resins.

### 4.3 Discussion

The ion exchange experiments were all relatively easy to perform. A solution was made and set quantities of ion exchange resin were added while stirring vigorously. Due to the simplicity of the experiment, it was not expected that it would produce results of much note. However, significant trends have been found within the data and some unexplained phenomena have been observed, despite the error margins being considerable.

#### **Ion Exchange I**

The first ion exchange experiment was performed without analysing an unprocessed sample, but was ultimately deemed to be indicative of a possible success. Enrichment factors in some samples suggested that  $^{48}\text{Ca}$  was enriched in solution, but this was in comparison to the earlier mineralisation experiment values. These had been acquired in a completely different analysis with a high chance of a differing calibration. Indeed, in the end it turned out that  $^{48}\text{Ca}$  is primarily depleted in solution during ion exchange experiments.

#### **Ion Exchange II**

The second ion exchange experiment improved upon the first by including an unprocessed calcium chloride solution, using more ion exchange resin and recording more intermediate steps. The stock calcium sample allowed for the normalisation of results and the intermediate steps resulted in the formation of convincing fits. Figure 4.3 shows the results. It can be seen that the error margins are considerable, being as large as or larger than the biggest deviation in enrichment factor. Unfortunately, the source of the large errors is entirely due to the ICP-MS, which in its old age is not equipped to handle differences in enrichment this small: it is primarily used with samples that contain a previously enriched source.

Despite the large error margins, the values show a very clear trend that appears to be linear within this range. It points downwards, however, depleting the solution of  $^{48}\text{Ca}$  as more calcium ions are taken away. This is in contrast to the first experiment, where it was thought some enrichment had been observed instead. It thus seems that  $^{48}\text{Ca}$  is adsorbed with a preference higher than that of  $^{43}\text{Ca}$  and  $^{44}\text{Ca}$ . Section 2.7 discussed the possible mechanisms behind ion exchange preferences: a kinetic effect can cause faster reacting ions to occupy ion exchange resins, whereas an equilibrium effect causes certain ion species to knock others out due to a higher binding affinity. It is generally expected that lighter ions are faster in reactions, while larger ions have a higher resin affinity, as demonstrated in figure 2.6. Since  $^{48}\text{Ca}$  concentrates in solution, it thus seems that the kinetic effect is dominant, causing predominantly the lighter ions to be adsorbed into the resin.

A few more remarks can be made about the second ion exchange experiment. Firstly, it can be noted that the remaining fraction of  $^{48}\text{Ca}$  only barely dips below 0.5, despite six grams of resin having been added to only three grams of dissolved calcium chloride. It was first thought that the capacity of the resin was sufficient for it to process nearly 50% of its own weight in calcium chloride, but figure 4.5 shows that the capacity took on a very different value during the ion exchange experiments, resulting in a relatively low fraction of calcium removed.

Secondly, the enrichment factors are plotted as a function of the remaining fraction of  $^{48}\text{Ca}$ , as opposed to the remaining fraction of all calcium, consisting mostly of  $^{40}\text{Ca}$ . The reason for this was touched upon earlier: the argon-40 used by the ICP-MS makes it impossible to measure  $^{40}\text{Ca}$  with any accuracy and forces the use of different measures. As long as the enrichment factor stays close to unity, which is unfortunately the case in all results displayed here, using the  $^{48}\text{Ca}$  fraction is reasonable.

Thirdly, as had been observed during the mineralisation experiments, the ratio  $^{48}\text{Ca}/^{44}\text{Ca}$  undergoes a much stronger change than  $^{48}\text{Ca}/^{43}\text{Ca}$ . The cause is unclear and may, again, be

attributed to a difference in concentration or a difference in nuclear spin. It is expected that  $^{40}\text{Ca}$  behaves in line with  $^{44}\text{Ca}$  and  $^{48}\text{Ca}$  thanks to its spin being identical to that of these two isotopes.

A last point can be made about the nature of the fits. These were chosen to be linear primarily because the data sets suggest it, but it is not expected that this linear trend continues all the way to the point where there is no calcium left in solution. Being ratios by nature, enrichment factors tend to either blow up or become very small as the absolute quantities of isotopes diminishes. In the event that  $^{48}\text{Ca}$  is adsorbed much more readily than  $^{43}\text{Ca}$ , for example, it is likely that the former will disappear from solution before the latter ceases to be detected by ICP-MS. The ratio  $^{48}\text{Ca}/^{43}\text{Ca}$  would then yield zero. The fact that linear fits apply very well to the data can be attributed to the small enrichment effect of the process and the large fraction of calcium left in solution by the end of the experiment.

### **Ion exchange III**

The third ion exchange experiment was performed with some small changes to the second one. Because it is expected that the largest enrichment effects become visible as the calcium has all but disappeared from solution, the amount of calcium chloride used was decreased to one third of its original value and the quantity of ion exchange resin was almost doubled. The results, shown in figure 4.4, are much more striking than the ones that came before. They are presented in the same format as the the second ion exchange experiment results, but with a few additions and a few changes.

The linear fit of the  $^{48}\text{Ca}/^{43}\text{Ca}$  data, shown in figure 4.4 corresponds reasonably well to the measurements, but it seems to be much less pronounced than the one in figure 4.3, featuring only half of the previously measured slope. There are some hypotheses as to why this discrepancy exists. The third experiment featured much less calcium than the second in a similar volume, making the overall concentration much lower. This could have caused some local calcium starvation around newly added resin beads. Although the solution was always stirred vigorously and the beads were added at a slow rate, the differing concentrations caused the third experiment beads to have an effectively faster entry. Another hypothesis is based on the time between the addition of the ion exchange resin and the taking of samples. Although the solution was always given minutes at minimum, the timing was not matched between the two experiments and was not recorded very well in experiment logs. For demonstrating the kinetic effect, a short time is advantageous, whereas the equilibrium effect favours a very long experiment time. There is no known timescale for the difference between these two cases, however, making it difficult to quantify possible differences between differently timed experiments.

Another type of fit was added to the  $^{48}\text{Ca}/^{43}\text{Ca}$  data. This one is of the variety  $f(x) = x^a$ , where  $a$  is the power coefficient. Because there are no other variables within the fit function, it passes through the coordinates  $(0, 0)$  and  $(1, 1)$  perfectly, which makes sense in the current experiment. It passes suspiciously well through the collected data points, yielding a power coefficient with a relatively small margin of error. It could be coincidental that the points are positioned exactly right for a power law to fit the data, especially since a linear fit seems to work reasonably well as well. It is difficult to say with error margins this large.

The elephant in the room is the  $^{48}\text{Ca}/^{44}\text{Ca}$  ratio of this experiment, shown in figure 4.4. The  $^{48}\text{Ca}/^{43}\text{Ca}$  values of the same experiment were added for comparison. Its enrichment factors are large and unlike anything that has been seen during this project. Single stage enrichment processes were expected to enrich or deplete on the order of percentage points at most, and these measurements reached an increase of almost 8%. For comparison, the next largest deviation from the standard was found in the  $^{48}\text{Ca}/^{44}\text{Ca}$  measurement of the second ion exchange experiment, where it took on a value of 0.974. This brings up the second peculiarity about the samples: they are enriched instead of depleted. All ion exchange experiments so far have

yielded samples in which  $^{48}\text{Ca}$  was depleted relative to  $^{43}\text{Ca}$  and  $^{44}\text{Ca}$ . The course of the measurements is also quite interesting: it points towards depletion for the first two points and then veers up into enrichment. A linear fit was made for consistency, but it does not match the data very well. Again there is a number of hypotheses as to why these results are as they are.

The first considers the idea that the points are legitimate and there was no large measurement error or experimental mishap. This is somewhat unlikely. Contrary to the last few points, the second point in the series does point to a depletion of  $^{48}\text{Ca}$  and corresponds reasonably well to the data of the second experiment in figure 4.3. In order for the last points in the series to be correct, either all other data collected in the second and third ion exchange experiments have to be wrong, or there has to be some kind of previously unseen effect that specifically removes  $^{44}\text{Ca}$  from solution. The latter is, in principle, possible. As was mentioned before, the time between addition of the resin and the extraction of some solution for analysis was not fixed and likely differed somewhat between the second and third experiment. If the equilibrium effect overcomes the kinetic effect in a matter of hours and demonstrates a clear dominance, a reversal in enrichment could be seen. There is one objection to this theory, however, and that is that  $^{44}\text{Ca}$  would need to be more slowly reacting than  $^{48}\text{Ca}$  and that  $^{44}\text{Ca}$  would have to have a long-term advantage over  $^{48}\text{Ca}$  to be adsorbed into the resin. Both of these situations are the opposite of what would be expected.

The second hypothesis is that there was no high enrichment and that the analysis produced the last two points erroneously. Again, this is possible, but highly unlikely. In order to rule out any bias within the ICP-MS analysis, the samples were not submitted in chronological order. The final two points in the graph actually consisted of four samples that were positioned somewhat centrally in the sample batch. No samples around these points exhibited extraordinary enrichment factors. The ICP-MS runs a calibration cycle at the beginning and end of a run, but also calibrates between samples in the case of a large batch, meaning that there may arise an unreasonable difference between samples if they belong to differently calibrated sample sets. This was not the case for this batch. Only two calibration runs were performed: one before the analysis of the samples and one after the analysis. All samples were thus measured with the same settings, and still a select few showed anomalous ratios. There is a possibility that the machine produced faulty values for exactly the right samples, exactly in accordance with the duplicates within the sample set, but this is not very probable.

The third and last hypothesis poses that the enrichment values are faulty and the ICP-MS functioned correctly, but that something in the samples disrupted the measurement. This counteracts the arguments of the previous paragraph: if some contaminant intrinsic to the samples disrupted the analysis, it does not matter how far they were spaced apart within the sample set, whether there were any duplicates or with which calibration they were measured. However, there is no clear indication how samples might be contaminated such that they would produce these results. The presence of an impurity with mass number 44 such as  $\text{CO}_2$  would be a first thought, but this would cause a decrease in the perceived  $^{48}\text{Ca}/^{44}\text{Ca}$  ratio instead of an increase. There is also no indication for the presence of such a contamination in the other samples or in the calibration solutions. After all, the other measurements did produce sensible results. This is the same reason why a contamination in the other mass numbers, 43 and 48, is unlikely. They would have to be present in exactly the right quantities in all samples, including the calibration solutions, except in the four samples that caused high enrichment values. Since the only difference between the second and last two data points is the addition of ion exchange resin, it would be logical to think that something in the resin suppressed or bound the  $^{44}\text{Ca}$  specifically. This type of process is by definition an enrichment procedure and makes for a legitimate, albeit surprising, result.

## FTIR spectroscopy

The FTIR graph shown in figure 4.6 represents only a small portion of the total data set that was produced during analysis. The machine measured from 400 to 4000  $\text{cm}^{-1}$ , but the vast majority of this range produced uninteresting results and has been left out. The horizontal scale denotes the wavenumber of the measured radiation, which corresponds to the inverse of the wavelength in centimetres. It is a measure of frequency, with the conversion factor being the speed of light:  $\nu = c \cdot \tilde{\nu}$ , where  $\nu$  is the frequency,  $c$  the speed of light and  $\tilde{\nu}$  the wavenumber. As is customary for these graphs, the horizontal axis has been inverted. The vertical scale shows the normalised amplitude of the transmitted light. Since the absolute amplitudes of individual peaks do not have much meaning on their own, curves are normalised and made to match as well as possible for easier comparison.

It can be seen that the different plots in the figure do not correspond very well, despite being analyses of nearly identical substances. Herein lies the difficulty of comparing different samples using FTIR spectroscopy: the method is extremely sensitive to varying concentrations of crushed resin, as well as the moisture the sample attracts between its creation and the moment it is analysed. The curves shown in figure 4.6 have therefore been normalised such that they overlap maximally. Fortunately, the changes that are looked for between the curves is not vertical. A calcium ion is bound differently than two sodium ions and takes a different energy to be excited vibrationally. Different energies correspond to different radiation frequencies and therefore to different wavenumbers. The peak shift would thus be horizontal.

A significant shift consists of a difference between the calcium loaded resin and the two sodium loaded resins. Although the regenerated resin may contain traces of calcium, it is suspected that it contains mostly sodium and should thus largely follow the sodium loaded resin. Few convincing horizontal shifts have been found over the entire spectrum, but in this range two have been observed. At a wavenumber of about 1040  $\text{cm}^{-1}$ , it can be seen that the sodium loaded and regenerated resins peak at a slightly different value than the calcium loaded resin. Vertical lines signify the small difference between the calcium and sodium peaks. Although the shift is easiest to quantify in that region, it can be seen that the structures left of the peaks show the deviation more clearly. Another slight deviation can be spotted around 1180  $\text{cm}^{-1}$ , again signified by a set of vertical lines. This shift is less convincing because the absorption peaks are quite broad and in the case of the regenerated resin somewhat craggy.

Classifying the various absorption peaks correctly is challenging because absorptions for different regions of a molecule tend to overlap. Fortunately, there are many tables that list absorption values for specific vibrations in specific groups and from those some indication of the absorption sources may be gleaned. The 1040  $\text{cm}^{-1}$  peak has been classified by multiple sources to be the stretching of S=O, found in the sulfonate groups of the ion exchange resin. It could also be symmetric SO<sub>3</sub> stretching, however. The calcium-loaded resin exhibits a higher wavenumber for this absorption peak, meaning that it takes more energy to excite the specific mode. This can be made understandable by considering that a calcium atom is much heavier than a sodium atom. Having calcium attached to the sulfonate group would make it more arduous to move the sulphur atom. Additionally, sodium atoms connect to only one sulfonate group whereas calcium connects to two, thereby likely making the construction slightly more rigid. The difference is minimal, however, suggesting that the oxygen atom is the main actor in the vibration. The 1180  $\text{cm}^{-1}$  peak can be traced back to either another S=O stretch or a SO<sub>3</sub> symmetric stretch. Similar arguments to the ones used for 1040  $\text{cm}^{-1}$  apply.[49][50]

The shifts found in the FTIR analysis are significant and can be justified to satisfaction. However, they are much too small to be of any practical use. It is expected that it would be very difficult to irradiate resin beads and excite calcium more than sodium, let alone excite specific calcium isotopes while the resin is submerged in infrared-absorbent water. It is likely, however, that much larger peak shifts exist outside of the currently measured spectrum.



# Chapter 5

## Electrophoresis

Roughly the same group that made recent advances in calcium enrichment through chromatography has also expanded into electrophoresis, explained in section 2.8. One of their calcium enrichment schemes combines the two more promising electrophoresis methods into multi-channel counter-current electrophoresis (MCCCE), shown in figure 2.11. The main idea is to use a counter-current scheme while taking advantage of the heat dissipation that is possible with capillaries. The core of the experiment consists of a perforated boron nitride block that contains a large number of narrow channels. Thanks to boron nitride's low permittivity relative to water, the electric field is concentrated within the block. This causes almost all electrophoresis to take place there. The high thermal conductivity and channel structure of the boron nitride block also allows it to effectively drain heat from the resistively heated solution, transferring it to a cooling system. In this way, higher electric fields may be attained without fear of the solution reaching boiling temperatures. The pressure-driven liquid flow within the apparatus was set up opposite to the electrophoretic ion velocity to maximise the separation between isotopes within the confines of the experiment. Although the setup geometry did not allow for a high production volume, the experiment reported enrichment factors as high as 6. This is exceptional even for gaseous enrichment schemes. Thus the only obstacle that remains for MCCCE is upscaling to industrial production levels while remaining energy efficient. Pump power requirements and resistive heating losses pose the biggest challenges in this regard.[41]

In 1969, an experiment was performed on the enrichment of isotopes using **molten salts**. The experiment used an inventive method in which a difference in voltage caused both electromigration and a counter-current. It consisted of compartments connected by tubes filled with sand to avoid turbulence where the fragile isotope separation process takes place. The graphite electrodes were placed into the outer compartments so that they were partly submerged and the entire setup was placed inside an oven so that the salts were kept molten during the experiment. The setup is shown in figure 5.1. In the electromigration process, calcium ions moved towards the negatively charged cathode, whereas chloride recombined at the positively charged anode and formed chlorine gas. By leading this gas back into the compartment with the cathode, it once again formed molten calcium chloride which could participate in the experiment once more. Thanks to this flow of chlorine gas and the law of communicating vessels, a counter-current was instituted that perfectly counteracted the flow of calcium ions. The final effect was that the net flow of calcium ions was exactly zero, meaning that the faster-moving ions collected at the cathode and the slower ones moved towards the anode.[51]

This self-regulating system is sensitive to tiny differences in electromigration velocity and can be used in all salts that produce a gas upon recombination of their non-metal component, making the method highly universal. In the specific case of calcium, an enrichment factor of nearly 9 was observed with respect to  $^{48}\text{Ca}$  and a factor over 4 for  $^{44}\text{Ca}$ . However, although these factors are very large indeed for single enrichment stages, the costs associated with producing large amounts of enriched calcium using this method may be daunting. The process requires temperatures in excess of 770° C to keep the salt molten and considerable electrical currents to maintain the electrolysis. This may not be cost effective, considering calutrons already have a much higher enrichment factor, have existing infrastructure and are likely much

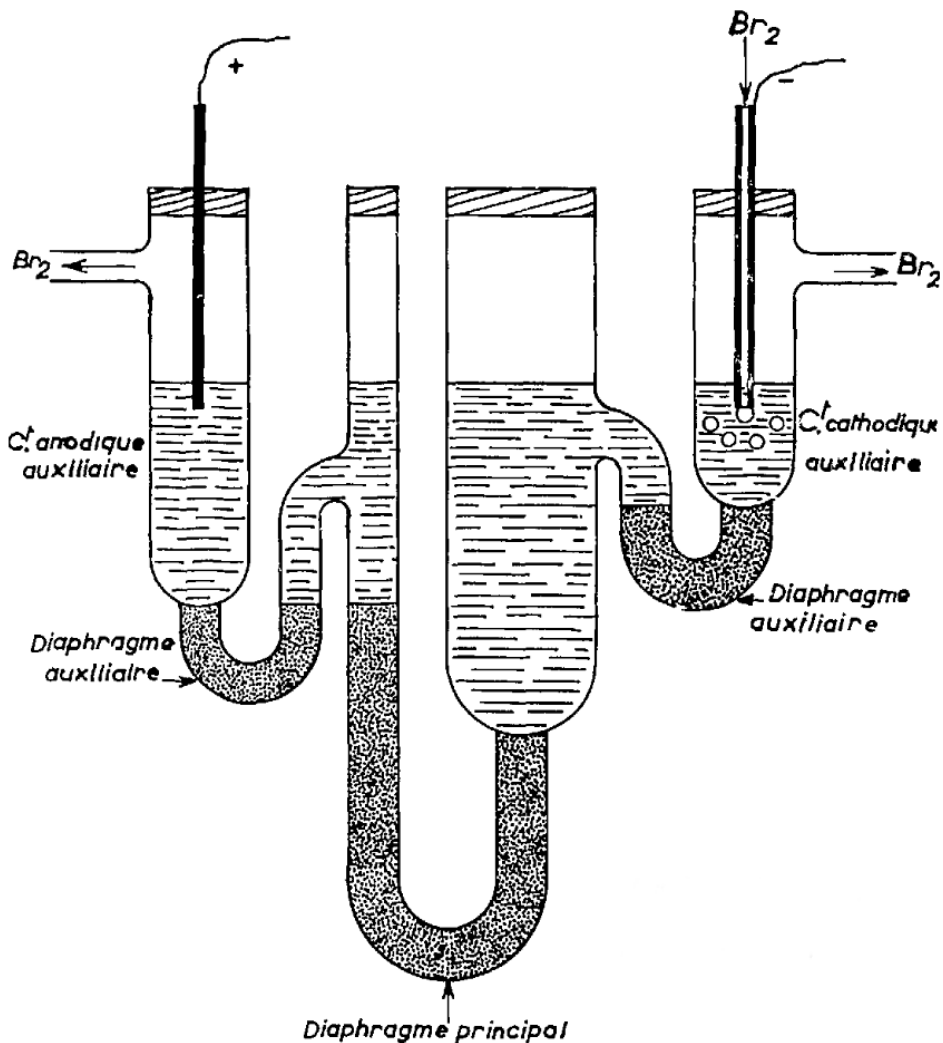


FIGURE 5.1: A calcium enrichment scheme by molten salt counter-current electromigration. In this case, calcium bromide is used instead of calcium chloride, but the basic function of the experiment is identical.[51]

less dangerous in the event of an accident. Unfortunately the method does not apply to room temperature experiments, where the salts are dissolved in water or another inexpensive solvent. Electromigration and electrolysis work as in the case of molten salts, but the recombination of chlorine gas with calcium simply does not happen under regular conditions. An external solvent flow therefore needs to be instituted that precisely counteracts the flow of ions, explained more in-depth in section 2.8. As the article outlining the molten salt experiment states, this is a laborious and delicate procedure.[51]

Substances akin to molten salts exist at lower temperatures: **room temperature ionic liquids** (RTILs). These are salts that are liquid near room temperature and can be used as entirely ionic solvents. Regular salts are generally solid up to high temperatures thanks to the strong ionic bonds between the anions and cations. RTILs therefore often feature a large and highly asymmetric organic cation, as well as a smaller anion that does not readily fit into this structure. This imperfect binding causes ionic liquids to behave like a liquid, but the binding is still strong enough to cause a viscosity much higher than that of organic solvents: RTILs are known to possess viscosities of a few tens to hundreds of mPa·s. Water only has a viscosity of 0.89 mPa·s and acetone one of 0.31 mPa·s [52]. Despite being entirely ionic themselves, ionic liquids are not always good solvents of other salts. In fact, most RTILs that have been tested so far have demonstrated an insignificant solubility of calcium chloride: only one instance was recorded

where a saturated  $\text{CaCl}_2$  solution consisted of more than 10%  $\text{CaCl}_2$  by mass [53].

Ionic liquids are thus not a suitable room temperature replacement of molten salts when it comes to self-regulating counter-current experiments. However, they have proven useful in another enrichment scheme. A lithium enrichment experiment has been carried out in which an ionic liquid was used to impregnate an organic membrane. This membrane was then coated with a protective layer to prevent the ionic liquid from escaping, after which it could serve as a barrier in an electrophoresis experiment. A compartment was split in two by the sheet and electrodes were inserted on either side of it to apply a high voltage. Solutions were then pumped along either side of the membrane: a  $\text{LiCl}$  solution on the side of the positive electrode and one of  $\text{NaCl}$  on the other side. The lithium that passed through the barrier was then analysed by a mass spectrometer and the isotope ratio between  ${}^6\text{Li}$  and  ${}^7\text{Li}$  was determined as a function of total lithium transmission through the membrane. The highest enrichment factors were found for the lowest total transmission. They were found to be 1.4 for a total transmission of  $\sim 5 \cdot 10^{-4}\%$  and 1.2 for a transmission of 0.01%, which is very high for such a simple experiment. It is already on par with the gas centrifuge and far exceeds the capabilities of the gaseous diffusion scheme, which is similar to this method in that it also separates isotopes with a membrane in a continuous fashion. It is not thoroughly explained how the exact enrichment process works, however, and there is no elaboration on its applicability to ions such as calcium. Nevertheless, it is an interesting method that could prove invaluable in the future.[54]

## 5.1 Experiment

The previous experiments have all dealt with materials and methods that are not far from everyday conditions. The occasional corrosive chemical and heating plate were the most dangerous objects, making experiments easy to set up and relatively safe to perform. For the planned experiments, however, a DC voltage of several hundred volts was required, reaching 2 kV at its highest point. Combined with the fact that these voltages were meant to be applied over a distance of less than ten centimetres, exercising caution was considered wise. Unfortunately, caution takes time and time is short. Therefore not nearly all planned experiments have come to fruition. In the end, only a preliminary experiment was realised physically and most of the work done concerning electrophoresis consisted of simulations. Larger and more complex follow-up experiments than the one realised have been devised and tested using homemade as well as open source simulation software.

As expanded upon in section 2.8, counter-current electrophoresis has proved to be one of the most effective ways to enrich ions in a low viscosity solution. The counter-current makes it possible to maintain a high voltage over what is effectively an infinite distance. The voltage and liquid current are balanced in such a way that they almost cancel out, making  ${}^{40}\text{Ca}$  and  ${}^{48}\text{Ca}$  concentrate at opposite ends of the experiment. It is these areas at the extremes of the setup, especially the one rich in  ${}^{48}\text{Ca}$ , that should be isolated and further enriched.

During the course of this project, a new method has been devised that focuses on these areas. The experimental setup consists of an arbitrarily long chain of electrodes positioned a regular distance away from each other in a row. Voltage is applied to them in such a way that they alternately receive a positive and a negative voltage. The resulting electric fields then point alternatingly forwards and backwards along the electrode chain, resulting in ions moving either forwards or backwards, depending on their position within the experiment. If a salt is dissolved in a field that is pointing forwards, the positive calcium ions will move in the forward direction until they encounter the negative electrode that attracted them. The  ${}^{40}\text{Ca}^{2+}$  ions are likely to reach their end goal first, since they are faster in electromigration and in diffusion. Just as the first  ${}^{40}\text{Ca}^{2+}$  ions arrive, the field is switched, and the forwards field becomes a backwards one. Conversely, the neighbouring field switches from negative to positive. Thus a portion of the ions that reached the electrode move into the next zone and are pulled towards the next

electrode. The slower ions that do not reach the electrode in time for the switch are pulled back. This continues with as many electrodes as is necessary. Every switch brings new material to the next region, enriched by a little bit more than that in the previous cell.

Ideally, electrodes would be perfectly insulated so that no electrolysis takes place. In this experiment it is imperative that calcium ions do not lose their electric charge because they need to be manipulated further by electric fields after encountering their first electrode. This proved to be more difficult than initially thought. Thanks to its small and dipolar molecular makeup, water has an extremely high electric permittivity, making it difficult for electric fields to concentrate in solutions. If an object made of plastic were to be inserted into the water, it would ‘absorb’ the electric field as shown in figure 5.2. Insulation works the same way. If only electrode, insulation and water are considered in an infinitely large plate capacitor, the electric field in the water and in the insulator is given by:

$$E_w = \frac{\Delta V}{2\epsilon_w/\epsilon_i \cdot d_i + d_w} \quad E_i = \frac{\Delta V}{2d_i + \epsilon_i/\epsilon_w \cdot d_w} \quad \Rightarrow \quad \frac{E_i}{E_w} = \frac{\epsilon_w}{\epsilon_i} \quad (5.1)$$

where  $E$  signifies the magnitude of the electric field,  $\Delta V$  the voltage difference between the capacitor plates,  $\epsilon$  the electric permittivity and  $d$  the thickness of the material. Subscripts  $w$  and  $i$  denote water and insulator material, respectively. The fraction  $\epsilon_w/\epsilon_i$  is quite large for most insulator material choices: the relative permittivity of plastics hovers around 3 and that of water is approximately 80, although this number is known to change drastically when used as a solvent for salts, going as low as 20 [55][56]. The goal with these equations is to adjust the parameters so that the field in the water is as high as possible and the field in the insulator as low as possible. The former can be realised by keeping the dimensions of the experiment small and the latter by making the fraction  $\epsilon_w/\epsilon_i$  as small as possible. An insulator with a high permittivity may be used and the permittivity of water may be lowered by adding more salt. This also has the effect of decreasing the hydration number, thus increasing the effective mass difference between the relevant isotopes. High permittivity insulators include exotic materials such as  $\text{PbMgNbO}_3 + \text{PbTiO}_3$  with a relative permittivity of 22,600, but more accessible materials exist such as aluminium oxide ( $\text{Al}_2\text{O}_3$ ) which has a dielectric constant of 9 and would also suffice in this case [57]. Furthermore, aluminium oxide can be grown onto aluminium by anodisation. In this process, a current is run through the aluminium while it sits in an acid bath. The oxygen produced at the surface by the electrolysis forms a thick oxidation layer, but this layer is not completely homogeneous. Pores in the  $\text{Al}_2\text{O}_3$  layer form as a result of the acidic solution and allow the electrolysis to continue for longer than would otherwise be possible. This is advantageous in situations where the oxide is meant to protect against corrosion and other damage, but can be problematic in the case of electrical insulation. However, in the spirit of experimentation and for its ease of procurement and manufacture, it was decided to attempt anodised aluminium electrodes regardless. In the case that they fail in the preliminary experiment, they can be insulated with water-tight plastic tape.

The shape of the electrodes is another point of difficulty. Their primary function is to generate an electric field that is both strong and reasonably homogeneous over distances much larger than the electrode diameter. This field is to transport ions in a periodic fashion and should above all be close to identical to its neighbouring cells. On the other hand, the mechanism requires ions to pass through or around electrodes before a switch occurs. Due to the symmetric nature of the experiment, at most half of all newly arriving ions may pass into the next zone. This is in the case of perfect ion transmission, however, and requires both a completely permeable and infinitely thin electrode. In reality, a much smaller fraction of all ions that reach the electrode proceed into the next cell. To maximise how many do pass on, the electrode shape has to be carefully chosen. Although thin parallel plates are the most straightforward option for their ability to generate the most homogeneous electric field, they are not ideal in terms of ion mobility. They exhibit much higher fields at their corners than near their centre, as

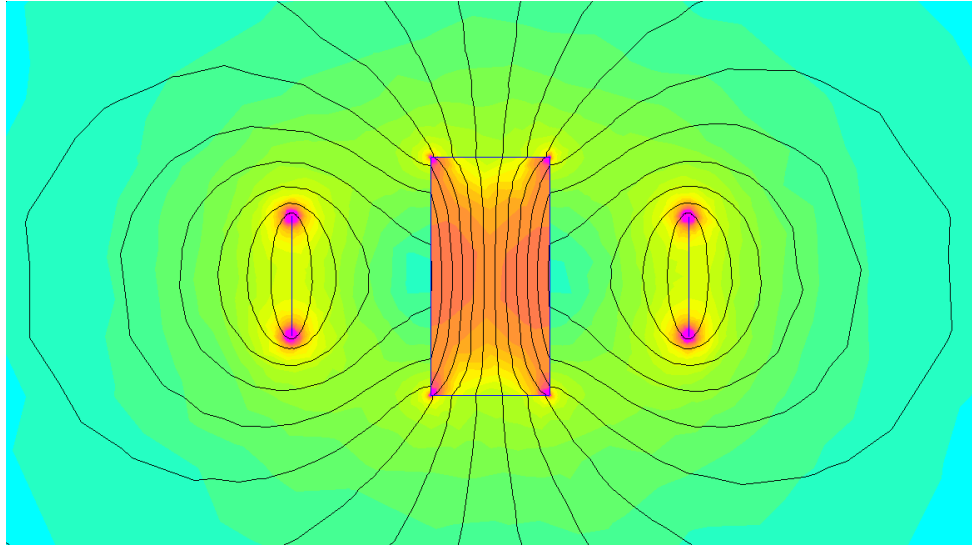


FIGURE 5.2: A FEMM simulation of two thin parallel plate electrodes on either side of a polystyrene block. The entire experiment is submerged in water. Blue represents a high electric field whereas yellow going into white signifies a low field.[58]

shown in figure 5.2, but this is not considered to be sufficient to let ions pass. Most that reach the electrode would cling to the front surface and would never be able to move around to the back.

In a previous experiment involving MCCCE, explained earlier in this section and pictured in figure 2.11, ions were also required to move through a set of electrodes to be collected. Three cylindrical platinum electrodes were used in a row so that they did not impede the flow of the fluid too much. The experiment used an actual pump-driven solvent flow and is therefore not the best example, but it does present an alternative electrode configuration [41]. Purely cylindrical electrodes with an even insulation layer suffer from much the same problems as the parallel plate configuration, however. In fact, the electric field is in this case strongest on the front and backside of the cylinders, stimulating ions to stay in their respective cells. The relevant fields are visualised in figure 5.3. To remedy this problem, the shape of the electrodes and the insulation layer may be changed. Instead of using a perfectly round shape, an oval cross-section may be employed. Figure 5.3 also shows the shifted electric field magnitudes as a result of this. Two methods may be utilised: the electrode may be oval perpendicular to the ion motion or the insulator may be oval parallel to the ion motion. These configurations encourage the collection of ions on the sides of the electrodes and could thus send ions into the next cell once the fields switch. Another electrode arrangement is the grid, or perforated plate. The plate-like shape allows for the generation of a homogeneous electric field while the holes allow ions to pass through. It is a matter of hole geometry whether ions collect on the outside of the plate or within the holes. A cross-section of such a plate through a row of holes essentially looks the same as a series of cylinders in a row. The optimisation problem is therefore similar: the insides of the holes should feature a concentrated electric field so that the ions collect in the middle of the electrode and can be passed on during the next electric field switch.

There are some parameters that are likely to matter little if homogeneous fields can be realised. The exact width and height of the experiment do not influence the electric field and so may be chosen as is convenient. In an eventual high-volume production scheme, these may be taken to be large, but for a proof-of-concept experiment they should be taken to be quite small. This decreases remixing by turbulence and convection currents. The experiment thus reduces to a one-dimensional problem with a few vital parameters. These are: the distance between electrodes, the field switching period and the voltage difference between neighbouring

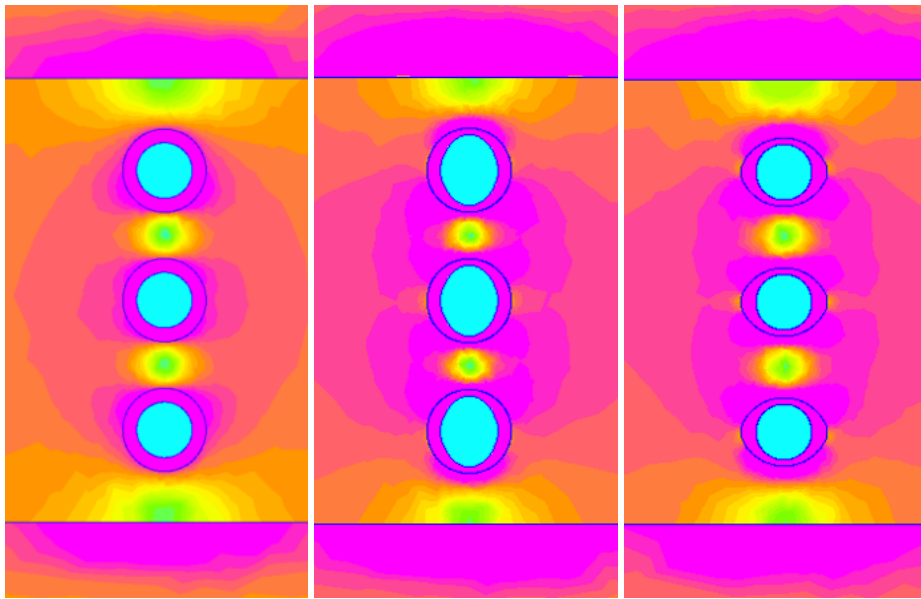


FIGURE 5.3: Various electrode shapes. The electrode insulation and the experiment boundary are made of polystyrene, and the rest of the experiment is filled with water. The colour gradient signifies the absolute magnitude of the electric field, here presented without scale for the sake of qualitative example. Again, blue signifies a high electric field whereas yellow represents a low field. Note that the leftmost simulation shows the strongest fields at the front and back of the electrodes, whereas the others emit strong fields at their sides.

electrodes. These parameters are linked so that the third parameter can be determined if the first two are known. After all, ions travel a known distance in a set time under the influence of a set field, fixing the electrode distance. In order to visualise what length each stage should have and how long a single period should be, the electromigration time  $t$  can be compared to the thermal broadening of ion bands. In the ideal case, the isotope separation is larger than the width of the broadening:

$$\Delta l = \Delta\mu Et \quad \geq \quad \sigma = \sqrt{2Dt} \quad (5.2)$$

Here,  $\Delta l$  denotes the separation difference between isotopes,  $\Delta\mu$  the difference in electrical mobility between  $^{40}\text{Ca}$  and  $^{48}\text{Ca}$ ,  $\sigma$  the width of the electromigration bands and  $D$  the diffusion coefficient of calcium ions. This equation can be rewritten to find the minimal time needed:

$$t \geq \frac{2D}{(\Delta\mu E)^2} \quad (5.3)$$

In reality, the broadening will not just be caused by thermal effects. Turbulence and convection increase the broadening width and would essentially just cause a larger diffusion coefficient in equation 5.3.[41]

From equation 2.7, the fractional difference in velocity between isotopes is known, namely  $\Delta v/v = v_{40}/v_{48} - 1 = 8.2 \cdot 10^{-4}$ , and  $v = \mu E$  so that  $\Delta v/v = \Delta\mu/\mu$ . Furthermore, the electrical mobility is established to be  $\mu = 6.17 \cdot 10^{-8} \text{ m}^2/\text{Vs}$ . Filling in these values as well as  $D = 7.92 \cdot 10^{-10} \text{ m}^2/\text{s}$  [59] yields

$$t \geq \frac{6.19 \cdot 10^{11} \text{ V}^2\text{s/m}^2}{E^2} \quad l = \mu Et \geq \frac{3.82 \cdot 10^4 \text{ V}}{E} \quad \Delta U \approx lE \geq 3.82 \cdot 10^4 \text{ V} \quad (5.4)$$

where  $\Delta U$  is the voltage difference between electrodes. The first two equations are plotted in figure 5.4, showing that the times and lengths, although possible, are not quite small. Multiple hours are needed in most cases, with stage lengths of metres. Note that the experiment ideally

consists of many such stages and that the electric field needs to be kept constant along each. The last equation is only correct for infinite parallel plate capacitors: in most other cases the required voltage will be even larger. Needless to say, 38.2 kV is quite a high voltage and would present difficulties even without the electrodes being bathed in a conductive solution.

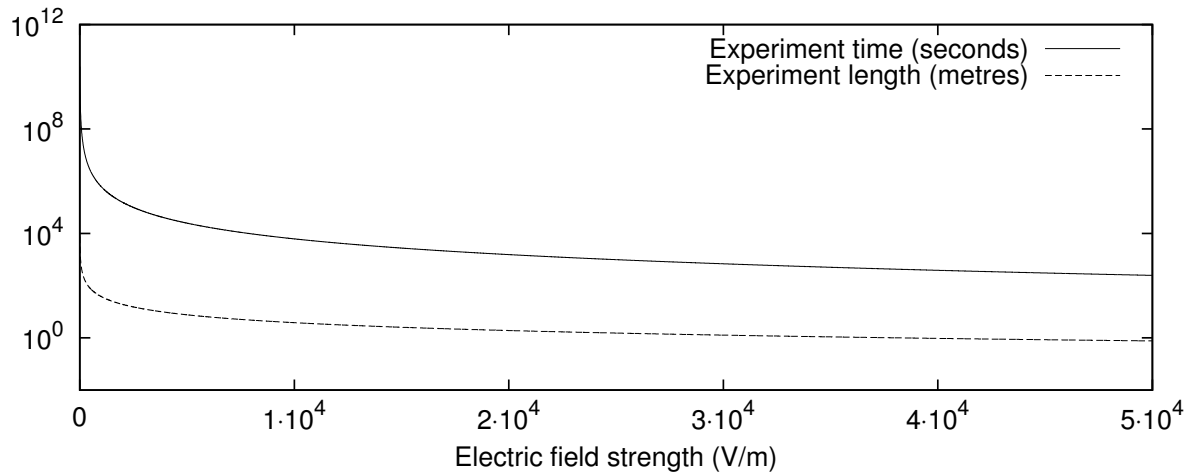


FIGURE 5.4: The experiment time and length as a function of the electric field.

The idea of the proposed experiment is thus not to separate isotopes by a great length at once: it is to separate the isotopes many times by very little. By dividing the great length of an enrichment experiment into much smaller parts, the electric field can be kept more uniform and the enrichment process more consistent. The main advantage of the scheme, however, is that it provides a cascade in itself under a relatively simple premise. Each cell receives calcium ions from its neighbours and sorts them very slightly according to mass. Additionally, the symmetry of the experiment causes the scheme to enrich in two directions. Since there is no preference for forwards or backwards movement with a perfectly periodic switch of the field, the lighter ions propagate more easily in either direction than the heavier isotopes. In essence, the setup provides an environment in which light ions ‘diffuse’ outwards much more quickly.

Disadvantages also exist for the enrichment scheme. In the consideration of counter-current electrophoresis, it was noted that heat generation is a limiting factor. The movement of ions continuously being pulled through the liquid can cause the setup to heat up to the point of boiling. The cooler solvent flow alleviates this problem somewhat, however, and there are schemes such as MCCCE that employ a heat sink to cool the fluid down. No liquid flow exists in the proposed experiment, however. The solution is ideally completely static apart from the ions it contains. Additionally, the movement of the ions is not made to be efficient, making production expensive. The main idea of the experiment is namely to waste as much of the heavy isotope’s movement as possible to keep it confined. Cooling of some manner would have to be employed to keep such an experiment going for any length of time. Perforated insulator blocks with a high heat capacity could be used to turn each stage into an MCCCE process.

Perhaps the most obvious disadvantage of the method is that it enriches an element in its faster moving isotopes. These are the ions that can pass through to the next cell more easily and ‘diffuse’ out of the experiment with high purity. Of course, where there is depletion of  $^{48}\text{Ca}$  in one location, there must be enrichment in another. The conservation of isotopes makes sure that heavier isotopes are enriched within the experiment as depleted calcium is removed. A downside of this is that a great quantity of material has to be removed before a small amount of enriched calcium is produced. Additionally, with the desired isotope stranded within the device, a continuous enrichment scheme is also made difficult. Enriching in one dimension and transporting enriched material in another is one possibility of solving this problem. For

example, the electrodes could be made to be quite wide so that the material can be transported along them using a solvent flow. This is likely to interfere with the ion flow, however, especially since the electrodes cannot be smooth. The turbulence generated by the flow on electrode holes would enhance remixing of the isotopes and counteract any enrichment progress. These problems have not been considered in detail in this project as the eventual mass-production of highly enriched calcium is not its main focus.

## Simulation

Simulation of the electric fields was done in FEMM (Finite Element Method Magnetics [58]) to gain an idea of the electric field shape in non-trivial experimental setups. Although FEMM is reasonably user-friendly and powerful program, it only works in two dimensions. More complex electrode shapes are difficult to simulate if their special features are not in the plane of simulation. For example, a perforated plate cannot be simulated accurately if it is viewed from the side. The simulation software is still valuable, however. The experiment that has been outlined in this section is in essence mostly one-dimensional, making FEMM the perfect tool for simulation.

A number of matters were simulated using FEMM. Firstly, the electrode shape and its insulation was analysed. In a previous experiment, circular platinum rods were used to supply the electric field [41]. When positioned in a row, they provide a reasonably homogeneous field while still allowing for the passage of ions. However, as was explained before, the circular shape of the electrodes is unsuitable for the current experiment, in which there is no liquid flow to help the ions pass through them. This is shown in figure 5.3, where the electric field hotspots are located at the front and back of the electrodes. The ions thus concentrate at their original side of the electrode and do not have the opportunity to move to the next cell when the field switches. Oval electrodes, on the other hand, work much better. By decreasing the radius of curvature on the sides of the cylinders, the field concentrates there and allows the ions to gather at a point where they can move to either cell when the field switches polarity. This is shown in figure 5.3. Electrodes themselves may not be easy to form into custom shapes and thus it was attempted to shape the electrode insulation such that the field would concentrate at the sides of the electrode-insulator combination. This was done by making the insulator walls thinner at the sides of the electrodes. The electric field is able to locally permeate more easily into the liquid and creates a similar situation as before, where the sides of the electrodes form hotspots with respect to the electric field magnitude.

The walls of the setup were very briefly the subject of investigation. Because of its one-dimensional nature, the experiment can be considered to be a tube or narrow channel with walls on all sides. The material and thickness of these walls greatly affect the field geometry between neighbouring electrode sets. For example, a metallic set of walls would be a very bad idea. No voltage difference can exist within a conductor and thus all of the experiment's walls would be at the same voltage. The only voltage difference would be directly between the electrodes and the walls, which would also be where the only electric field would be. This is demonstrated in figure 5.5. Although the concept of a dielectric constant is not entirely applicable to metals, this value can often be considered to be infinitely large. Choosing a material with a lower dielectric constant than that of water, on the other hand, causes the bulk of the electric field to concentrate within the solution. As mentioned before, water is extremely polarisable and owes its large permittivity to that. Most insulators thus possess a dielectric constant much lower than that of water and are good candidates for the construction of the experiment. These include easy to manufacture plastics such as PVC. The parallel walls of the experiment in the case of a low dielectric constant material also cause a fairly homogeneous field between electrodes, as can be seen in figure 5.6. The individual experiment cells, despite being relatively long and narrow, resemble large parallel plate capacitors thanks to this concentrating effect.

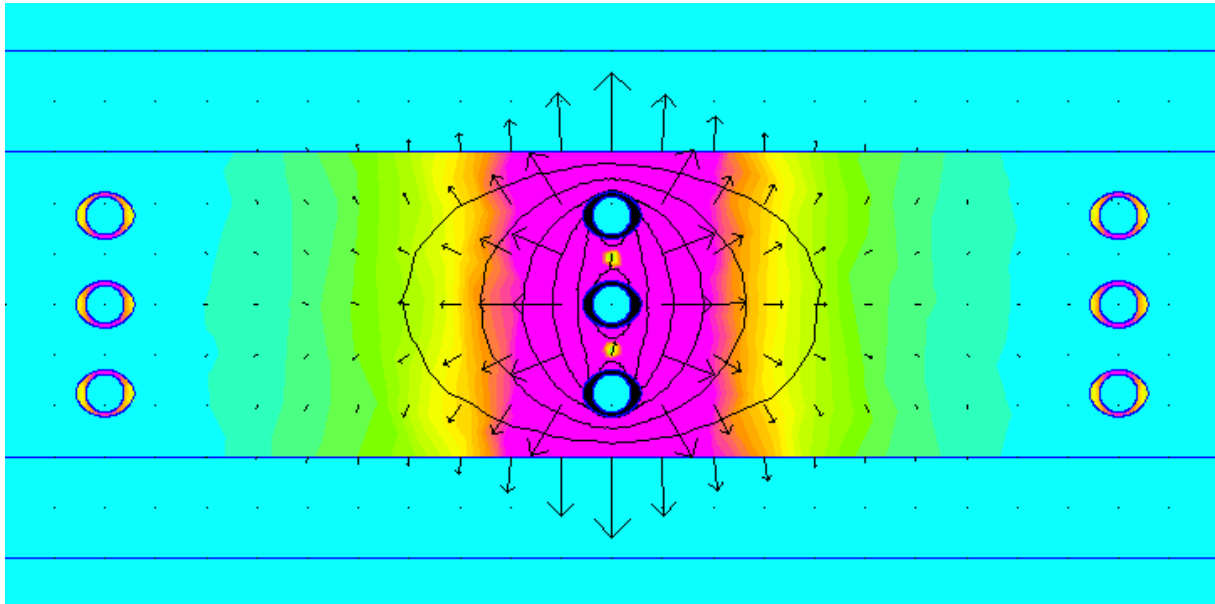


FIGURE 5.5: Electrodes submerged in water with walls made out of metal. The electrode insulation is made of polystyrene and the electric field is denoted qualitatively by colour gradient. The equipotential lines are shown, as well as the electric vector field. Compare these to the ones in figure 5.6.

This makes the naive assumption of  $E = \Delta U/d$  (where  $E$  is the electric field,  $\Delta U$  the voltage difference and  $d$  the distance between electrodes) much more accurate.

As noted before, the proposed experiment does not rely on a single stage separating calcium ions by a large distance, but rather on many small separations over many cells. During electrophoresis, the ion bands spread out into Gaussian distributions. It is the heads and tails of these distributions that are compressed near the electrodes and cut off when the field flips. Because of the difficulty that is involved in describing this behaviour analytically, a program was written to determine whether there could be any enrichment in a tabletop experiment. Two parameters are instrumental in making the experiment a success: the spatial period, dictated by the physical distance between the electrodes, and the temporal period, which is the time after which the field inverts. The latter is the only variable that is adjustable during experimentation and is likely to be the variable that is tuned to produce optimal results. The program thus fixed the spatial period while the temporal period was varied to find the length of time that causes maximal enrichment. A few assumptions are made in the operation of the simulations. These are discussed in the following paragraphs.

The first concerns the effect of the external field on ions in the solution. It is assumed that the average velocity of the ions is directly and instantaneously proportional to the electric field, with a proportionality constant called the electrical mobility:  $\vec{v} = \mu \cdot \vec{E}$ . In reality, the ions exist in a chaotic environment that causes them to move quickly and erratically in all directions. This rapid thermal motion, although much greater in magnitude than the effects of the electric field, almost averages out to zero and manifests itself primarily in the broadening of ion bands. Two effects thus act on the ions at all times and are simulated within the program: the electric force, modeled by a constant velocity granted to all calcium ions, and the random thermal forces, modeled by jumps in random directions. The magnitude of these jumps is dependent on the diffusivity of calcium ions and was taken from literature [59]. Different isotopes of calcium were given a differing velocity according to  $v \sim m^{-0.005}$  as explained in section 2.8, and the base velocity, taken to be the velocity of  $^{40}\text{Ca}$  ions, was also found in literature [36].

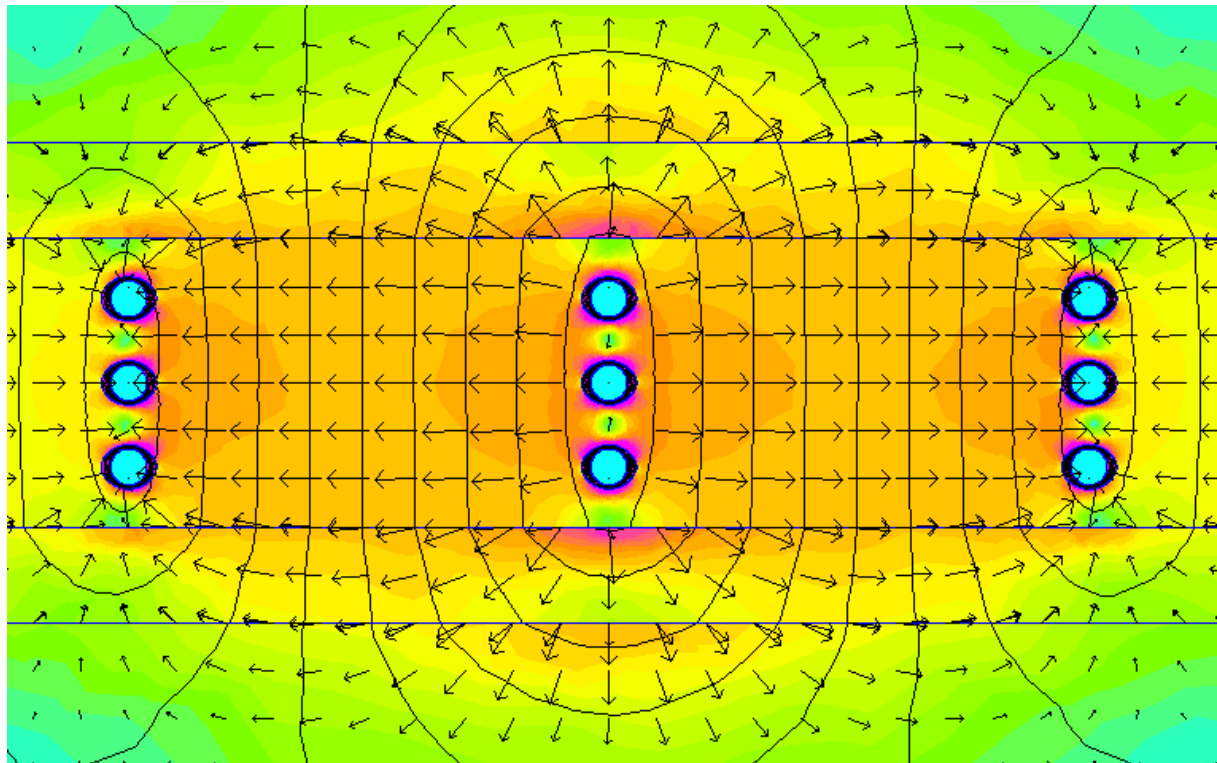


FIGURE 5.6: Electrodes submerged in water with walls and electrode insulation made out of polystyrene. The electric field is denoted qualitatively by colour gradient. Also visible are equipotential lines (solid black lines) and the electric vector field (black arrows). Compare this figure to figure 5.5

The second simplification manifests itself in the setup of the experiment. In reality, the electrodes are enormously thick compared to the size of an ion, necessitating more complex electrodes and electric field configurations to move ions as close to the cell edge as possible. The simulation does not take the thicknesses of the electrodes or the complex electric fields into consideration. One reason for this is that these variables are highly dependent on specific experiment configurations and are likely to differ significantly even within the same experiment. Additionally, it is not likely to matter much in practice. In the case that electric fields concentrate around the sides of the electrodes, ions should be able to enter both adjacent cells after the field switches. Although diffusion is an extremely slow process on larger length scales, ions should spread over millimetres within seconds. In other words, electrodes can be considered to be infinitely thin with reasonable accuracy. A similar argument holds for the simplification of fields into perfectly homogeneous and sharp-edged sections. In the simulation, each cell is assigned a single value for the magnitude of the electric field, equal and opposite to the fields in surrounding cells. Thanks to the infinitely small width of the electrodes, this results in sharp transitions from one region to the next. The reasons for this are the same as before. Firstly, the specific field configuration is highly dependent on the experimental setup and can certainly not be described in a one-dimensional simulation. Secondly, the specifics of the field boundaries are not likely to matter. Only very close to the electrodes the field can be seen to deviate significantly from a perfectly homogeneous one, as can be seen in figure 5.6.

Another assumption that had to be made is much less reasonable. Tens to hundreds of thousands of ions were simulated to accurately reproduce the thermal broadening of calcium bands. The fact that the very heads and tails of these distributions are cut off in the enrichment process means that they have to be well-defined within the simulation. Exactly how many calcium particles were needed for this was determined by trial and error. Because of the great number of individually moving ions, it was found to be impractical to consider the effects of the

ions' electrical charges on the local electric fields. Especially considering the great electric fields that are present within electrolytic solutions, this is a gross oversimplification. As an example of this, consider a single gram of calcium chloride that is separated in a simple parallel plate capacitor filled with water. The electric field that is generated by this can be described as:

$$E = \frac{\Delta U}{d} = \frac{Q}{Cd} = \frac{Q}{\varepsilon A} \quad (5.5)$$

where  $E$  is the electric field magnitude,  $\Delta U$  is the voltage over the capacitor,  $Q$  is the charge collected on one side of the capacitor,  $d$  is the distance between the plates,  $C$  is the capacitance of the capacitor,  $\varepsilon$  is the permittivity of the capacitor dielectric and  $A$  is the area of the capacitor plates. As can be seen, the distance between the capacitor plates  $d$  is not a variable in the final equation because both the electric field and the capacitance are inversely proportional to it. Taking the area of the capacitor plates to be  $5 \text{ cm}^2$  and the permittivity of the dielectric to be that of water, namely  $7.1 \cdot 10^{-10} \text{ F/m}$ , all that remains is to determine the charge at the capacitor plates. One gram of pure  $\text{CaCl}_2$  contains 0.36 grams of calcium atoms, amounting to  $2.2 \cdot 10^{23}$  individual  $\text{Ca}^{2+}$  ions generating a charge of  $6.9 \cdot 10^4 \text{ C}$ . Equation 5.5 then yields  $E = 2.0 \cdot 10^{17} \text{ V/m}$ . Over ten centimetres, this amounts to a voltage of 2 EV (that is exavolts, or  $10^{18}$  volts). Needless to say, these fields and voltages are far from the ones generated in experiments today. For a factor this large, there is surprisingly little information to find in literature. It seems that researchers in the literature cited so far take the migration of ions in an electric field for granted despite the enormous internal fields that are at play between the ions. However, even though in subject to many assumptions, the simulation is still significant. It is known that ions do migrate in an electric field far weaker than the fields present in solution, and it is likewise known that different isotopes have differing migration speeds. This is all that is required for a simplified qualitative analysis.

The simulation is meant to create a reasonably accurate representation of ion movement over time. A step size of one second was used, repositioning all ions at every step. Such a small step size was chosen because it is an intuitive stretch of time that is short enough to allow the temporal period of the experiment to be adjusted with some sensitivity. Additionally, calculating the movement of ions takes up only a small fraction of computation time compared to plotting the ion distributions, so choosing a step size that is very small compared to the total experiment time is not very disadvantageous. This is because the program makes histograms of the ion distributions every ten to thousand steps depending on the total experiment time and simulated field. It does this by collecting the positions of all ions and sorting them into a text file. The produced text files are later plotted using `Gnuplot` to form a timelapse of the simulated experiment. The resolution of the produced ion distribution histograms was set to one millimetre, but the ions can assume much more precise positions, which is especially useful around the infinitely thin electrodes.

The large number of ions that have to be simulated creates an optimisation challenge. By far the most time-costly operation of the program is to collect all the positions of the ions and put them in a text file for plotting. Fortunately, this process is not required at every step. It can be done once every few steps, preferably as often as possible without slowing down the simulation too much. Because the program is meant to provide qualitative insight rather than quantitative analysis, it is important that the simulation is recorded sufficiently throughout its operation. This allows the created histograms to form a coherent film that accurately portrays the behaviour of the experiment. If the electric field were to be updated according to the ion distributions, on the other hand, positions would have to be recorded at every step. Not only do all ion positions need to be determined for this, but the effect on the electric field has to be calculated and applied as well. Even simplified models for determining the effective electric field prolong the computation time immensely.

## Preliminary experiment

A preliminary experiment has been devised that should test a number of matters before a larger experiment can be attempted. It was intended to test the materials used in the experiment, to measure electrophoretic speeds and to investigate whether ions organise themselves under a high electric field. The experimental setup is pictured in section 5.2. It consists of two compartments that each house an aluminium electrode. These electrodes were perforated and then anodised to provide electrical insulation. During the experiment, the compartments can be quickly isolated from each other by a plug valve so that any difference in isotopic ratio between the two parts can be kept in place. Samples can be taken after the voltage between the electrodes has been reduced to zero and it has become safe to alter the experiment. These samples are then analysed by ICP-MS as before. TDS meters can be inserted into the fluid and left operational during the experiment to monitor ion concentrations. It is known that these meters cause disturbances in the electric field and effect an overall decrease in the electric field magnitude, but this effect is believed to be sufficiently small. The bulk of the construction is made from PVC and contains the compartments as well as the valve. It is based on a plate that contains four holes so that the construction may be fastened to a wooden object with screws. The covering plate was chosen to be made out of transparent perspex so that the water level and the exact meter positions could be monitored. It is important that the TDS meters are sufficiently submerged within the fluid since they rely on resistance measurements between fixed electrodes. The plate also houses high voltage connectors that have been precisely positioned so that electrodes are nearest to the outside walls. The ground connections of the two connectors are in electrical contact with each other through a metal strip to provide a common base voltage. During the experiments, one of the electrodes was also connected to this metal strip so that the voltage could be regulated entirely through the other connector.

In order to prevent high electric fields resulting from sharp edges, the holes and edges of the electrodes were chamfered and sanded before anodising. During some experimentation with the oxide thickness resulting from anodisation, it was found that the electrode thickness would grow for the first half hour of treatment as a result of the growing oxidation layer and would then start to decline. This is likely due to the oxidation layer being eaten away by the acid just as fast as it is generated. The underlying aluminium is thus converted to aluminium oxide by electrolysis through the oxide pores, after which it is dissolved by the acid that was used to create the pores in the first place. The end-result is that the oxide layer keeps the same thickness while the aluminium below is eaten away.

Before the main experiments, tests were conducted to determine whether the experimental setup could contain the high electric fields that would be generated by the planned voltages. The limiting factor with regard to the voltage is electrical breakdown that may occur within the system. Electric fields could become sufficiently strong to cause electric arcing through the air or water, creating ionised paths that conduct electricity through otherwise insulating material. Such a diversion of voltage would be detrimental to the experiment, and could even be harmful to the setup, not to mention its operators. For safety reasons, the power supply is equipped with a mechanism that triggers a shutdown if a predetermined current is detected.

Firstly, with just air in the experiment, one electrode was grounded as described before and the other electrode received a slowly increasing voltage. Electric arcing is preceded by a humming noise reminiscent of overhead power lines on humid days, and manifests itself as a soft noise in this experiment. The hum was not heard at any point as the voltage was gradually increased to 2 kV, which had been designated as the maximum for this experiment. Afterwards, the device was cleaned and filled with demineralised water. In order to avoid direct electrical contact with the connector, the water level had a strict upper limit. Above this level, it would reach the clamp with which the electrode was in electrical contact with the connector and would cause electrolysis once voltage would be applied. Despite the anodised electrodes, the safety mechanism engaged as the voltage rose to 550 V. Further testing revealed that the

current at this point had a magnitude of roughly 1.5 mA, but no other signs of a current were detected, such as bubbles of hydrogen gas. It is likely that the minute amounts of electrolysed material were either not visible to the naked eye or immediately dissolved in the water. After the positive electrode was wrapped in electrical tape, the test was repeated with no detectable electrical current up to 2 kV. The TDS meter closest to the ground electrode was then added to the setup and the experiment was repeated. Near 1.7 kV to 1.8 kV, a faint humming noise was heard, signalling an imminent electrical breakdown. With the meter in the other slot near the high voltage electrode, the voltage reached 1.6 kV before a similar noise was heard. The differing breakdown voltages indicate that the setup had lost some of its symmetry through the application of the electrical tape. With both TDS meters inserted, the voltage could safely be increased to 2 kV with no danger of electrical arcing. Instead of concentrating in a single meter, the field in this case is distributed more evenly, making the setup more robust to high voltages.

The preliminary experiment had a number of goals. Firstly, it was intended to test the materials of the electrodes, measurement devices and container in the context of a high voltage experiment. The experiment was intended to produce a strong and homogeneous electric field with no electrolysis or corrosion of the container. Especially the aluminium oxide insulation of the electrodes had been in doubt, but it was also thought that the PVC compartments or perspex covering plate might undergo reactions with a concentrated calcium chloride solution. From reports published online, it was suspected that the latter was not the case: PVC performs well to moderately well in contact with a  $\text{CaCl}_2$  solution [60] and perspex shows “slight attack” after three days in contact with a saturated solution [61].

The second goal of the experiment was to measure electrophoresis speeds. Diffusion, as noted in section 2.8, is an extremely slow process in liquids, taking multiple years to traverse a single metre. What seems to be relatively quick diffusion in everyday processes such as the sweetening of tea is actually effected by convection and turbulence much more than diffusion. It is thus suspected that a difference could be observed between normal diffusion and electrophoresis in the given experiment. The preliminary experiment was first made shock-free and thermally stable. The former was done by screwing the construction into a large plank and then fastening said plank securely to a heavily-laden table. Although this did not provide a completely shock-free environment, it is believed that most disturbing effects were hereby taken away. These include nearby footsteps and opening doors. Because the experiment is quite small and the room is draft-free, no thermostat was deemed necessary to provide thermal stability.

In order to test the difference in speed between thermal diffusion and electrophoresis, one compartment may be filled with a calcium chloride solution while the other contains demineralised water. To test the speed of thermal diffusion, the valve is opened carefully. Because both compartments feature a TDS meter, the concentration can be monitored as a function of time. Once both meters display an equal TDS value, the compartments can be considered to be in equilibrium and the experiment ends. To test the speed of electrophoresis, exactly the same experiment is performed, but with a high voltage over the electrodes. The compartment containing the  $\text{CaCl}_2$  solution is set at a high positive voltage to drive the positively charged calcium ions away. Because of their much higher mobility and smaller charge [36], it is thought that the chloride ions do not impede the calcium atoms much. This presumption is reinforced by the fact that electrophoresis experiments have been performed in the past.

The last goal of the setup is to find an effect akin to the one seen in thermal diffusion, explained in section 2.4. The compartments are connected to each other and the setup is filled with a calcium chloride solution. A high voltage is then applied over the solution for multiple hours, after which the valve is swiftly closed and samples can be taken from the separate compartments. The rationale behind the experiment is that lighter ions may be more influenced by the electric field than heavier ones. This was demonstrated in a previous experiment [41]. It is thus suspected that the calcium ions might order themselves according to weight within a

static field. Once again, it is imperative that all other effects are excluded from the experiment. Simple turbulence and convection are likely to have a much larger effect than the electric field if they are let to run their course. In order to suppress these disruptive effects, the same setup is used as described in this section.

## 5.2 Results

Many of the results shown in this section would initially have been considered part of the process. However, with time it became clear that simulation of the proposed experiment and the design of the preliminary experiment were projects in and of themselves. Their results are documented here.

### Simulation

Many different kinds of simulations were run. The most prominent ones showed the progress of a single enrichment experiment over time. They produced short films that showed the evolution of the ion distributions over time. Although very enlightening, animation does not transfer very well to paper. A single frame is nonetheless shown in figure 5.7 to serve as an example.

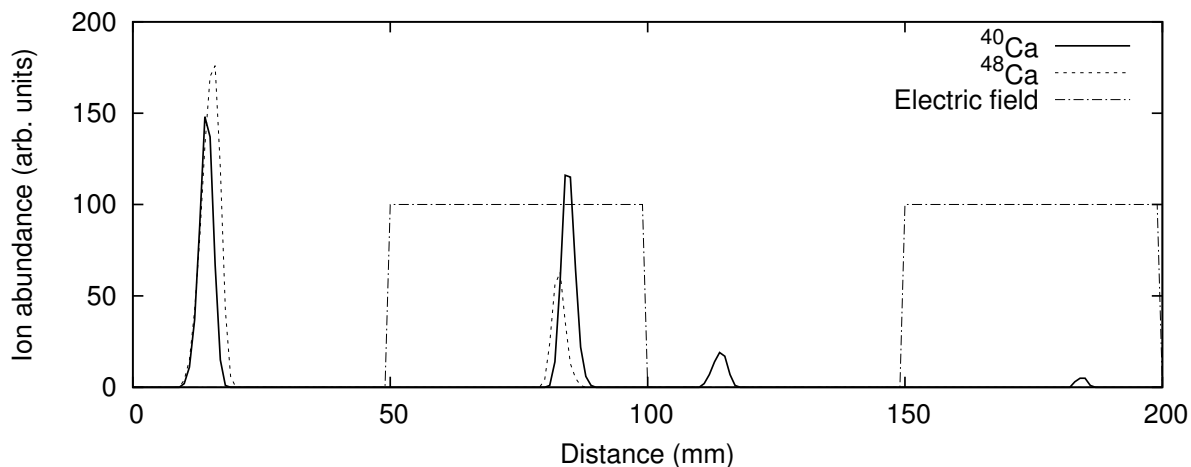


FIGURE 5.7: A frame out of an ion distribution animation. The shown simulation is more than a minute of simulated time under way, with an electric field of 20 V/mm and a switching period of 21 seconds. The electric field has been rescaled so that it fits within the graph: a field of 100 signifies a positive field, making the ions move right, while a field of 0 indicates a negative electric field, moving ions to the left. A wildly exaggerated mass-dependence ( $v \sim m^{-0.3}$ ) has been adopted for clarity.

A range of simulations was run to determine the change in enrichment factor as a function of the field-switch period. The results of two such runs are shown below in figure 5.8. The score is determined by subtraction of the number of  $^{40}\text{Ca}$  ions from the number of  $^{48}\text{Ca}$  ions. Raw data can be found in appendix C.

It can be noted that the second graph in figure 5.8 features error bars while the first does not. This is simply due to the fact that the errors in the first case are so small that they are not visible. They have been included in the raw data presented in appendix C, however. The error margins were generated by performing all simulations five times and comparing the results.

Lastly, the progress of single experiments was plotted to determine the evolution of the enrichment factor over time. One such plot is shown in figure 5.9.

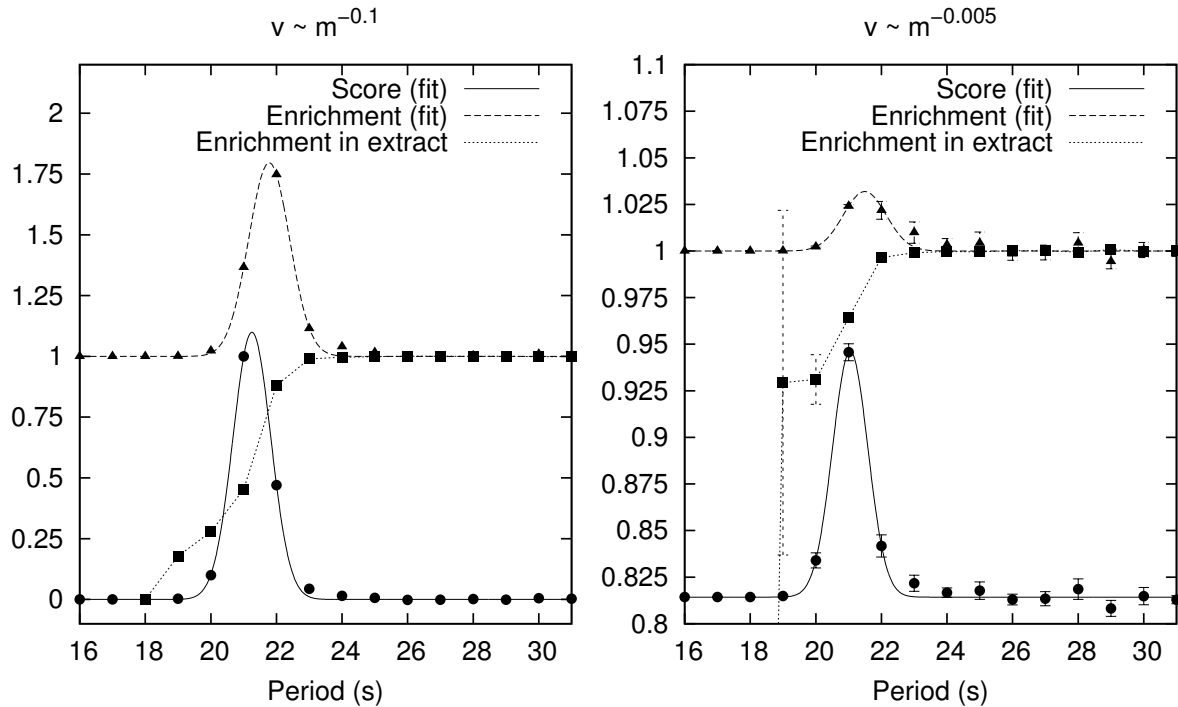


FIGURE 5.8: Enrichment factors in the simulated experiments. Both the enrichment factors within the experiment and those of extracted material are shown and fitted with Gaussian curves. A score value signifies the fitness of each experiment and is shown on an arbitrary scale. Other than the mass-dependence indicated above each graph, experiment parameters were identical to those in figure 5.7, with a total simulated runtime of 2000 seconds or  $\sim 0.56$  hours.

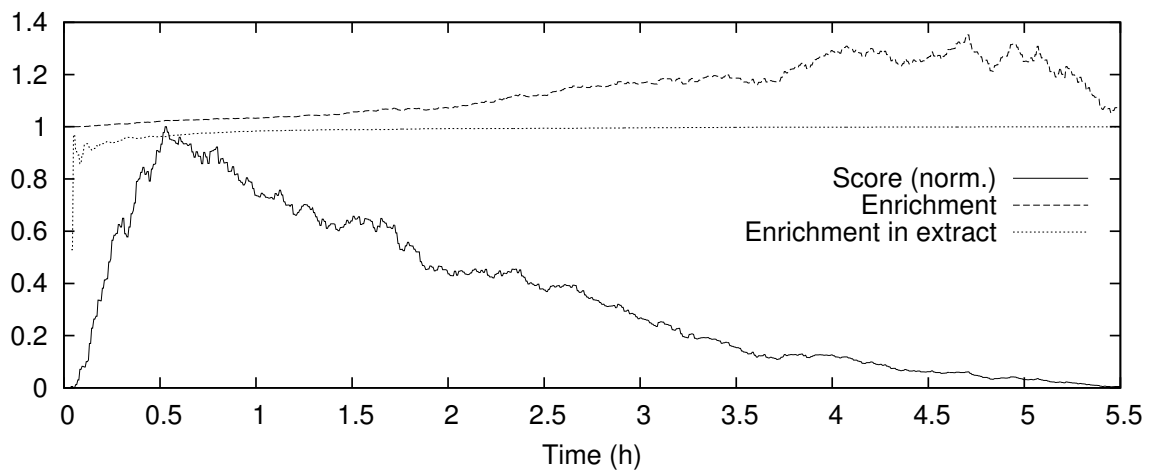


FIGURE 5.9: Enrichment factors of material involved in a simulated experiment. The enrichment factor of material still inside the experiment and that of material that has been extracted are shown side by side. A normalised score function has also been plotted. Parameters are identical to the ones used in figure 5.7, with  $v \sim m^{-0.005}$ .

## Preliminary experiment

The preliminary experiment underwent numerous design phases before a final design was realised. This final model is shown in the following illustrations.

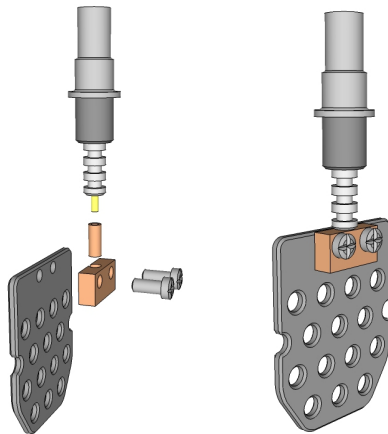


FIGURE 5.10: The electrode and its connection to the high voltage connector. The gold connector pin is squeezed into a copper tube which is then pressed against a bare section of the electrode with two screws.

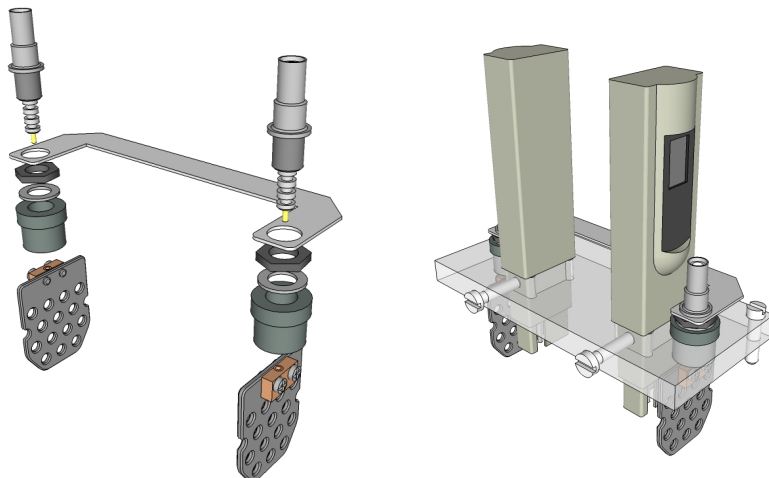


FIGURE 5.11: The grounding plate assembly and covering plate assembly. In the left illustration are shown, from top to bottom, the high voltage electrode, grounding plate, fastening nut and ring, connector seating and electrode assembly. The connector seating contains threading and fastens the connector to the covering plate, as shown in the right illustration. There, two TDS meters are shown along with their fastening screws. The screws that connect the covering plate to the main body are also shown.

Unfortunately, the described experimental setup took such a long time to devise that not many experiments could be performed. Although initially meant to test ion migration time, the TDS meters proved too sensitive to measure appropriate calcium chloride concentrations. However, an experiment was still performed to investigate the effects of an electric field on the distribution of calcium ions in solution. 20.00(5) g calcium chloride was dissolved in 100.0(1) mL water, which was then put under a voltage of 2 kV over 16 hours. The valve was swiftly closed before the voltage was decreased to zero. Samples were taken from the positive and negative compartments and analysed by ICP-MS. The data is shown in figure 5.14 and the raw data can be found in appendix D.

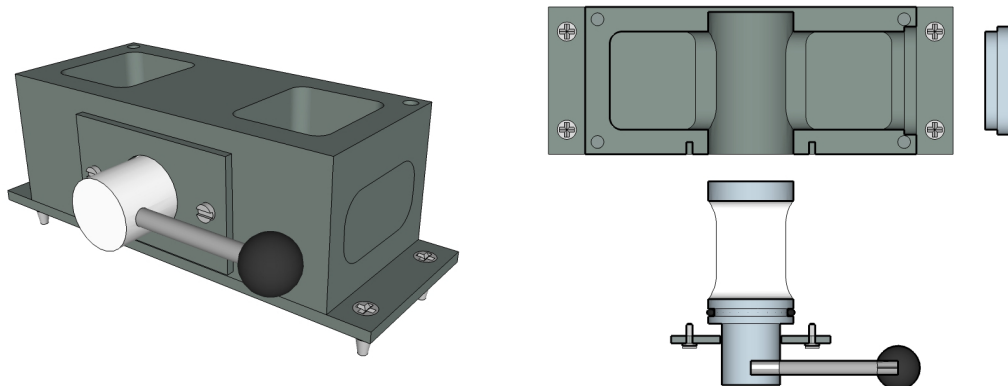


FIGURE 5.12: An overview and horizontal cross-section of the main body of the preliminary experiment. It consists of a compartment housing and a plug valve, as well as several minor components such as a bottom plate, compartment plug and valve holder plate. The latter two are especially visible in the cross-section. The valve handle can be rotated to an upward or downward position to separate the compartments.

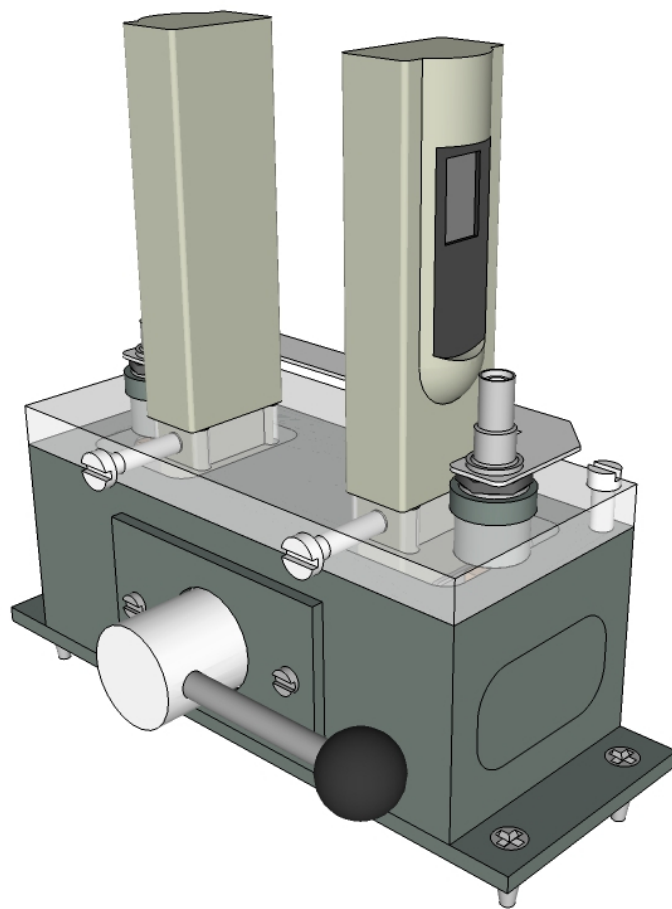


FIGURE 5.13: The final assembly, with the covering plate connected to the main body. The electrodes fit into their respective compartments to form the electric field. Thanks to the thorough encapsulation of the electrodes, the device is safe to handle even under high voltage.

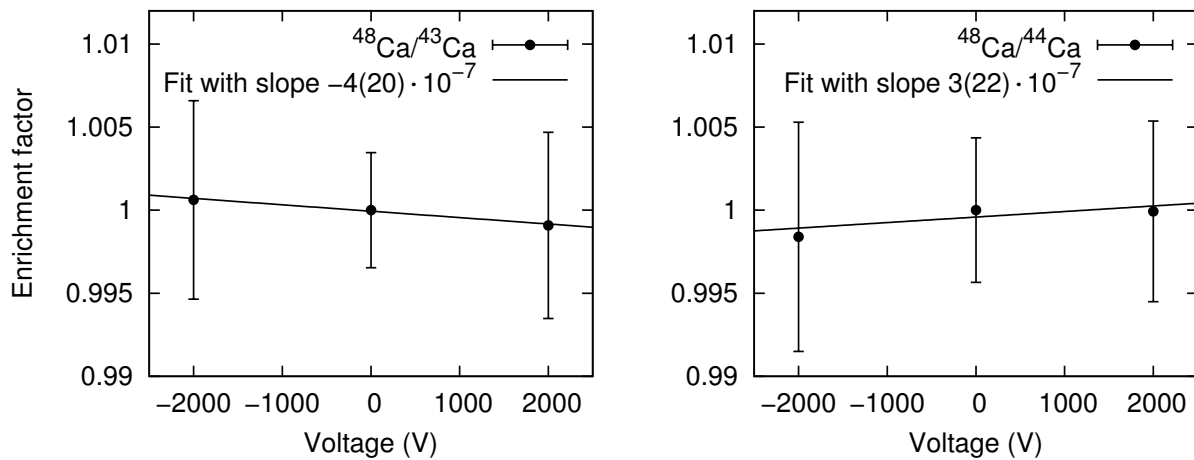


FIGURE 5.14: Enrichment factors for a high voltage experiment in which calcium chloride was left in a 2 kV electric field for almost sixteen and a half hours. The 0 V samples were collected from the initial solution whereas the  $\pm 2000$  V samples were collected from their respective compartments after the experiment had been completed.

### 5.3 Discussion

The experiments pertaining to electrophoresis are quite varied, with some only manifesting themselves in simulations while others occupy themselves with experimental setup. In the following sections, not only are the significance and meaning of the results discussed, but also the thought processes behind many aspects of the experiments.

#### Simulation

Qualitative simulations that show the evolution of ion distributions have helped to understand the behaviour of ions in a periodic electric field. Although single frames such as the one shown in figure 5.7 are not too enlightening, many of these can be put together into a short film that can be very informative. It can be found, for instance, how far the  $^{40}\text{Ca}$  front has advanced relative to the  $^{48}\text{Ca}$  band. Around 80 mm in figure 5.7, it can be seen that  $^{40}\text{Ca}$  has a significant lead over  $^{48}\text{Ca}$ , further enhanced by its larger abundance at that position in the experiment. Naturally, enrichment can readily be spotted in each frame. In the example, it can be seen that there is enrichment of  $^{48}\text{Ca}$  in the first stage of the experiment and depletion in the rest. Past 100 mm, no  $^{48}\text{Ca}$  is visible at all, but this is an effect of the unreasonably high mass-dependence that was adopted for the sake of example.

Two points can be made about the method of simulation, even when a more reasonable mass-dependence is assumed. Firstly, it can be seen that the  $^{40}\text{Ca}$  and  $^{48}\text{Ca}$  ion abundances are on the same order of magnitude. In fact, there are exactly as many ions of each isotope. This was done for ease of plotting and calculation, and does not influence the simulation. After all, effects that calcium ions have on each other were not incorporated into the program. Additionally, simulating the natural isotope abundances would be counterproductive. In the frame shown in figure 5.7, there are  $10^5$  members of each ion species. Adopting the natural abundances, either the number of  $^{48}\text{Ca}$  ions would have to drop to 187, or the number of  $^{40}\text{Ca}$  ions would have to rise to  $5.3 \cdot 10^7$ . The former would be better for computation speed while the latter has better accuracy. In section 5.1 it was explained why it is necessary that a large number of ions is incorporated in the simulation. Because neither of the realistic options is very attractive, it was decided to use equal numbers of  $^{40}\text{Ca}$  and  $^{48}\text{Ca}$  ions.

Secondly, the ion bands shown in the figure are much narrower than would be expected in an actual experiment. It was explained in section 2.8 that thermal diffusion by itself is an extremely slow process, so it is not surprising that a simulation that only takes diffusion into account would produce narrow bands. However, in an actual experiment, it is likely that other effects would cause bands to broaden. These include convection currents and vibrations, which may be caused by something as simple as footsteps or a bump against the table. It is difficult to predict the exact influence of these effects and they differ between different experimental setups. Therefore it was assumed that they cause broadening in a completely random fashion, much like thermal broadening. The final result is a system that operates solely under the effects of thermal diffusion, but with a drastically heightened temperature. In order to be conservative in adding unknown effects to the simulation, the magnitude of broadening was kept below the expected values. It is not expected that this influences the end results qualitatively.

The results shown in figure 5.8 plot the enrichment factor and score of an experiment as a function of the temporal period. Clear peaks can be spotted centering around a period of 21 seconds, around which the enrichment factor in the extracted material rises rapidly from zero to one. This is the material that has reached the end of the simulation, 30 cm from the start. As mentioned before, it is logical that there should be depletion in the extracted material if there is enrichment within the experiment. This simply means that more  $^{40}\text{Ca}$  than  $^{48}\text{Ca}$  ions reach the end in the given time. At periods shorter than 18 seconds, it can be seen that no ions reach the end in the given time. The temporal period is simply too short for any ions to reach the end of the first cell and they stay trapped there. Between 18 and 24 seconds, the fastest calcium ions can reach the end of the cell through a combination of the electric field and the random thermal motion. This is where the enrichment is located, since  $^{40}\text{Ca}$  ions have a slightly higher mobility than  $^{48}\text{Ca}$  and can thus reach the end of the cell in slightly higher numbers. The final regime consists of temporal periods longer than 24 seconds. Here, all ions can reach the end of their run before the field switches. No distinction is therefore made between  $^{40}\text{Ca}$  and  $^{48}\text{Ca}$ , and the enrichment factor returns to unity.

The peaks are quite narrow, indicating that an actual experiment would easily miss them if the scanning resolution were too low. Especially since the parameters of an experiment are likely to be very different from those anticipated in simulation, it would be difficult to find resonance by way of the internal enrichment factor alone. Fortunately, there is another indicator that can be used to find the sweet spot in an experiment. The enrichment factor is highest when there is just a small amount of calcium exiting the experiment. This calcium would ideally be slightly depleted in  $^{48}\text{Ca}$ , but the mere presence of a small amount of calcium exiting is enough indication that the enrichment peak is near.

A balance has to be struck between enrichment and production. Higher enrichment means lower production: as more  $^{40}\text{Ca}$  ions exit the experiment, so too do more  $^{48}\text{Ca}$  ions. In order to avoid having a high enrichment factor but no production volume, the score value was introduced. It is simply the number of  $^{48}\text{Ca}$  ions minus the number of  $^{40}\text{Ca}$  ions still present in the experiment. Because the simulation uses equal numbers of  $^{40}\text{Ca}$  and  $^{48}\text{Ca}$  particles, the score starts at zero and returns to zero once all ions have exited. The peak signifies the point at which the absolute difference between isotope abundances is greatest, which is again around a period of 21 seconds. It is interesting to note, however, that the peak in score does not correspond exactly to the peak in enrichment. This is likely because more material has been removed at the enrichment peak than at the score peak. In figure 5.8, the score data has been rescaled and repositioned to fit within the graphs.

The difference between the two graphs in figure 5.8 is large. In the first one, where  $v \sim m^{-0.1}$ , the enrichment factor reaches values over 1.75 whereas the other graph only comes up to 1.025. The latter is unfortunately closer to the harsh reality of an actual experiment, with a small mass-dependence of  $v \sim m^{-0.005}$ . The small enrichment factor within the device is also reflected in the enrichment factor of the material that exits it. Unlike in the  $v \sim m^{-0.1}$  case, the

enrichment factor of the extracted material rises to unity almost immediately, indicating that the removed material is hardly depleted of  $^{48}\text{Ca}$ .

Figure 5.9 shows the progress of a single enrichment experiment over time. This simulation was performed primarily to investigate how long an experiment could be left to run without emptying itself of all calcium, but it also shows other interesting aspects of the process. It can be seen that the enrichment in the extract goes to unity extremely quickly, indicating that the enrichment is not performed very efficiently. Nonetheless, especially after four hours of operation, the enrichment within the experiment has gotten to be quite high, even though the mass-dependence of the ion velocity was set to be realistically small. The plotted score shows that the absolute difference between the ion species has decreased drastically by that point, however, indicating that there is very little calcium left within the device.

Both production and enrichment can be found at the peak of the score curve, which centres a bit over half an hour. Because this corresponds to roughly 2000 seconds, figure 5.8 can be used as a reference to determine the enrichment factor more accurately. Looking at the point generated for a period of 21 seconds, it can be seen that the enrichment factor at that point amounts to 1.025.

## Preliminary experiment

For the preliminary experiment, there were two basic requirements. The first was that the system should be able to generate an intense electric field over approximately ten centimetres without posing a threat to the operator. The second was that the liquid inside the system should be able to be divided into two parts, with one part belonging to one electrode while the other belonged to the other electrode. These demands proved difficult to meet in conjunction.

For the safe generation of an intense electric field, it is advantageous to shield the electrodes from the outside world as much as possible. This was realised by enveloping them in a structure of PVC and perspex, none of which are conductive. The electrodes were attached to high voltage connectors that prevent current leakage. Because aluminium is difficult to solder, screws were fitted into holes that were drilled into the anodised aluminum. The section of the electrode between the screw holes was then sanded to locally eliminate the insulating aluminium oxide layer and a copper construction with the high voltage connector squeezed inside was pressed against the aluminium by the screws. The process is shown in figure 5.10.

In order to keep the electrodes safely out of reach during operation, the electrode-connector assembly was further shielded by a perspex plate. This plate would not only separate the electrode fully from the connector, but would also serve as a covering plate for the experiment. In figure 5.11, it can be seen that TDS metres were also inserted into this covering plate and held at the appropriate height with teflon screws. Two more such screws allowed the covering plate to be attached to construction that would hold the liquid. The same figure shows how the ground connections of the two connectors were brought into contact with each other through a metal strip.

The final insulating feature of the experiment was the base and main body. This base was to hold the calcium chloride solution and connect to the covering plate to form a closed object. Another main feature of the construction was the valve mechanism. Many different types of valves were considered, such as a gate valve, iris valve and diaphragm valve. However, these were difficult to reconcile with the requirements that the insulating enclosure needed to be preserved and the valve needed to separate the two compartments quickly and without too much turbulence. For example, the gate valve is difficult to make water tight and would always stick out of the construction when in the opened position. Iris valves, on the other hand, would likely be too slow to close without offering a convincing guarantee of being water tight. A custom valve was considered, in which two combs would slide against each other to provide a seal with very little movement. The expected construction difficulties were formidable, however, and eventually a plug valve was used instead. This type of valve consists of a cylinder

that can be made to rotate in place by way of a lever located outside of the construction. Because the cylinder contains a large gap, it can be rotated such that it creates a channel from one compartment to the other. It can be rotated back to an orientation that closes the connection after the experiment has been completed. Although this does create some turbulence within the solution, it is expected that the seal is created quickly enough to avoid extensive remixing. The main body with valve is shown in figure 5.12 and the entire construction assembled is showcased in figure 5.13.

Unfortunately, the experiment itself is much more exciting than its results, which are presented in figure 5.14 along with linear fits. It can be seen that the enrichment factors do not deviate from unity very much and that the error margins are considerable. This ensures that no hard conclusions can be made based on these results. Indeed, if an isotope-dependent effect exists at all, it must be quite small.



# Chapter 6

## Conclusions

The project investigated a wide range of possibilities for the enrichment of calcium, both in literature and experiment, with the goal of finding an enrichment method to produce large amounts of calcium rich in the isotope  $^{48}\text{Ca}$ . Motivation for this study came from the CANDLES project, which aims to investigate neutrinoless double beta decay using large amounts of the isotope. Enrichment methods were thus required to be reasonably fast and cheap per unit calcium processed. Thanks to the exceptionally large mass difference between the desired  $^{48}\text{Ca}$  isotope and the dominant  $^{40}\text{Ca}$  isotope, it was initially expected that the study would produce promising results.

The findings of different portions of the project have been documented within their respective chapters. Three main subjects were studied in total:

- Mineralisation has shown mild promise. Despite not featuring large enrichment factors, significant trends in the results are considered to be especially interesting because of the pre-existing mineralisation industry, currently used for the mass-production of calcium chloride flakes.
- Ion exchange resins have produced the highest enrichment factors in this study. Although it was already known from literature that expensive crown ethers show isotopic preference, the current study found that much cheaper polystyrene sulfonate resins likewise produce significant results. Again, this is especially interesting because of the widespread use of the resins in large-scale industries, such as water purification.
- Electrophoresis was the most technically challenging subject of the study and did not come to complete experimental fruition. Moreover, the experimental results that were yielded by the preliminary experiment showed no enrichment. Nevertheless, simulations have shown that enrichment in the proposed scheme is a real possibility.

As is often the case, more research is needed before definite conclusions may be drawn. The results of all experiments but the preliminary experiment are encouraging, but are either small with large errors, as in the mineralisation case, large and inconsistent, such as the ion exchange resin results, or purely produced by simulations, as most electrophoresis results are. Especially in need of clarification are the ambiguous mineralisation and ion exchange resin results, the enrichment rates of which could be quite high.

Shortcomings of the study can be summarised in three points. The first is that all experiments are by necessity of tabletop scale. Although the project is meant to find a method suitable for mass-production, no such trials could be attempted, nor could any experiment easily be attempted that requires special laboratory glassware, such as a chromatographic column. The second shortcoming is the absence of  $^{40}\text{Ca}$  isotope measurements. This is entirely inherent to the ICP-MS, which uses  $^{40}\text{Ar}$ . Using a thermal ionisation mass spectrometer (TIMS) would allow for the measurement of the lightest calcium isotope. The third shortcoming is the scarcity of experiments in the electrophoresis section. Despite devoting a large amount of time to the subject, only a few concrete results were achieved.

Future experiments could therefore improve upon the current study by performing more decisive experiments. To this end, more accurate measuring equipment could be used, and a

TIMS could be used instead of the  $^{40}\text{Ar}$ -based ICP-MS. Ion exchange experiments have yielded unexpectedly high enrichment factors and could be built upon further. The electrophoresis experiments outlined in section 2.8 could also be attempted, although they remain technically challenging.

Several small-scale calcium enrichment experiments of varying complexity have been performed over the course of a year and have yielded encouraging results. The simple methods demonstrated provide powerful tools for the cheap bulk procurement of low-enriched calcium, potentially finding use in the creation of superheavy nuclei and the search for neutrinoless double beta decay.

# Appendix A

## Mineralisation data

The following tables include the complete and processed data from the mineralisation experiments.

TABLE A.1: Mass spectrometry data from the first mineralisation experiment.

Sample	$^{43}\text{Ca (ppb)}_{\text{std}}$	$^{44}\text{Ca (ppb)}_{\text{std}}$	$^{46}\text{Ca (ppb)}_{\text{std}}$	$^{48}\text{Ca (ppb)}_{\text{std}}$
Water	$47 \pm 20$	$48 \pm 21$	$-3832 \pm 1047$	$35 \pm 24$
Water	$9.0 \pm 0.5$	$10.7 \pm 0.4$	$-2348 \pm 659$	$-0.3 \pm 4$
Stock $\text{CaCl}_2$	$16010 \pm 158$	$16100 \pm 159$	$13510 \pm 1190$	$15680 \pm 144$
Stock $\text{CaCl}_2$	$16310 \pm 176$	$16350 \pm 223$	$13650 \pm 505$	$15930 \pm 196$
Intermediate	$6022 \pm 60$	$6119 \pm 93$	$4033 \pm 987$	$5856 \pm 99$
Intermediate	$6058 \pm 38$	$6171 \pm 46$	$3498 \pm 771$	$5891 \pm 33$
Intermediate	$6907 \pm 70$	$7003 \pm 89$	$3887 \pm 134$	$6705 \pm 50$
Product	$7134 \pm 76$	$7226 \pm 73$	$5309 \pm 780$	$6950 \pm 76$
Product	$7089 \pm 75$	$7188 \pm 61$	$4361 \pm 387$	$6904 \pm 91$
Product	$7268 \pm 21$	$7351 \pm 27$	$4897 \pm 1024$	$7049 \pm 15$

TABLE A.2: Mass spectrometry data from the second mineralisation experiment.

Stage	$^{43}\text{Ca (ppb)}_{\text{std}}$	$^{44}\text{Ca (ppb)}_{\text{std}}$	$^{46}\text{Ca (ppb)}_{\text{std}}$	$^{48}\text{Ca (ppb)}_{\text{std}}$
-1	$45220 \pm 590$	$45070 \pm 610$	$43790 \pm 649$	$44260 \pm 576$
-1	$44620 \pm 141$	$44470 \pm 149$	$42360 \pm 568$	$43770 \pm 95$
-1	$45080 \pm 307$	$44850 \pm 289$	$43240 \pm 469$	$43980 \pm 237$
-1	$45060 \pm 288$	$44840 \pm 254$	$43090 \pm 461$	$44020 \pm 328$
2	$25240 \pm 115$	$25170 \pm 75$	$23540 \pm 342$	$24520 \pm 78$
2	$25360 \pm 251$	$25410 \pm 251$	$23420 \pm 233$	$24680 \pm 289$
2	$25160 \pm 135$	$25090 \pm 151$	$23360 \pm 334$	$24450 \pm 129$
2	$25370 \pm 234$	$25370 \pm 188$	$23300 \pm 487$	$24670 \pm 219$
3	$29580 \pm 179$	$29480 \pm 169$	$27860 \pm 444$	$28770 \pm 196$
3	$29610 \pm 176$	$29480 \pm 147$	$27390 \pm 256$	$28810 \pm 195$
3	$29730 \pm 142$	$29630 \pm 192$	$28090 \pm 306$	$28940 \pm 120$
3	$29670 \pm 99$	$29590 \pm 142$	$27420 \pm 112$	$28920 \pm 114$
5	$35720 \pm 200$	$35500 \pm 247$	$33820 \pm 357$	$34810 \pm 213$
5	$35670 \pm 131$	$35500 \pm 113$	$33500 \pm 106$	$34690 \pm 133$
5	$35870 \pm 157$	$35670 \pm 181$	$33830 \pm 364$	$34920 \pm 167$
5	$35720 \pm 193$	$35680 \pm 175$	$33640 \pm 96$	$34870 \pm 145$



## Appendix B

### Ion exchange resin data

TABLE B.1: Mass spectrometry data from the first ion exchange experiment.

Experiment	$^{43}\text{Ca}$ (ppb) <sub>std</sub>	$^{44}\text{Ca}$ (ppb) <sub>std</sub>	$^{46}\text{Ca}$ (ppb) <sub>std</sub>	$^{48}\text{Ca}$ (ppb) <sub>std</sub>
1	$215.2 \pm 2.0$	$213 \pm 5$	$3526 \pm 812$	$225 \pm 8$
1	$219 \pm 5$	$214 \pm 4$	$3471 \pm 601$	$220 \pm 6$
1	$210.3 \pm 2.0$	$209 \pm 4$	$3605 \pm 691$	$219 \pm 4$
1	$220 \pm 5$	$216 \pm 4$	$3952 \pm 828$	$222 \pm 4$
2	$358.8 \pm 2.9$	$353.1 \pm 2.8$	$3730 \pm 695$	$362.5 \pm 2.3$
2	$371 \pm 7$	$368 \pm 9$	$4961 \pm 629$	$373 \pm 10$
2	$2847 \pm 273$	$2873 \pm 288$	$5955 \pm 803$	$2883 \pm 290$
2	$2884 \pm 299$	$2912 \pm 304$	$6997 \pm 452$	$2919 \pm 300$

TABLE B.2: Mass spectrometry data from the second ion exchange experiment.

Added resin (g)	$^{43}\text{Ca}$ (ppb) <sub>std</sub>	$^{44}\text{Ca}$ (ppb) <sub>std</sub>	$^{46}\text{Ca}$ (ppb) <sub>std</sub>	$^{48}\text{Ca}$ (ppb) <sub>std</sub>
$0.00 \pm 0.05$	$31120 \pm 246$	$33110 \pm 288$	$26930 \pm 318$	$31200 \pm 243$
$0.00 \pm 0.05$	$50210 \pm 672$	$53390 \pm 760$	$49620 \pm 1155$	$50750 \pm 689$
$2.00 \pm 0.05$	$30130 \pm 606$	$32250 \pm 663$	$25640 \pm 962$	$30220 \pm 668$
$2.00 \pm 0.05$	$30320 \pm 340$	$32470 \pm 389$	$25760 \pm 776$	$30400 \pm 336$
$4.00 \pm 0.05$	$24520 \pm 240$	$26370 \pm 262$	$20430 \pm 416$	$24580 \pm 202$
$4.00 \pm 0.05$	$24510 \pm 693$	$26330 \pm 726$	$19300 \pm 1053$	$24520 \pm 686 =$
$5.60 \pm 0.05$	$23940 \pm 659$	$25890 \pm 742$	$18330 \pm 1243$	$24010 \pm 650$
$5.60 \pm 0.05$	$24020 \pm 306$	$26100 \pm 353$	$18030 \pm 895$	$24090 \pm 254$
$6.00 \pm 0.05$	$19310 \pm 408$	$21090 \pm 473$	$11790 \pm 1383$	$19320 \pm 418$
$6.00 \pm 0.05$	$19590 \pm 239$	$21450 \pm 319$	$12440 \pm 898$	$19590 \pm 233$

TABLE B.3: Mass spectrometry data from the third and final ion exchange experiment.

Added resin (g)	$^{43}\text{Ca}$ (ppb) <sub>std</sub>	$^{44}\text{Ca}$ (ppb) <sub>std</sub>	$^{46}\text{Ca}$ (ppb) <sub>std</sub>	$^{48}\text{Ca}$ (ppb) <sub>std</sub>
$0.00 \pm 0.05$	$17900 \pm 54$	$17770 \pm 117$	$17250 \pm 594$	$18000 \pm 147$
$0.00 \pm 0.05$	$17180 \pm 54$	$17370 \pm 66$	$15760 \pm 248$	$17250 \pm 42$
$4.00 \pm 0.05$	$7004 \pm 46$	$7137 \pm 49$	$6152 \pm 514$	$7019 \pm 42$
$4.00 \pm 0.05$	$6713 \pm 71$	$6952 \pm 86$	$5811 \pm 311$	$6729 \pm 85$
$6.00 \pm 0.05$	$2329 \pm 7$	$2183 \pm 18$	$1970 \pm 159$	$2331 \pm 18$
$6.00 \pm 0.05$	$2264 \pm 14$	$2117 \pm 6$	$1528 \pm 74$	$2256 \pm 5$
$10.00 \pm 0.05$	$882 \pm 8$	$812 \pm 7$	$258 \pm 233$	$870 \pm 13$
$10.00 \pm 0.05$	$866 \pm 7$	$798 \pm 5$	$387 \pm 227$	$870 \pm 14$



## Appendix C

### Simulation data

The following simulation data was acquired using  $10^5$   $^{40}\text{Ca}$  and  $10^5$   $^{48}\text{Ca}$  particles.

TABLE C.1: Data from a simulation in which the ion velocity is dependent on mass according to  $v \sim m^{-0.1}$ . Enrichment values pertain to the isotope  $^{48}\text{Ca}$  relative to  $^{40}\text{Ca}$ .

Period (s)	Score	Enrichment	Enr. in extract
16	$0 \pm 0$	$1 \pm 0$	
17	$0 \pm 0$	$1 \pm 0$	
18	$0.0 \pm 0.3$	$1 \pm 0$	0
19	$72 \pm 10$	$1.00072 \pm 0.00010$	$0.18 \pm 0.03$
20	$2190 \pm 124$	$1.0226 \pm 0.0013$	$0.279 \pm 0.006$
21	$21917 \pm 65$	$1.3660 \pm 0.0014$	$0.453 \pm 0.006$
22	$10307 \pm 75$	$1.748 \pm 0.006$	$0.8805 \pm 0.0009$
23	$962 \pm 47$	$1.115 \pm 0.006$	$0.9895 \pm 0.0005$
24	$325 \pm 74$	$1.040 \pm 0.009$	$0.9965 \pm 0.0008$
25	$136 \pm 47$	$1.016 \pm 0.005$	$0.9985 \pm 0.0005$
26	$-46 \pm 63$	$0.995 \pm 0.007$	$1.0005 \pm 0.0007$
27	$-30 \pm 68$	$0.997 \pm 0.007$	$1.0003 \pm 0.0008$
28	$30 \pm 40$	$1.003 \pm 0.004$	$0.9997 \pm 0.0004$
29	$-22 \pm 65$	$0.998 \pm 0.005$	$1.0003 \pm 0.0007$
30	$117 \pm 39$	$1.009 \pm 0.003$	$0.9987 \pm 0.0004$
31	$59 \pm 32$	$1.004 \pm 0.002$	$0.9993 \pm 0.0004$

TABLE C.2: Data from a simulation in which the ion velocity is dependent on mass according to  $v \sim m^{-0.005}$ .

Period (s)	Score	Enrichment	In extract
16	$0 \pm 0$	$1 \pm 0$	
17	$0 \pm 0$	$1 \pm 0$	
18	$0.6 \pm 0.4$	$1 \pm 0$	0
19	$7 \pm 7$	$1 \pm 0$	$0.93 \pm 0.09$
20	$216 \pm 44$	$1.0022 \pm 0.0005$	$0.931 \pm 0.013$
21	$1438 \pm 50$	$1.0241 \pm 0.0008$	$0.9642 \pm 0.0013$
22	$301 \pm 65$	$1.022 \pm 0.005$	$0.9965 \pm 0.0008$
23	$82 \pm 47$	$1.010 \pm 0.006$	$0.9991 \pm 0.0005$
24	$26 \pm 27$	$1.003 \pm 0.003$	$0.9997 \pm 0.0003$
25	$38 \pm 51$	$1.004 \pm 0.006$	$0.9996 \pm 0.0006$
26	$-14 \pm 31$	$0.998 \pm 0.003$	$1.0002 \pm 0.0003$
27	$-10 \pm 42$	$0.999 \pm 0.004$	$1.0001 \pm 0.0005$
28	$47 \pm 60$	$1.004 \pm 0.005$	$0.9995 \pm 0.0007$
29	$-66 \pm 47$	$0.994 \pm 0.004$	$1.0008 \pm 0.0005$
30	$6 \pm 51$	$1.0005 \pm 0.004$	$0.9999 \pm 0.0006$
31	$-16 \pm 24$	$0.9988 \pm 0.0018$	$1.00018 \pm 0.00027$



## Appendix D

### Static electric field data

TABLE D.1: Mass spectrometry data from the static electric field experiment.

Voltage (V)	$^{43}\text{Ca}$ (ppb) <sub>std</sub>	$^{44}\text{Ca}$ (ppb) <sub>std</sub>	$^{46}\text{Ca}$ (ppb) <sub>std</sub>	$^{48}\text{Ca}$ (ppb) <sub>std</sub>
2000	$21520 \pm 68$	$21730 \pm 82$	$19770 \pm 435$	$21620 \pm 64$
2000	$21550 \pm 127$	$21810 \pm 65$	$19340 \pm 220$	$21720 \pm 151$
0	$23040 \pm 66$	$23280 \pm 98$	$20910 \pm 369$	$23190 \pm 87$
0	$22870 \pm 29$	$23170 \pm 55$	$21230 \pm 113$	$23050 \pm 6$
-2000	$21810 \pm 132$	$22090 \pm 154$	$19520 \pm 97$	$21970 \pm 153$
-2000	$21730 \pm 61$	$22060 \pm 122$	$19370 \pm 487$	$21910 \pm 111$



# Bibliography

- [1] B. R. Martin. *Nuclear and Particle Physics: An Introduction*. 2007.
- [2] J. Grumann et al. "Investigation of the stability of superheavy nuclei around Z=114 and Z=164". In: *Zeitschrift für Physik* 228.5 (1969), pp. 371–386.
- [3] E. H. Ibe. *Terrestrial Radiation Effects in ULSI Devices and Electronic Systems*. 2015, pp. 23–25.
- [4] J. Suhonen and O. Civitarese. "Weak-interaction and nuclear-structure aspects of nuclear double beta decay". In: *Physics Reports* 300 (1998), pp. 123–214.
- [5] A. Dueck, W. Rodejohann, and K. Zuber. "Neutrinoless double beta decay, the inverted hierarchy, and precision determination of  $\theta_{12}$ ". In: *Physical Review* 83 (2011).
- [6] S. R. Elliott and P. Vogel. "Double Beta Decay". In: *Annual Review of Nuclear particle Science* (2002).
- [7] M. Auger et al. "The EXO-200 detector, part I: detector design and construction". In: *Journal of Instrumentation* 7 (May 2012).
- [8] M. Sisti et al. "Status of the CUORE and results from the CUORE-0 neutrinoless double beta decay experiments". In: *Nuclear Physics B Proceedings Supplement* (Feb. 2015).
- [9] M. Agostini et al. "Production, characterization and operation of  $^{76}\text{Ge}$  enriched BEGe detectors in GERDA". In: *The European Physical Journal C* 75.39 (Feb. 2015).
- [10] A. Barabash. "SuperNEMO double beta decay experiment". In: *Journal of Physics: Conference Series* 375 (2012).
- [11] S. Umehara et al. "Search for Neutrino-less Double Beta Decay with CANDLES". In: *Physics Procedia* 61 (2015), pp. 283–288.
- [12] B. C. Reed. "Centrifugation during the Manhattan Project". In: *Physics in Perspective* 11 (2009), pp. 426–441.
- [13] Alex Wellerstein. *Zippe's Centrifuges*. <http://blog.nuclearsecrecy.com/tag/proliferation/page/2/>. Accessed: 16-8-2016. 2012.
- [14] A. J. Dempster. "A New Method of Positive Ray Analysis". In: *Physical Review* 11.4 (Apr. 1918).
- [15] T. R. Mazur. *Magnetically Activated and Guided Isotope Separation*. Nov. 2015.
- [16] J. R. Oppenheimer. *Magnetic Shims*. US2719924 A. 1945.
- [17] L. Beaton. "The slow-down in nuclear explosive production". In: *New Scientist* 309 (Oct. 1962), pp. 141–143.
- [18] Committee on Decontamination and Decommissioning of Uranium Enrichment Facilities. *Affordable Cleanup? Opportunities for cost reduction in the decontamination and decommissioning of the nation's uranium enrichment facilities*. National Academy Press, 1996.
- [19] IBI Labs. *Uranium Hexafluoride*. <http://ibilabs.com/uranium-uranyl-thorium-compounds/uranium-compounds/uranium-hexafluoride>. Accessed: 9-8-2016.
- [20] Portsmouth/Paducah Project Office. *Paducah Gaseous Diffusion Plant Transition*. <http://energy.gov/pppo/paducah-gaseous-diffusion-plant-transition>. Accessed: 9-8-2016.

- [21] W. H. Furry and R. Clark Jones. "The Separation of Isotopes by Thermal Diffusion". In: *Reviews of Modern Physics* 18.2 (Apr. 1946), pp. 151–224.
- [22] A. S. Krass et al. *Uranium Enrichment and Nuclear Weapon Proliferation*. 1983.
- [23] T. Partanen. *Cascade Profile Calculator*. <http://www.tm-partanen.site88.net/index.php>. Accessed: 9-8-2016.
- [24] Corning Incorporated. *Calcium Fluoride CaF<sub>2</sub> - Physical and Chemical Properties*. [https://lightmachinery.com/media/1542/h0607\\_caf2\\_product\\_sheet.pdf](https://lightmachinery.com/media/1542/h0607_caf2_product_sheet.pdf). Accessed: 9-8-2016. 2003.
- [25] A. A. Zavitsas. "Aqueous Solutions of Calcium Ions: Hydration Numbers and the Effect of Temperature". In: *The Journal of Physical Chemistry B* 109.43 (Sept. 2005), pp. 20636–20640.
- [26] T. Megyes et al. "Solvation of Calcium Ion in Polar Solvents: An X-ray Diffraction and ab Initio Study". In: *The Journal of Physical Chemistry A* 108 (Mar. 2004), pp. 7261–7271.
- [27] S. Umehara et al. "Chromatographic Separation of Calcium Isotopes using Benzo-18-Crown-6-Ether Resin and Acetic Acid Solution". In: *Austin Chromatography* 3.1 (Mar. 2016).
- [28] C. J. Pedersen. "Cyclic Polyethers and Their Complexes with Metal Salts". In: *Journal of the American Chemical Society* 89.26 (Dec. 1967), pp. 7017–7036.
- [29] DOWEX<sup>TM</sup> Ion Exchange Resins. Tech. rep. The Dow Chemical Company, 2015.
- [30] Smokefoot. *idealized image of water softening by cation exchange*. <https://en.wikipedia.org/wiki/File:CationExchCartoon.png>. Accessed: 9-8-2016. 2013.
- [31] L. Paar, J. Elbert, and K. Manfredi. *Organic Chemistry Laboratory Experiments for Organic Chemistry Laboratory*. 2008.
- [32] SACHEM. *Displacement Chromatography 101*. <http://sacheminc.com/solutions/biotechnology/displacement-chromatography-101/>. Accessed: 9-8-2016.
- [33] COMSOL. *Diffusion Coefficient*. <https://www.comsol.nl/multiphysics/diffusion-coefficient>. Accessed: 9-8-2016. 2016.
- [34] THERMOPEDIA. *Diffusion Coefficient*. <http://www.thermopedia.com/content/696/>. Accessed: 9-8-2016. 2011.
- [35] College of DuPage. <http://bio1151.nicerweb.com/Locked/media/ch20/electrophoresis.html>. Accessed: 9-8-2016.
- [36] C. A. Vincent. "The Motion of Ions in Solution under the Influence of an Electric Field". In: *Journal of Chemical Education* 53.8 (1976), pp. 490–493.
- [37] I. C. Bourg et al. "Isotopic mass dependence of metal cation diffusion coefficients in liquid water". In: *Geochimica et Cosmochimica Acta* 74.8 (Apr. 2010), pp. 2249–2256.
- [38] B. van Zeghbroeck. *Principles of Semiconductor Devices*. Feb. 2002.
- [39] Beckman Coulter. *Introduction to Capillary Electrophoresis*.
- [40] J. R. Glynn Jr. et al. "Capillary Electrophoresis Measurements of Electrophoretic Mobility for Colloidal Particles of Biological Interest". In: *Applied and Environmental Microbiology* 64.7 (1998), pp. 2572–2577.
- [41] T. Kishimoto et al. "Calcium isotope enrichment by means of multi-channel counter-current electrophoresis for the study of particle and nuclear physics". In: *Progress of Theoretical and Experimental Physics* 33.3 (Mar. 2015).
- [42] N. Gussone et al. "Model for kinetic effects on calcium isotope fractionation ( $\delta^{44}\text{Ca}$ ) in inorganic aragonite and cultured planktonic foraminifera". In: *Geochimica et Cosmochimica Acta* 67.7 (Oct. 2002).

- [43] T. F. N  gler et al. "The  $\delta^{44}\text{Ca}$ -temperature calibration on fossil and cultured Globigerinoides sacculifer: New tool for past sea surface temperatures". In: *Geochemistry Geophysics Geosystems* 1 (Sept. 2000).
- [44] J. Skulan and D. J. DePaolo. "Calcium isotope fractionation between soft and mineralized tissues as a monitor of calcium use in vertebrates". In: *Proceedings of the National Academy of Sciences* 96.24 (Nov. 1999).
- [45] Minerals Technologies. *What is PCC — Precipitated Calcium Carbonate?* <http://www.mineralstech.com/Pages/SMI/Precipitated-Calcium-Carbonate-%28PCC%29.aspx>. Accessed: 9-8-2016.
- [46] W. A. Shaw. *Fundamentals of Zero Liquid Discharge System Design*. <http://www.powermag.com/fundamentals-of-zero-liquid-discharge-system-design/>. Accessed: 29-9-2016. 2011.
- [47] S. Umehara et al. In: *Progress of Theoretical and Experimental Physics* (May 2015).
- [48] K. Gericke. *Vibrational states and spectra of diatomic molecules*. [http://www pci.tu-bs.de/aggericke/PC4e/Kap\\_III/Vibration.htm](http://www pci.tu-bs.de/aggericke/PC4e/Kap_III/Vibration.htm). Accessed: 10-8-2016. 2008.
- [49] B. Stuart. *Infrared Spectroscopy: Fundamentals and Applications*. 2004.
- [50] J. B. Lambert. *Introduction to Organic Spectroscopy*. 1987.
- [51] M. Menes. * lectromigration en sels fondus et application   la s paration des isotopes des elements alcalins et alcalino-terreux*. Tech. rep. Commissariat   l' nergie atomique, 1969.
- [52] Accu Dyne Test. *Viscosity, Surface Tension, Specific Density and Molecular Weight of Selected Liquid*. [https://www.accudynetest.com/visc\\_table.html?sortby=sort\\_centeripoise%20DESC](https://www.accudynetest.com/visc_table.html?sortby=sort_centeripoise%20DESC). Accessed: 9-8-2016.
- [53] A. B. Pereiro et al. "Solubility of inorganic salts in pure ionic liquids". In: *The Journal of Chemical Thermodynamics* 55 (June 2012), pp. 29–36.
- [54] T. Hoshino and T. Terai. "High-efficiency technology for lithium isotope separation using an ionic-liquid impregnated organic membrane". In: *Fusion Engineering and Design* 86 (May 2011), pp. 2168–2171.
- [55] Triad RF Systems. *Dielectric Constant, Strength and Loss Tangent*. <http://www.rfcafe.com/references/electrical/dielectric-constants-strengths.htm>. Accessed: 9-8-2016.
- [56] N. Gavish and K. Promislow. "Dependence of the dielectric constant of electrolyte solutions on ionic concentration". In: *arXiv* (Aug. 2012).
- [57] R. Singh and R. K. Ulrich. "High and Low Dielectric Materials". In: *The Electrochemical Society* (June 1999), pp. 26–30.
- [58] D. Meeker. *Finite Element Method Magnetics*. <http://www.femm.info/wiki/HomePage>. Accessed: 29-9-2016. 2014.
- [59] E. Samson, J. Marchand, and K. A. Snyder. "Calculation of ionic diffusion coefficients on the basis of migration test results". In: *Materials and Structures* 36 (Apr. 2003), pp. 156–165.
- [60] PVC Chemical Resistance Chart. Tech. rep. SpillTech, 2009.
- [61] Workshop Handbook. Tech. rep. theplasticshop.co.uk, 2011.